



Ga-68 pentixafor PET/CT imaging of vascular expression of chemokine receptor 4 (CXCR4) as a marker of arterial inflammation in patients with human immunodeficiency virus infection and its comparison with F-18 FDG PET/CT Imaging

Ismahel Opeyemi Lawal

Dissertation submitted for the degree of Doctor of Philosophy in the Faculty of Health Sciences at the University of Pretoria

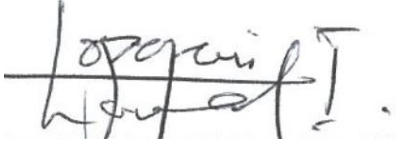
Supervisor: Prof Mike M. Sathekge

Co-supervisor: Prof Anton C. Stoltz

November 2020

DECLARATION

I hereby declare that this dissertation that I herewith submit in accordance with the requirements for the degree of Doctor of Philosophy at the University of Pretoria is my original work and has not been previously submitted to any other institution of higher learning. All sources cited or quoted in this work are indicated and acknowledged with a comprehensive list of references.



.....

Ismaheel O. Lawal

24 November 2020

DEDICATION

To my father, Imam Abubakar Lawal, for his love for education and academic excellence, and for inculcating same into me early in my upbringing

ACKNOWLEDGEMENTS

The output from my Ph.D. study reflects the amazing inspiration and support I received from mentors, colleagues, friends, and family members. To all these people, most of whom are not herein mentioned by name, I remain eternally grateful.

The greatest impetus to undertake a Ph.D. study came from my supervisor, Prof Mike Sathekge. During these years of my study, I received a lot of support and guidance from him. He provided funding for my study and was singularly instrumental for my remuneration during my Ph.D. program. You are always available to listen to my concerns, allay my fears, provide solutions to my problems, and encourage me to soldier on in the face of the challenges I encounter during my study. Thank you for your kindness and generosity to me and my family over these years.

In my co-supervisor, Prof Anton Stoltz, I found a supportive guide. I cherish your words of encouragement. Even when you were battling with your own health issues, you remained a strong pillar of support, providing me with guidance. Your death was a devastating blow to me; the passage of time has not been able to heal the wound your departure inflicted on us. I will always remember you as a dedicated, hardworking, selfless, and supportive teacher.

The nature of the work undertaken during my Ph.D. study could not have been done without a lot of help from colleagues. I receive a lot of help from many kind colleagues at work, including Johncy Mahapane, Cindy Davis, and Janke Kleynhans for helping with the synthesis of the radiotracer used in my study; Ceceila Corbet for helping with the scheduling of patients for PET scans; Adele Koegelenberg and Lynn Boshoff for helping set up the imaging protocols; and Letjie Maserumule, Honest Ndlovu, Khayinsile Hlongwa, and Janet Reed for helping with patients recruitment. I received encouragement and support from many colleagues with whom we have become friends over these years, including Chantale De Villiers, Kgomotso Mokoala, Neo Mokgoro, Aisha Ismaila, Zodwa Mahlangu, Thabo Lengana, Tebatso Boshomane, Alfred Otte Ankrah.

I thank the Nuclear Medicine Research Infrastructure (NuMeRI) for sponsoring my study. I also received generous support and help from the fantastic people at NuMeRI, including Prof Jan Rijn Zeevaart, Prof Thomas Ebenhan, and Mr. Yunus Munga. PentixaPharm (Wuerzburg, Germany) provided us with the peptide (pentixafor) used in one of my studies. I

thank Drs. Hakim Bouterfa and Jens Kaufmann for facilitating this kind gesture. Thank you, Ms. Motlalepula Marumo, for always helping with procurement and claim issues.

I have always enjoyed plenty of support and love from my parents (Imam Abubakar Lawal and Hajia Omotayo Lawal) and siblings (Khadijat Sulaiman-Lawal, Rukayat Ajiboyo-Lawal, Zainab Jimoh-Lawal, Jamiu Lawal, and Tunde Lawal). My father taught me to cherish education and academic excellence as a young boy while growing up. It is this love that has been driving my academic pursuits. I thank you all for your love, prayers, and unwavering support that have seen me to this stage of my career. I thank members of my extended family, multitude of friends and pass teachers who continue to support my growth in many wonderful ways.

To Ameenah (my wife), Atiyyah (my daughter), and Ammar (my son), you are the best anyone can ever wish for. I take this opportunity to appreciate your commitment to my success, your support, sacrifice, love, and prayers. Thank you for your understanding and patience in enduring my long absences, for always allowing me to work at home undisturbed during evenings and weekends, and for your attentiveness in listening to stories about my work. I pray that our sacrifices will be rewarded with success and prosperity so that I make up for the many missed opportunities in the years to come.

Praise be to Allah by whose grace great things are brought to completion. I thank You for the gift of life, your protection over us, and your guidance in our affairs.

TABLE OF CONTENTS

Declaration	ii
Dedication	iii
Acknowledgements	iv
Chapter 1 Introduction Molecular Imaging of Vascular Inflammation in HIV Infection	1
Chapter 2 <i>Ismaheel O. Lawal, Alfred O. Ankrah, Anton C. Stoltz, Mike M. Sathekge</i> Radionuclide imaging of inflammation in atherosclerotic vascular disease among people living with HIV infection: Current practice and future perspective <i>Eur J Hybrid Imaging. 2019;3:5.</i>	10
Chapter 3 <i>Ismaheel O. Lawal, Anton C. Stoltz, Mike M Sathekge</i> Molecular imaging of cardiovascular inflammation and infection in people living with HIV infection <i>Clin Transl Imaging. 2020;8(3):141-155</i>	39
Chapter 4 <i>Ismaheel O. Lawal, Alfred O. Ankrah, Gbenga O. Popoola, Thabo Lengana, MD, Mike M. Sathekge</i> Arterial inflammation in young patients with human immunodeficiency virus infection: A cross-sectional study using ¹⁸ F-FDG PET/CT <i>J Nucl Cardiol. 2019;26(4):1258-1265.</i>	76
Chapter 5 <i>Ismaheel O. Lawal, Kgomotso G. Mokoala, Gbenga O. Popoola, Thabo Lengana, Alfred O. Ankrah, Anton C. Stoltz, Mike M. Sathekge</i> Impact of optimized PET imaging conditions on ¹⁸ F-FDG uptake quantification in patients with apparently normal aortas <i>J Nucl Cardiol. Published online ahead of print on 06 August 2019</i>	93
Chapter 6 <i>Ismaheel O. Lawal, Gbenga O. Popoola, Johncy Mahapane, Jens Kaufmann, Cindy Davis, Honest Ndlovu, Letjie C. Maserumule, Kgomotso M.G. Mokoala, Hakim Bouterfa, Hans-Jürgen Wester, Jan Rijn Zeevaart, Mike M. Sathekge</i> [⁶⁸ Ga]Ga-Pentixafor for PET imaging of vascular expression of CXCR-4 as a marker of arterial inflammation in HIV-infected patients: A comparison with ¹⁸ F-FDG PET imaging <i>Biomolecules. 2020;10(12):1629.</i>	115

Chapter 7	<i>Ismaheel O. Lawal, Akintunde T. Orunmuyi, Gbenga O. Popoola, Thabo Lengana, Kgomotso M.G. Mokoala, Alfred O. Ankrah, Mike M. Sathekge</i> FDG PET/CT for evaluating systemic arterial inflammation induced by anthracycline-based chemotherapy of Hodgkin lymphoma: A retrospective cohort study <i>Medicine (Baltimore).</i> 2020;99(48):e23259.	134
Chapter 8	Summary	157
Chapter 9	General conclusion and future perspectives	160
Annexures	Ethics approval certificates PhD committee approval letter	163

Chapter 1

Introduction

Molecular Imaging of Vascular Inflammation in HIV Infection

Since the start of the pandemic in the early 1980s, a total of about 75.5 million people have been infected by the human immunodeficiency virus (HIV) globally. In 2019, about 38 million people were living with HIV infection, including 1.7 million people who became newly infected with the virus in that year [1]. HIV infects and destroys CD4-bearing immune cells, including CD4⁺ T-lymphocytes, monocytes/macrophages, and dendritic cells. The hallmark of untreated HIV infection is, therefore, severe immune suppression predisposing the infected individual to acquisition and re-activation of opportunistic infections. Antiretroviral agents acting on different viral pathways have been applied in combination in the treatment of HIV infection. Combination antiretroviral therapy (cART) has been effective in reversing immune suppression caused by HIV infection and has converted what was once a debilitating disease with a grim prognosis to a chronic manageable condition. The effectiveness of cART in the management of HIV infection has resulted in an improvement in the lifespan of people living with HIV (PLHIV) [3], and is now approaching the life expectancy of the HIV-uninfected general population [4]. cART inhibits viral replication but is unable to achieve complete viral eradication as replication-competent viral particles are present in sanctuary sites such as the central nervous system, testes, intestinal mucosa, lymph nodes, and other lymphoid tissues even in patients who achieved suppressed HIV viremia on cART [5].

The continuous presence of viral particles in sanctuary sites induces chronic immune activation evident by high circulating biomarkers of macrophage activation in patients effectively treated with cART [6]. This chronic immune activation coupled with other pro-atherogenic conditions prevalent in PLHIV such as endothelial dysfunction induced by HIV invasion of the vascular endothelium, impaired coagulation system, reduced vessel wall elasticity, dyslipidemia, and cART-induced metabolic derangements, predisposes this patient population to an excess risk of atherosclerotic cardiovascular disease (ASCVD) compared with HIV-uninfected populations even after correcting for traditional risk factors for ASCVD [7].). In PLHIV, there are soluble factors with pro-atherogenic properties that act through a reduction in cholesterol efflux from macrophages leading to an enhanced formation of foam cells [8]. Due to the interplay of these multiple factors, PLHIV have a risk of ASCVD that is twice that of the HIV-uninfected population [7]. In the cART era, ASCVD is a rising cause of mortality and morbidity among PLHIV [7].

Arterial inflammation is the prominent process in endothelial dysfunction that occurs early during atherogenesis in ASCVD [9]. Arterial inflammation precedes the appearance of the fatty streak, arterial wall stiffness, plaque formation, or occlusive arterial disease. Arterial inflammation is characterized by the invasion of arterial endothelium by inflammatory cells such as T-lymphocytes and monocytes [10]. Activated inflammatory cells increase glucose utilization by upregulation of glucose transporter expressed on their cell membrane. Fluorine-18 Fluorodeoxyglucose (^{18}F -FDG) is a radioactive analog of glucose trapped avidly by activated inflammatory cells. Positron emission tomography with computed tomography (PET/CT) of ^{18}F -FDG is, therefore, a useful imaging modality for non-invasive imaging of inflammation and infection. ^{18}F -FDG PET/CT has found a useful application in the interrogation of arterial inflammation as a risk for ASCVD and its complications.

^{18}F -FDG is the commonest PET tracer used in clinical imaging of inflammation and infection. However, it generally presents many challenges in its clinical utility, especially in imaging arterial inflammation [11]. Some of the pertinent problems with ^{18}F -FDG PET imaging in arterial inflammation are:

1. Stringent requirements for patient preparation, including dietary modification in the 24 to 48-hour period before imaging, restriction on physical exercise or other exerting activities over the same period, four to six-hour of fasting before scanning, etc.
2. There is a long uptake time between ^{18}F -FDG injection and commencement of PET/CT imaging. This is usually 60 minutes for all other ^{18}F -FDG PET indications. In the case of arterial inflammation imaging, a longer uptake time is required.
3. Certain medications interfere with ^{18}F -FDG uptake in neoplastic or inflammatory lesions. Patients on corticosteroids are required to stop their medication before ^{18}F -FDG PET/CT imaging.
4. A requirement for controlled ambient environmental conditions during the uptake time. All physical activities are restricted while the patient is kept warm in a dimly lit quiet room.
5. Physiologic ^{18}F -FDG uptake may cause contamination of photons into an adjacent vascular bed during tracer uptake quantification. Myocardial ^{18}F -FDG uptake may contaminate signals from coronary arteries and aorta. Similarly, physiologic pharyngeal

uptake, as well as uptake in neck muscles, may contaminate signal quantification in the carotid arteries.

6. The vascular smooth muscles trap ^{18}F -FDG avidly in ASCVD, thereby contributing significantly to the arterial tracer quantification during PET imaging of arterial inflammation [12]. The PET signal contributed by vascular smooth muscle cells is unwanted as ^{18}F -FDG uptake in inflammatory cells present in the arterial endothelium is the desirable signal representing inflammation.

Despite these limitations, there are important studies that have utilized ^{18}F -FDG for PET imaging of arterial inflammation in PLHIV. In chapter two, a summary of the current evidence on the use of ^{18}F -FDG PET/CT for vascular inflammation imaging is presented. In this chapter also, other targets expressed by activated inflammatory cells that can be targeted for radionuclide imaging of inflammation in ASCVD are presented. In addition to arterial inflammation as a precursor to atherogenesis and its complications, PLHIV are at an increased predisposition to infection involving various components of the cardiovascular system, including the endocardium, myocardium, and epicardium. Chapter three provides an update on the current evidence on the use of radionuclide techniques for cardiovascular inflammation and infection imaging.

Prior works on ^{18}F -FDG PET imaging of arterial inflammation in PLHIV included the older patient population. Older patients already have a multitude of ASCVD risk factors other than HIV infection. The contribution of these other ASCVD risk factors above that due to HIV infection may be difficult to separate. In chapter 4, the report on a cross-sectional study comparing arterial inflammation evaluated with ^{18}F -FDG PET/CT in young HIV-infected patients and HIV-uninfected age- and gender-matched controls is presented.

The average thickness of the human arterial wall is less than twice the spatial resolution of the clinical PET system [13,14]. This leads to a significant underestimation of tracer uptake quantification during PET imaging of arterial inflammation. A longer uptake time, beyond the 60 minutes commonly applied in routine PET imaging, leads to improved background tracer clearance with resultant improvement in the target-to-background ratio (TBR) [15]. On this background, the cardiovascular committee of the European Association of Nuclear medicine, in 2016, published a set of recommendations for application during ^{18}F -FDG PET/CT imaging of inflammation in ASCVD to improve the PET quantification parameters [16]. The results of an

original article that assessed the impact of these recommended patient preparations and imaging criteria on quantified PET parameters for arterial inflammation imaging are presented in chapter 5.

Due to the multiple challenges encountered with the use of ^{18}F -FDG as PET tracer for arterial inflammation imaging, a need exists to evaluate other PET tracers for arterial inflammation. Chemokine receptor-4 (CXCR4) is a cytokine receptor expressed on activated inflammatory cells. It mediates gene expression that drives actin polymerization, cytoskeleton rearrangement, and cell migration [17]. CXCR4 is also the co-receptor utilized by HIV during its entry into CD4-bearing immune cells [18]. Gallium-68 pentixafor is a PET radioligand that targets CXCR4 expressed on macrophages. Chapter 6 presents the results of a head-to-head comparison of ^{18}F -FDG PET/CT and ^{68}Ga -pentixafor PET/CT for imaging arterial inflammation in PLHIV. Among the different radiotracers with potential for use for vascular inflammation imaging, ^{68}Ga -pentixafor was chosen because it does not suffer from many of the challenges associated with ^{18}F -FDG for this indication. Some of the merits of ^{68}Ga -pentixafor for PET imaging of vascular inflammation include:

1. ^{68}Ga -Pentixafor binds to macrophages which represent direct imaging of inflammation within the atherosclerotic lesion [19]. While ^{18}F -FDG is taken up by the activated macrophages, some are also taken up by the vascular smooth muscle [12].
2. No special patient preparation is necessary.
3. No fasting is required.
4. No special ambient condition is necessary during the uptake time.
5. Imaging is done after 60 minutes of uptake time. This is due to the prompt uptake and excellent background clearance with a good target to background ratio [20].
6. Lower radiation burden compared with ^{18}F -FDG PET imaging [20].
7. Physiologic tracer uptake is limited to the spleen, adrenals, and bone marrow [19,20]. No significant physiologic tracer uptake occurs in the myocardium, brain, or skeletal muscle to interfere with vascular tracer uptake assessment.
8. ^{68}Ga is obtained from $^{68}\text{Ge}/^{68}\text{Ga}$ generator, making the tracer readily available without the need for an onsite cyclotron.

PLHIV are also at increased risk of malignant diseases. Factors predisposing to this excess risk of malignancies include increased predisposition to infection with oncogenic viruses,

chronic antigen stimulation, chronic inflammation, cytokine dysregulation, and prevalence of behavioral factors such as smoking [21]. Based on the strength of their association with acquired immunodeficiency syndrome (AIDS), HIV-associated malignancies can be classified as AIDS-defining and non-AIDS-defining. In the cART era, the incidence of AIDS defining cancers has been on the decline while there has been a rise in the incidence of non-AIDS-defining cancers [22]. Hodgkin lymphoma (HL) is a non-AIDS-defining cancer with a rising incidence among PLHIV in the cART era. Lymphomas are the commonest cause of cancer-related death among PLHIV [23]. Anthracycline-based chemotherapy is the mainstay of treatment of HL. The effectiveness of anthracycline-based chemotherapy has led to a remarkable improvement in the survival of patients with HL. Cardiovascular toxicity, including increased predisposition to ASCVD, is one of the long-term complications of anthracyclines [24,25]. There is a valid concern that HIV-infected patients with HL treated anthracycline-based chemotherapy may have a heightened risk of ASCVD. Since arterial inflammation precedes the formation of frank arterial atheroma, ¹⁸F-FDG PET/CT may be a useful non-invasive imaging modality to detect arterial inflammation as a risk for ASCVD in HIV-infected patients with HL who were treated with an anthracycline-based chemotherapy regimen. Chapter 7 presents the report of the study of ¹⁸F-FDG PET/CT imaging of arterial inflammation in a mixed group of HIV-infected and HIV-uninfected survivors of HL who were treated with an anthracycline-based chemotherapy regimen.

References

1. UNAIDS. Global HIV & AIDS statistics – 2020 fact sheet. Available from: <https://www.unaids.org/en/resources/fact-sheet>. Accessed 12 October 2020.
2. Simon V, Ho DD, Abdool Karim Q. 2006. HIV/AIDS epidemiology, pathogenesis, prevention, and treatment. *Lancet*. 2006;368:489-504.
3. Teeraananchai S, Kerr SJ, Amin J, Ruxrungtham K, Law MG. Life expectancy of HIV-positive people after starting combination antiretroviral therapy: a meta-analysis. *HIV Med*. 2017;18:256-266.
4. Wandeler G, Johnson LF, Egger M. Trends in life expectancy of HIV-positive adults on antiretroviral therapy across the globe: comparisons with general population. *Curr Opin HIV AIDS*. 2016;11:492-500.
5. Lamers SL, Rose R, Maidji E, Aagsalda-Garcia M, Nolan DJ, Fogel GB, et al. HIV DNA Is Frequently Present within Pathologic Tissues Evaluated at Autopsy from Combined Antiretroviral Therapy-Treated Patients with Undetectable Viral Loads. *J Virol*. 2016;90:8968-8983.
6. Nabatanzi R, Bayigga L, Cose S, Rowland Jones S, Joloba M, Canderan G, et al. Monocyte Dysfunction, Activation, and Inflammation After Long-Term Antiretroviral Therapy in an African Cohort. *J Infect Dis*. 2019;220:1414-1419.
7. Shah ASV, Stelzle D, Lee KK, Beck EJ, Alam S, Clifford S, et al. Global Burden of Atherosclerotic Cardiovascular Disease in People Living With HIV: Systematic Review and Meta-Analysis. *Circulation*. 2018;138:1100-1112.
8. Maisa A, Hearps AC, Angelovich TA, Pereira CF, Zhou J, Shi MD, et al. Monocytes from HIV-infected individuals show impaired cholesterol efflux and increased foam cell formation after transendothelial migration. *AIDS*. 2015;29:1445-57.
9. Wong BW, Meredith A, Lin D, McManus BM. The Biological Role of Inflammation in Atherosclerosis. *Can J Cardiol*. 2012;28:631-641.
10. Ross R. Atherosclerosis an inflammatory disease. *N Engl J Med*. 1999;340:115-126.
11. Rogers IS, Tawakol A. Imaging of coronary inflammation with FDG-PET: Feasibility and clinical hurdles. *Curr Cardiol Rep*. 2011;13:138-144.

12. Al-Mashhadi RH, Tolbod LP, Bloch LØ, Bjørklund MM, Nasr ZP, Al-Mashhadi Z, ¹⁸Fluorodeoxyglucose Accumulation in Arterial Tissues Determined by PET Signal Analysis. *J Am Coll Cardiol.* 2019;74:1220-1232,
13. Burg S, Dupas A, Stute S, Dieudonné A, Huet P, Le Guludec D, et al. Partial volume effect estimation and correction in the aortic vascular wall in PET imaging. *Phys Med Biol.* 2013;58:7527-7542.
14. Huet P, Burg S, Le Guludec D, Hyafil F, Buvat I. Variability and uncertainty of ¹⁸F-FDG PET imaging protocols for assessing inflammation in atherosclerosis: suggestions for improvement. *J Nucl Med.* 2015;56:552-559.
15. Bucerius J, Mani V, Moncrieff C, Machac J, Fuster V, Farkouh ME, et al. Optimizing ¹⁸F-FDG PET/CT imaging of vessel wall inflammation: the impact of ¹⁸F-FDG circulation time, injected dose, uptake parameters, and fasting blood glucose levels. *Eur J Nucl Med Mol Imaging.* 2014;41:369-383.
16. Bucerius J, Hyafil F, Verberne HJ, Slart RH, Lindner O, Sciagra R, et al. Position paper of the Cardiovascular Committee of the European Association of Nuclear Medicine (EANM) on PET imaging of atherosclerosis. *Eur J Nucl Med Mol Imaging.* 2016;43:780-792.
17. Walenkamp AME, Lapa C, Herrmann K, Wester HJ. CXCR4 Ligands: The Next Big Hit? *J Nucl Med.* 2017;58:77S-82S.
18. Feng Y, Broder CC, Kennedy PE, Berger EA. HIV-1 entry cofactor: functional cDNA cloning of a seven-transmembrane, G protein-coupled receptor. *Science.* 1996;272:872-877.
19. Hyafil F, Pelisek J, Laitinen I, Schottelius M, Mohring M, Döring Y, et al. Imaging the Cytokine Receptor CXCR4 in Atherosclerotic Plaques with the Radiotracer ⁶⁸Ga-Pentixafor for PET. *J Nucl Med.* 2017;58:499-506.
20. Herrmann K, Lapa C, Wester HJ, Schottelius M, Schiepers C, Eberlein U, et al. Biodistribution and Radiation Dosimetry for the Chemokine Receptor CXCR4-Targeting Probe ⁶⁸Ga-Pentixafor. *J Nucl Med.* 2015;56:410-416.
21. Yarchoan R, Uldrick TS. HIV-associated cancers and related diseases. *N Engl J Med.* 2018;378:1029-1041.

22. Tanaka LF, Latorre MDRD, Gutierrez EB, Heumann C, Herbinger KH, Froeschl G. Trends in the incidence of AIDS-defining and non-AIDS-defining cancers in people living with AIDS: a population-based study from São Paulo, Brazil. *Int J STD AIDS*. 2017;28:1190-1198.
23. Grulich AE, Vajdic CM. The epidemiology of cancers in human immunodeficiency virus infection and after organ transplantation. *Semin Oncol*. 2015;42:247-257.
24. van Nimwegen FA, Schaapveld M, Janus CPM, Krol ADG, Petersen EJ, Raemaekers JMM, et al. Cardiovascular disease after Hodgkin lymphoma treatment: 40-year disease risk. *JAMA Intern Med*. 2015;175:1007-1017.
25. Bhakta N, Liu Q, Yeo F, Baassiri M, Ehrhardt MJ, Srivastava DK, et al. Cumulative burden of cardiovascular morbidity in paediatric, adolescent, and young adult survivors of Hodgkin's lymphoma: an analysis from the St Jude Lifetime Cohort Study. *Lancet Oncol*. 2015;17:1325-1334.

Chapter 2

Radionuclide imaging of inflammation in atherosclerotic vascular disease among people living with HIV infection: Current practice and future perspective

Ismaheel O. Lawal¹, Alfred O. Ankrah^{1,2}, Anton C. Stoltz³, Mike M. Sathekge¹

1. Department of Nuclear Medicine University of Pretoria & Steve Biko Academic Hospital, Pretoria South Africa.
2. Department of Nuclear Medicine and Molecular Imaging, University Medical Center Groningen & University of Groningen, Groningen, The Netherlands.
3. Infectious Disease Unit, Department of Internal Medicine, University of Pretoria & Steve Biko Academic Hospital, Pretoria South Africa.

Eur J Hybrid Imaging. 2019;3:5.

Abstract

People living with human immunodeficiency virus (HIV) infection have twice the risk of atherosclerotic vascular disease compared with non-infected individuals. Inflammation plays a critical role in the development and progression of atherosclerotic vascular disease. Therapies targeting inflammation irrespective of serum lipid levels have been shown to be effective in preventing the occurrence of CVD. Radionuclide imaging is a viable method for evaluating arterial inflammation. This evaluation is useful in quantifying CVD risk and for assessing the effectiveness of anti-inflammatory treatment. The most tested radionuclide method for quantifying arterial inflammation among people living with HIV infection has been with ^{18}F -FDG PET/CT. The level of arterial uptake of ^{18}F -FDG correlates with vascular inflammation and with the risk of development and progression of atherosclerotic disease. Several limitations exist to the use of ^{18}F -FDG for PET quantification of arterial inflammation. Many targets expressed on macrophages, a significant player in arterial inflammation, have the potential for use in evaluating arterial inflammation among people living with HIV infection. The review describes the clinical utility of ^{18}F -FDG PET/CT in assessing arterial inflammation as a risk for atherosclerotic disease among people living with HIV infection. It also outlines potential newer probes that may quantify arterial inflammation in the HIV-infected population by targeting different proteins expressed on macrophages.

Keywords:

Arterial inflammation, HIV, Cardiovascular disease, ^{18}F -FDG PET, Tc-99m Tilmanocept, Target-to-background ratio

Abbreviations

AIDS	Acquired immunodeficiency syndrome
AMI	Acute myocardial infarction
cART	Combination antiretroviral therapy
CCR5	Chemokine receptor 5
CCTA	Coronary computed tomography angiography
CVD	Cardiovascular diseases
CXCL12	C-X-C chemokine ligand 12
CXCR4	C-X-C chemokine receptor 4
DANBIRT	DOTA-butyl amino-NorBIRT
¹⁸ F-FDG PET/CT	Fluorine-18 labeled 2-fluoro-2-deoxyglucose positron emission tomography/computed tomography
¹⁸ F-FMCH	Fluorine-18 Fluoromethylcholine
¹⁸ F-FOL	Aluminium fluoride-18 NOTA-folate
HIV	Human immunodeficiency virus
hs-CRP	High-sensitivity C-reactive protein
ICAM-1	Intercellular adhesion molecule-1
LFA-1	Leucocyte function-associated antigen-1
MCP-1	Monocyte chemoattractant protein-1
MMPs	Metalloproteinases
PLWH	People living with HIV
SUVmax	Maximum standardized uptake values
TBR	Target to background ratio
TSPO	Translocator protein
VCAM-1	Vascular cell adhesion molecule-1

Introduction

Infection with human immunodeficiency virus (HIV) has remained a significant cause of morbidity and mortality globally. In 2017, 36.9 million were living with the infection with about 1.8 million new infections reported in the same year (UNAIDS 2018). The widespread availability of combination antiretroviral therapy (cART) that is highly effective in suppressing viral replication has led to a significant reduction in HIV-associated morbidity and mortality, as well as the transmission of the virus from person to person. In 2017, 21.7 million individuals with HIV infection were already on cART with 940,000 individuals dying from acquired immunodeficiency syndrome (AIDS)-related illnesses, a significant reduction compared with 1.4 million and 1.9 million individuals who died of AIDS-related diseases in 2010 and 2004 respectively (UNAIDS 2018). Improvement in survival seen in people living with HIV (PLWH) has mostly been due to the reduction in mortality associated with opportunistic infections. Atherosclerotic cardiovascular diseases (CVD) are a growing cause of death among PLWH in developed and developing countries (Morlat et al. 2014; Chow et al. 2018; Hyle et al. 2017; Shah et al. 2018). PLWH have a two-fold higher risk of CVD compared with non-infected individuals. Also, the burden of CVD among PLWH has tripled over the last two decades (Shah et al. 2018). In this review, we will describe the role of arterial inflammation in atherogenesis and the etiopathogenic factors responsible for the higher risk of CVD among PLWH. We will further discuss the molecular probes in current clinical use and those with potential for clinical translation for radionuclide imaging of arterial inflammation among PLWH.

Atheroma formation, propagation, and complication: the role of inflammation

Inflammation is an essential factor in atherosclerosis and is also a culprit in the catastrophic complications that can result from arterial atheroma. The endothelial lining of the intact arterial intima usually resists adhesion by leucocytes. Damage to the arterial intima, however, leads to adhesion by leucocytes and inflammation of the vessel lining. Some factors are known to cause arterial intima injury. These factors include smoking, hypertension, hyperglycemia, insulin resistance, and obesity. Arterial injury leads to expression of cell adhesion molecules by the endothelial cells, a process which favors adhesion of leucocytes to the vascular intima.

T lymphocytes and monocytes are principal players in early atherogenesis binding to the endothelial cells via cell adhesion molecules expressed on the activated vascular endothelial cells

(Cybulsky and Gimbrone Jr. 1991; Cybulsky et al. 2001). Following binding of T lymphocytes and monocytes to the endothelial cells, they undergo diapedesis into the sub-endothelial space where they become activated, and monocytes transform into macrophages. Chemoattractants guide cellular migration into the sub-endothelial space. Cytokines form a big family of chemoattractants, and they include monocyte chemoattractant protein-1 (MCP-1), interleukin-1 (IL-1) tumor necrosis factor-alpha (TNF- α), and Lyso-PC (a component of oxidized lipoprotein) (McMurray et al. 1993; Yamashita et al. 2002).

Inflammatory cells play a crucial role in fatty streak formation. Monocytes invade the vessel wall and transform to macrophages. These macrophages increase their expression of scavenger receptors and engulf oxidized lipoprotein to form foam cells. Macrophages also multiply and release growth factors and cytokines leading to amplification of inflammation in the vessel wall (Libby 2006).

The matured atheromatous plaque typically contains a lipid or necrotic core which is covered by a fibrotic cap made up of an admixture of smooth muscle cells and supporting extracellular matrix. The base of the lesion (so-called the shoulder) often contains foam cells and T lymphocytes. These various components of the plaque vary from one lesion to the other. Stable plaque contains a small core of lipid with a thick cap. The unstable plaque contains a larger lipid core with a thin cap and a large number of inflammatory cells. Both types of lesions present a different array of cardiovascular complications. The stable plaque evolves to cause vascular stenosis which may eventually result in total occlusion. The unstable plaque, so-called the vulnerable plaque, is ominous as it can evolve into complications with fatal consequences. Plaque rupture is the dreaded complication of the unstable atheromatous lesion (Fan and Watanabe 2013).

Inflammation plays an important role in plaque rupture. Macrophages are capable of producing matrix metalloproteinases (MMPs), which can digest the cap leading to rupture. T cells produce interferon- γ , which inhibits smooth muscle cell proliferation and the laying down of extracellular matrix (Fan and Watanabe 2013). Smooth muscle cells are responsible for the production of collagen that gives strength to the fibrous cap.

Increased risk of atherosclerosis among people with HIV infection

HIV infection, its treatment with cART, and a higher prevalence of traditional CVD risk factors all act in concert to predispose PLWH to a higher risk of atherosclerotic CVD.

HIV infection is associated with an upregulation of the inflammatory processes in the organ/systems generally and in the vessel walls specifically. Upregulation of the inflammatory system is present in both treated and untreated PLWH (Duprez et al. 2012; Kuller et al. 2008). The D:A:D study presents a useful insight into the magnitude of CVD risk and the mortality resulting from it among HIV-infected patients (Glass et al. 2006). The study which included 33,308 HIV-infected patients that were followed-up for 10 years (1999 to 2008) reported 2482 deaths during the observation period. Deaths due to cardiovascular disease were 289, AIDS-related deaths were 743, and non-AIDS defining malignancy deaths were 286. These high CVD-related deaths occurred despite the low prevalence of traditional CVD risks in the study population—75% of the patients were in the low-risk age groups (less than 45 years for males, less than 55 years for females), only 8.5% were hypertensive, 3.5% were obese (BMI > 30 kg/m²), 2.5% were diabetic, and 1.5% had a previous history of stroke or myocardial infarction (Glass et al. 2006).

Freiburg and colleagues recently published a prospective longitudinal cohort study of the risk of acute myocardial infarction in HIV-infected patients and their age-, race/ethnicity-, and clinical site-matched uninfected veterans. The study enrolled 82,459 participants from April 2003 through December 2009 and followed them up for a median period of 5.9 years (Freiberg et al. 2013). They recorded 871 cases of acute myocardial infarction (AMI). The incidence of AMI was significantly higher among HIV-infected participants in all age groups compared with HIV-uninfected participants. After adjusting for Framingham risk factors, co-morbidities, and substance abuse, HIV-infected participants had a significantly higher incidence of AMI compared with non-infected participants. The risk for AMI remained significantly higher even in HIV-infected participants with suppressed viral load compared with non-infected participants (Freiberg et al. 2013). The finding of Freiburg et al. suggests that the increased risk of AMI among PLWH is likely a function of HIV, cART, and the burden of co-morbid conditions including Framingham risk factors.

The exact mechanisms by which HIV infection leads to increased risk for CVD remain incompletely understood. Putative mechanisms may include chronic immune activation and inflammation associated with HIV infection, CD4 depletion, impaired coagulation system,

vascular endothelial dysfunction, and reduced elasticity of vessel wall, dyslipidemia, and other cART-induced metabolic derangements.

The HIV status is a pro-coagulant condition resulting from reduced levels of anti-thrombotic protein S, and increased levels of pro-thrombotic cardiolipin and lupus anticoagulant (Lijfering et al. 2006; Sene et al. 2008). Deficiency of protein C and antithrombin III, as well as raised levels of P-selectin and homocysteine, have also been reported (Majluf-Cruz et al. 2004; Flinn et al. 1984; Bernasconi et al. 2001; Musselwhite et al. 2011). The vascular endothelium in HIV-infected patients expresses tissue factor, von Willebrand factor, and plasminogen activator inhibitor-1 (Aukrust et al. 2000). Substance abuse is more common in HIV-infected individuals compared with uninfected individuals (Glass et al. 2006). Cocaine use and smoking, two of the common substances of abuse among HIV-infected patients, cause platelet activation (Mavroudis et al. 2013).

There is an ongoing improvement in the potency, tolerability, and safety of cART use in PLWH. Despite this, however, cART is another identified risk factor predisposing to CVD among PLWH (Durand et al. 2011; Mary-Krause et al. 2003). In the D:A:D study, increased incidence of myocardial infarction occurred with increasing period of exposure to cART (26% relative increase per year of exposure during the first four to 6 years of use). Patients not on cART had a lower incidence of myocardial infarction (D:A:D Study Group 2003). In another report on the D:A:D study cohorts, the increased risk of myocardial infarction was associated with didanosine and abacavir use and not with zidovudine, stavudine, or lamivudine use. The risk was, however, not present beyond 6 months after cessation of the medication (D:A:D Study Group 2008). Obel et al., in a prospective population-based nationwide cohort study of 2952 HIV-infected Danish patients, also confirmed the increased risk of myocardial infarction with abacavir use (Obel et al. 2010).

Carr et al. found, about two decades ago, an increased incidence of peripheral lipodystrophy, hyperlipidemia, and insulin resistance among PLWH receiving protease inhibitors (PI) as part of cART (Carr et al. 1998a). In this cross-sectional study, the authors found significantly lower total body fat, higher total cholesterol, and triglycerides among patients on PI compared with PI-naïve patients. Sixty-four percent of patients on PI had lipodystrophy compared with 3% of PI-naïve patients. One of the putative mechanisms by which PIs promote atherogenesis lies in their ability to increase CD36-dependent cholesteryl-ester accumulation in

macrophages. PIs also cause hypercholesterolemia and induce endothelial dysfunction. The catalytic region of HIV-protease, the HIV enzyme that PIs target, has about 60% homology to regions of cytoplasmic retinoic-acid binding protein type 1 (CRABP-1) and low-density lipoprotein receptor-related protein (LRP), two proteins that regulate lipid metabolism (Carr et al. 1998b).

Hui has reviewed the different mechanisms by which PIs disrupt lipid metabolism leading to metabolic syndrome, a predisposing condition to CVD (Hui 2003). PIs suppress the breakdown of sterol regulatory element binding proteins (SREBP) which are present in the liver and adipose tissues. Accumulation of SREBP in the liver increases fatty acid and cholesterol synthesis. Its accumulation in the adipose tissues causes lipodystrophy, reduces leptin expression, and promote insulin resistance. PIs also suppress proteasome-mediated breakdown of newly formed apolipoprotein B. This results in overproduction of triglyceride-rich lipoproteins. PIs contribute to insulin resistance and the development of frank diabetes via their ability to suppress the inhibition of GLUT-4 activity in the adipose tissue and skeletal muscle.

¹⁸F-FDG PET for arterial inflammation in people living with HIV infection

The central role that arterial inflammation plays in atherogenesis is now well characterized. Several trials are either underway or have recently reported their findings on the evaluation of the effectiveness of different anti-inflammatory agents on arterial inflammation for risk reduction among individuals at risk for or with established CVD. The CANTOS trial recently demonstrated a dose-dependent reduction in recurrent CVD and CVD death in patients with previous myocardial infarction treated with canakinumab, a therapeutic antibody targeting interleukin-1 (Ridker et al. 2017). The results in this and other trials among people without HIV infection make use of serum high-sensitivity C-reactive protein (hs-CRP) and other serum biomarkers of inflammation to assess for response to interventions. In PLWH, chronic upregulation of the inflammatory system may make the use of these serum biomarkers for response assessment unreliable. A need, therefore, exists for direct measurement of arterial inflammation for risk assessment and therapy response evaluation. Imaging represents a viable option to achieve this.

Positron emission tomography (PET) with Fluorine-18 labeled 2-fluoro-2-deoxyglucose (¹⁸F-FDG) is capable of demonstrating functional changes in disease states, a process that precedes morphological changes that are discernible on anatomic imaging. Abdelbaky et al.

showed, in a longitudinal ^{18}F -FDG PET/CT study, that arterial inflammation precedes subsequent calcification in the same location as a marker of plaque progression (Abdelbaky et al. 2013). PET imaging is now performed as hybrid imaging usually with CT or more recently with magnetic resonance imaging (MRI) offering complementary morphologic information to the functional data available from PET.

Invasion of the vessel wall by inflammatory cells is an early feature of the process of atherogenesis. Activated inflammatory cells, especially macrophages, accentuate their use of glucose to cope with the metabolically demanding process of inflammation. ^{18}F -FDG, an analog of glucose, is similarly trapped by the inflammatory cells. ^{18}F -FDG PET/CT has a broad application in imaging of cardiovascular inflammation and infection (Lawal and Sathekge 2016).

Arterial FDG accumulation, a marker of arterial inflammation, has been found to correlate with the level of expression of serum biomarkers of macrophage activation such as CD68 and MMP-9 (Tawakol et al. 2006; Graebe et al. 2009). In established plaque, ^{18}F -FDG uptake is higher in symptomatic compared with an asymptomatic plaque (Rudd et al. 2002), and in asymptomatic patients with arterial plaques, ^{18}F -FDG uptake predicts future vascular events (Rominger et al. 2009; Figueroa et al. 2013).

Studies have been done in PLWH using ^{18}F -FDG PET/CT to demonstrate arterial inflammation. The target to background ratio (TBR) of arterial FDG uptake, which is obtained by calculating the mean of multiple maximum standardized uptake values (SUVmax) from an artery of interest and dividing it by the mean standard uptake value obtained from an adjacent vein, is commonly used as a surrogate for arterial inflammation. TBR has been shown to be highly reproducible in different arterial regions in a test-retest study (Rudd et al. 2008).

Subramanian et al. in 2012 compared aortic TBR in three groups of patients (Subramanian et al. 2012). Group one contained chronic HIV-infected patients ($n = 27$). Group two contained non-HIV control group matched with the HIV group by age, gender, and Framingham risk score ($n = 27$). Group three contained non-HIV patients known with atherosclerotic disease ($n = 27$). TBR, a surrogate for arterial inflammation, was significantly higher in the HIV-infected group compared with non-HIV-infected patients in group two but similar to that of patients in group three with an established atherosclerotic disease. TBR remained significantly higher in the HIV group even after correcting for traditional cardiovascular risk factors. TBR correlated with sCD163 level (a marker of macrophage

activation) but not with CRP or D-dimer in the HIV-infected group (Subramanian et al. 2012). The HIV patients included in this study were prospectively recruited, and ^{18}F -FDG PET/CT imaging was 3 h post tracer injection. Imaging patients after 3 h provided the best uptake time for visualizing vascular inflammation. The non-HIV infected patients in groups two and three of the study were, however, taken from a retrospective pool of data. These were patients who had ^{18}F -FDG PET/CT imaging for other indications other than evaluation of vascular imaging, and they acquired their images after an uptake period of 60 min. The impact of this differential uptake time in the study population is not known. A longer uptake time allows for better background clearance, and this may impact on the calculated TBR.

In the same year, Yarasheski and colleagues reported on carotid TBR in HIV-infected patients with suppressed viremia but with CVD risk factors and compared it with carotid TBR from five non-HIV controls with no risk factor for CVD (Yarasheski et al. 2012). They found a significantly higher carotid TBR in HIV-infected patients compared with the non-infected control group. Yarasheski et al. also evaluated the aortic TBR but in only nine of their study participants (five HIV patients and four controls) (Yarasheski et al. 2012). They did not find any significant difference in the aortic TBR between the HIV-infected and non-HIV control group. The absence of differences in the aortic TBR between HIV-infected and uninfected patients may be related to the small number of patients studied. A further limitation of this study lies in its comparison of the non-HIV patients with no risk factors for CVD with HIV-infected patients who had evidence of established arterial disease (as demonstrated by thickened carotid intima-media on ultrasound), as well as risk factors for CVD. It is unknown if the higher carotid TBR seen in the HIV-infected group is due to the effect of HIV infection or CVD risk present in these patients.

In a clinical trial, HIV-infected patients with sub-clinical coronary artery disease, arterial inflammation on ^{18}F -FDG PET/CT and LDL-cholesterol were randomized in 1:1 to receive atorvastatin or placebo. Lo et al. reported no difference between the two groups regarding TBR obtained at baseline and a repeat TBR after 12 months of treatment (Lo et al. 2015). There was a significant reduction in non-calcified coronary plaque volume and the number of high-risk plaques assessed on coronary computed tomography angiography (CCTA) in the atorvastatin group compared with the placebo group. The authors of this study affirmed the technical difficulty experienced in matching similar areas on the baseline and follow-up PET/CT scans.

The technical difficulty may be responsible for the lack of significant change between the two groups despite significant demonstrable changes in plaque volume and number as seen on CCTA.

Some researchers evaluated the effect of ART in 12 HIV-infected cART-naïve patients who had a baseline ^{18}F -FDG PET/CT and a repeat study done after 6 months of ART (Zanni et al. 2016). The researchers compared aortic TBR and ^{18}F -FDG uptake in axillary nodes between the baseline scan and repeat scan post 6 months of cART. While there was a significant reduction in ^{18}F -FDG uptake in the lymph nodes, they did not observe a similar reduction in aortic ^{18}F -FDG uptake. Three of the HIV-infected patients showed lesion progression on CCTA. The study was not sufficiently powered to demonstrate a change in arterial inflammation. Progression of the atherosclerotic disease in some of the study population was probably responsible for the lack of a significant difference in TBR in response to ART.

A study evaluated the relationship between TBR and HIV viremia in a recent report consisting of three groups of patients (Tawakol et al. 2017). The three groups of HIV-infected patients were (1) cART-treated patients with undetectable viremia, $n = 33$; (2) cART-untreated or treated patients with detectable viremia, $n = 7$; and (3) cART-untreated patients with undetectable viremia—the so-called elite controllers, $n = 5$. TBR as a measure of arterial inflammation was not significantly different between all HIV-infected patients compared with HIV-uninfected controls. When 15 statin-naïve HIV-infected patients on cART with undetectable viremia were matched (age, gender, and FRS) with 15 statin-naïve HIV-uninfected controls, arterial inflammation was higher in HIV-infected patients compared to control. TBR obtained at different sites in the arterial bed were concordant.

Using aortic TBR as a surrogate marker for arterial inflammation, our group recently reported the presence of arterial inflammation in young PLWH (40 years and younger) with otherwise low-risk factors for CVD compared with age- and gender-matched HIV-uninfected controls (Lawal et al. 2018). In one of the largest studies to have evaluated arterial inflammation in PLWH using FDG PET, we found no significant impact of the duration of HIV infection, CD 4 count, and viral load at the time of imaging on the vascular inflammation. Our study showed that arterial inflammation is already present in PLWH at a younger age even if they have no significant other traditional CVD risk factors other than being HIV-infected (Fig. 1). Our finding, as well as findings by others, has stimulated interest in evaluating various anti-inflammatory

agents such as statins and methotrexate for primary prevention of CVD among PLWH (Mosepele et al. 2018; Hsue et al. 2018).

One study reported no significant difference in TBR in 26 HIV-infected patients with suppressed HIV viremia on ART, low FRS, and without CVD compared with 25 healthy controls (Knudsen et al. 2015). Carotid IMT was similarly not different between the two groups. Serum markers of inflammation (hs-CRP), activated macrophages (CD163), and endothelial dysfunction (E-selectin, VCAM-1, ICAM-1, MMP-9) were also not different between the two groups. Only PAI-1 (a marker of coagulation) was significantly higher in the HIV-infected group compared with the healthy controls. Table 1 summarizes studies reporting on the use of ^{18}F -FDG PET/CT in the evaluation of arterial inflammation in HIV-infected individuals.

^{18}F -FDG remains the most tested tracer for the evaluation of arterial inflammation in PLWH. It, however, has got several limitations to its use. The most important of these limitations appear to be lack of specificity of ^{18}F -FDG. It is taken up intensely in the myocardium and, to a variable extent, in the tissues of the neck (such as muscle, pharyngeal wall, brown fat). These areas of physiologic ^{18}F -FDG uptake can cause photon spillover into the adjacent arterial segment of interest (such as coronary and carotid arteries) during arterial ^{18}F -FDG uptake quantification. Also, a long uptake time is required for blood pool clearance of ^{18}F -FDG to allow for optimum arterial tracer quantification. Bucarius and colleagues demonstrated a higher arterial ^{18}F -FDG uptake in patients imaged after a longer uptake time (> 145 min) compared with patients imaged earlier (≥ 97 to ≤ 111 min) (Bucarius et al. 2014). In the study, while meanTBRmax demonstrated a progressively increasing trend with uptake time, the SUVmax of ^{18}F -FDG uptake in the aorta decrease with delayed imaging suggesting that improvement in meanTBRmax seen in the study was as a result of better background clearance on delayed imaging.

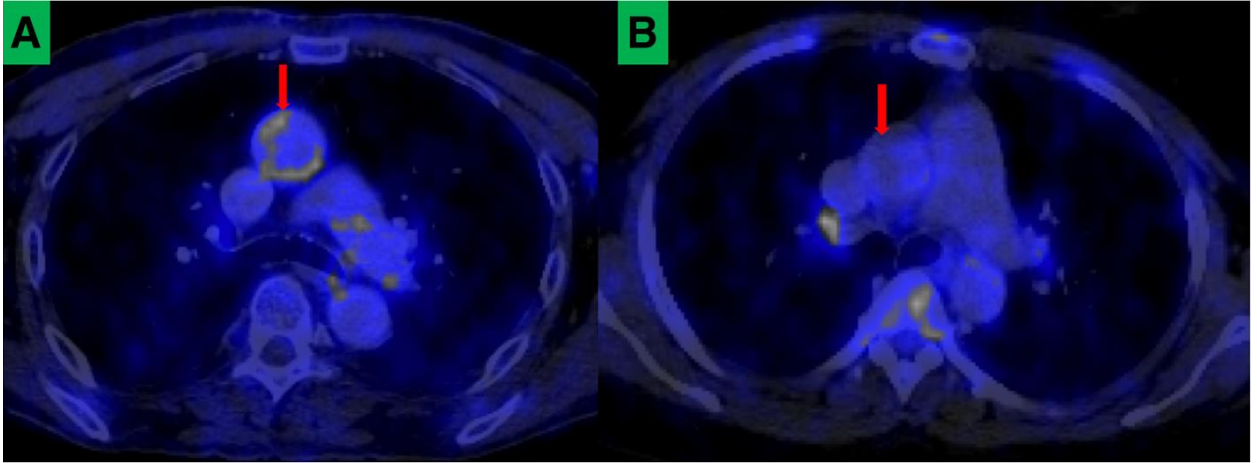


Fig 1 ^{18}F -FDG PET/CT images showing axial sections through the chest of an HIV-infected patient (a) and HIV-uninfected patient (b) matched for age and gender. Increased ^{18}F -FDG uptake is seen in the ascending aorta (red arrow) of the HIV-infected patient but not in the HIV-uninfected control

Consequently, the European Association of Nuclear Medicine Cardiovascular committee has recommended a 2-h uptake time between ^{18}F -FDG injection and commencement of PET imaging (Bucerius et al. 2016). Given these challenges and many others including the need for fasting and a fasting blood sugar of ≤ 7.0 mmol/L, there is an effort toward finding a more specific tracer for arterial wall inflammation imaging and for plaque characterization, which may find clinical application in PLWH (Vigne et al. 2018). Bucerius and co-workers recently published a review of the molecular targets for atherosclerotic imaging (Bucerius et al. 2018).

Table 1 Summary of studies utilizing ¹⁸F-FDG PET/CT in the evaluation of arterial inflammation in HIV infected patients

Authors, Year of publication	Number of HIV-infected patients	Vessels where TBR was obtained	Summary of findings	comments
Subramanian et al. 2012	27	Ascending aorta	Higher TBR in HIV-infected patients than non-infected patients. TBR in HIV-infected patients comparable to TBR in non-HIV infected patients with atherosclerosis	
Yarasheski et al. 2012	9	Carotid arteries Aorta	TBR higher in HIV patients compared with non-HIV patients in the carotids but not in the aorta	
Lo et al. 2015	40	Ascending aorta	No significant reduction in TBR was seen between HIV infected patients randomized to atorvastatin and HIV-infected patients treated with placebo	Technical difficulty hampered proper comparison of baseline scan and follow-up scan obtained after one year of treatment
Zanni et al. 2016	12	Ascending aorta	No significant change in TBR after six months of ART in treatment-naïve HIV-infected patients	3 of the study patients developed progression in coronary plaques as demonstrated on CCTA
Tawakol et al. 2017	45	Aorta	TBR was significantly higher in statin-naïve, HIV-infected patients on ART with undetectable viremia compared with matched (age, gender, and FRS) statin-naïve HIV-uninfected controls	
Knudsen et al. 2014	26	Carotid, arteries, different regions of the aorta	No difference in TBR in all arterial beds between HIV infected and non-infected individuals.	
Lawal et al. 2018	121	Ascending aorta	Higher aortic TBR in young individuals with HIV infections with otherwise low-risk for CVD compared with age and	

			gender-matched HIV-uninfected controls	
--	--	--	--	--

Potential targets for characterization of atherosclerosis in HIV-infected patients

Several alternative tracers to ^{18}F -FDG have been explored in preclinical studies and clinical studies (mostly in HIV-uninfected patients) to image arterial wall inflammation. While differences exist in the morphology and characteristics of plaques seen in PLWH and HIV-uninfected patients, inflammation is a common denominator in the atherosclerotic CVD seen in both groups. These tracers, therefore, hold potential for application in PLWH (Fig. 2).

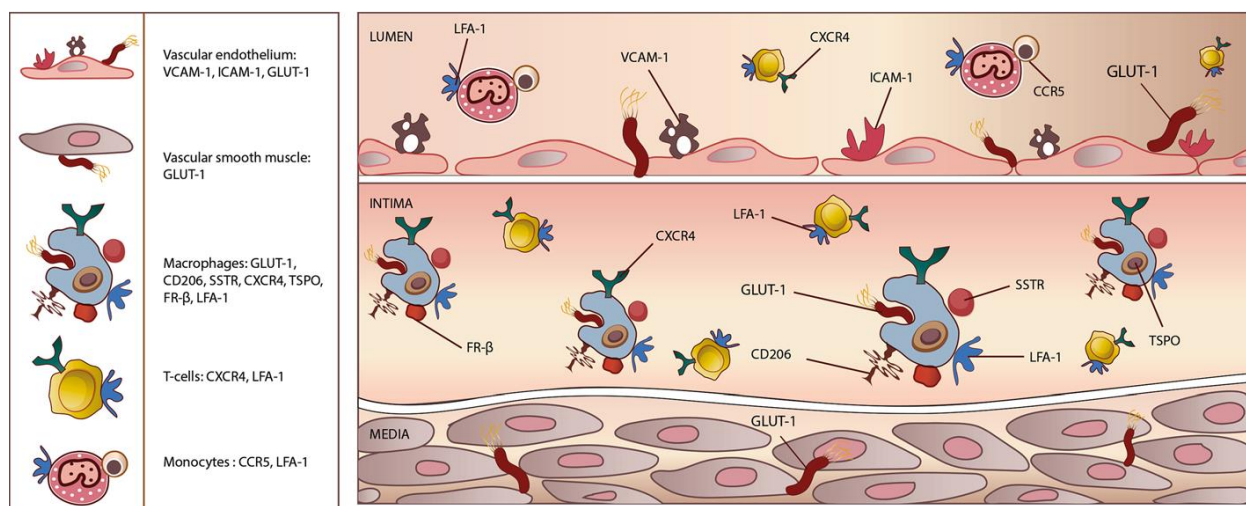


Fig 2 An illustration of the vessel wall and lumen showing current and potential targets on the vessel wall and inflammatory cells that can be explored for radionuclide imaging of vessel wall inflammation among people living with HIV infection

$^{99\text{m}}\text{Tc}$ -Tilmanocept SPECT/CT

$^{99\text{m}}\text{Tc}$ -Tilmanocept binds to the mannose receptor (CD206) expressed on macrophages.

Macrophages are the primary driver of arterial inflammation, thus are present in abundance in the vascular sub-endothelium. $^{99\text{m}}\text{Tc}$ -tilmanocept was approved for intradermal/subcutaneous/peritumoral injection in sentinel lymph node mapping in solid tumors. Zanni et al. recently demonstrated $^{99\text{m}}\text{Tc}$ -tilmanocept localization to CD206-expressing macrophages in an in vitro experiment (Zanni et al. 2017). Following subcutaneous tracer injection, they showed higher tracer uptake in the aortas of HIV-infected patients compared with

HIV-uninfected patients. Radiolabeled tilmanocept does not have significant binding to the myocardium or skeletal muscle. This lack of muscle uptake will address the problem of photon spillover seen with ^{18}F -FDG imaging. Tilmanocept has been successfully labeled with gallium-68 (^{68}Ga) and used in in-vivo studies done in non-human primates (Liss et al. 2014; Lee et al. 2017). Some ongoing clinical trials are evaluating the safety and feasibility of intravenous administration of radiolabeled tilmanocept for different clinical indications (NCT02865434, NCT03332940, NCT03157167). An intravenously administered ^{68}Ga -tilmanocept for PET imaging will provide better image resolution and makes quantification of arterial tracer uptake easier.

Somatostatin receptor-based imaging

Activated pro-inflammatory macrophage M1 express somatostatin type II receptors. Excellent binding of ^{68}Ga -DOTATATE, a synthetic radiolabeled somatostatin analog, has been extensively reported in neuroendocrine imaging. Tarkin et al. demonstrated a high correlation between vessel wall uptake of ^{68}Ga -DOTATATE and CVD risk factors (Tarkin et al. 2017). In the same study, ^{68}Ga -DOTATATE showed a higher TBR and a better discriminatory ability (between high-risk versus low-risk coronary atherosclerotic lesions) than ^{18}F -FDG. ^{68}Ga -DOTATATE does not demonstrate significant myocardial uptake, making it an excellent tracer for imaging of inflammation in coronary plaques. Using ^{68}Ga -DOTATOC, Lee et al. confirmed the correlation between arterial tracer uptake and patients' Framingham risk score (Lee et al. 2018).

^{68}Ga has a longer positron range compared with ^{18}F , hence PET imaging with ^{68}Ga suffers from a lower spatial resolution. Copper-64 (^{64}Cu) is a cyclotron-produced positron emitter with a physical half-life of 12.7 h and a shorter positron range compared with ^{68}Ga (1 mm versus 4 mm). Malmberg et al. performed a head-to-head comparison of ^{64}Cu -DOTATATE and ^{68}Ga -DOTATOC for imaging of large vessel atherosclerotic disease (Malmberg et al. 2015). Expectedly, ^{64}Cu -DOTATATE demonstrates a higher uptake in arterial walls. When imaging is done early, a higher pool blood tracer concentration will be seen with a ^{64}Cu -labeled peptide. The longer half-life of ^{64}Cu allows for delayed imaging up to 24 h post tracer injection. This delayed imaging will ensure an excellent background clearance giving a high target (arterial wall uptake) to background (blood pool) ratio.

Chemokine receptor-based imaging

Chemokines are a group of heparin-binding proteins that partake in plaque formation, progression, destabilization, and rupture.

C-X-C chemokine receptor 4 (CXCR4) is a transmembrane G protein-coupled chemokine receptor. The receptor mediates changes in gene expression that leads to actin polymerization, cytoskeletal rearrangement, and cell migration (Walenkamp et al. 2017). CXCR4 receptor and its natural ligand, C-X-C chemokine ligand 12 (CXCL12), play a vital role in cellular migration during embryogenesis, neo-angiogenesis, tumor cell multiplication, migration and invasion, immunity, and infection. CXCR4 is a co-receptor for the entry of HIV into CD⁺ T cells (Feng et al. 1996). CXCR4 and its alternative ligand, macrophage inhibitory factor (MIF), play an essential role in the recruitment of leucocytes into vessel wall following endothelial injury—a prelude to the process of atherogenesis. CXCR4 is also crucial for the continued leucocyte migration during atheromatous progression. High level of CXCR4 expression is seen in hematopoietic progenitor cells and inflammatory cells including T lymphocytes and monocyte/macrophages (Bleul et al. 1997; Gupta et al. 1999).

A few studies have evaluated the utility of pentixafor, a synthetic ligand for CXCR4, labeled to ⁶⁸Ga in the imaging of arterial inflammation in atherosclerosis. Hyafil and colleagues demonstrated ⁶⁸Ga-Pentixafor uptake in atherosclerotic lesions induced in rabbits which were confirmed to localized to macrophage-rich regions of the plaques (Hyafil et al. 2017). The intensity of uptake was reduced when the CXCR4 receptor was blocked by pre-treatment with AMD3100. In the same study, PET/MR was performed on eight patients (four with carotid stenosis greater than 50% and four with carotid stenosis less than 30%). No ⁶⁸Ga-pentixafor was seen in patients with stenosis less than 30% while two patients with stenosis more significant than 50% had intense tracer uptake in their carotid lesion. Uptake of pentixafor was confirmed on immunohistochemistry to correspond to the macrophage-rich region with only mild uptake in lymphocyte-rich areas.

In a larger human study of 38 patients, 611 foci of ⁶⁸Ga-Pentixafor⁶⁸Ga-pentixafor uptakes were seen in the vessels (Li et al. 2017). The intensity of uptake correlated positively with the presence of CVD risk factors (male gender, diabetes, hypertension, hypercholesterolemia). TBR obtained by two independent reviewers shows good reproducibility ($r = 0.6$, $p < 0.01$). The positive correlation of tracer uptake and the presence of CVD was

confirmed in another study of 51 patients with 1411 plaques where tracer uptake correlated with calcified plaque burden, age, hypertension, hypercholesterolemia, smoking history, and prior cardiovascular event (Weinberg et al. 2018).

Chemokine receptor 5 (CCR5) is another chemokine receptor expressed on a subgroup of monocytes facilitating their entry into plaques. ^{111}In -DOTA-DAPTA was recently synthesized and demonstrated in a mouse study to target CCR5 for plaque inflammation imaging (Wei et al. 2018). The lower resolution of the SPECT system may limit the clinical utility of this tracer. The same tracer labeled with ^{64}Cu has been successfully synthesized and holds a greater promise for this indication (Luehmann et al. 2014).

Arterial imaging based on lipid synthesis and utilization

Different classes of lipids play a vital role in atheroma formation and progression. Increased de novo synthesis and uptake of lipid is essential in monocyte maturation to macrophages and subsequent transformation to foam cells (Ecker et al. 2010). There is, therefore, accentuation of lipid biosynthesis by the tissues of the vascular wall and by the mononuclear inflammatory cells.

Acetate is the substrate for the formation of acetyl coenzyme A, the building block of fatty acids. There is increased uptake of acetate by inflammatory cells and vascular smooth muscle during atherogenesis. ^{11}C -acetate can be used as an imaging tool for the evaluation of the early process of fatty acid synthesis in the atheromatous vascular wall. (Derlin et al. 2011). In a study which evaluated the feasibility of ^{11}C -acetate as marker of fatty acid synthesis in atherosclerotic vessel wall, arterial tracer uptake was found to correlate with known CVD risk factors such as age and male gender (Derlin et al. 2011).

Choline is a raw material for the synthesis of phosphatidylcholine (Gao et al. 2018). Phosphatidylcholine is a type of phospholipid and one of the three main groups of lipids seen in the atheromatous vessel wall (Insull Jr and Bartsch 1966). Like acetate, there is increased uptake of choline by the inflammatory cells within the atheromatous plaque such that its level of uptake reflects vessel wall inflammation. Early work with ^{18}F -fluoromethylcholine (^{18}F -FMCH) suggests that increased fatty acid accumulation in the vessel wall occurs by a different mechanism than vessel wall calcification (Bucerius et al. 2008). In the study, none of the lesions with calcification-only show ^{18}F -FMCH uptake. Conversely, nine lesions with combined vessel wall calcification and other forms of vessel wall alterations such as vessel wall thickening

demonstrated ^{18}F -FMCH uptake (Bucerius et al. 2008). This results which have also been replicated in a more extensive study with ^{11}C -choline indicates that upregulation of fatty acid utilization by the arterial wall as a marker of vascular inflammation is a different process from arterial calcification in atheroma formation and progression (Kato et al. 2009). The myocardium does not show significant physiologic uptake of radio-labeled choline. The liver, however, does show high tracer uptake. The high liver uptake may lead to a spillover of photon into the right coronary artery and may represent a drawback in the evaluation of tracer uptake in this vascular territory.

Translocator protein-based imaging

The translocator protein (TSPO), previously known as peripheral benzodiazepine receptor, is an 18 kDa protein found in the outer mitochondrial membrane where it participates in cholesterol transport and biosynthesis of steroids. It is highly expressed in activated macrophages and microglial cells. Different carbon-11 and fluorine-18 labeled probes targeting TSPO have been successfully synthesized and used for arterial inflammation imaging (Hellberg et al. 2018; Lamare et al. 2011). TSPO is abundantly expressed in the myocardium as well as the vascular smooth muscles. This high muscular uptake may limit its utility in vascular inflammation imaging.

Folate receptor-based imaging

Folate receptor β is richly expressed on activated macrophages where it mediates internalization of folate-linked molecules (Xia et al. 2009). Several molecular probes (SPECT and PET) targeting the membrane-bound folate receptors have been developed and evaluated for their ability to image animal models of atherosclerotic vascular disease. The PET probes appear to have the highest potential for clinical translation due to the higher spatial resolution of the PET system compared with the SPECT. Silvola and colleagues recently reported the synthesis and the ability of aluminum fluoride-18 NOTA-folate (^{18}F -FOL) to target macrophage-bearing folate receptor in the arteries of mammals (Silvola et al. 2018). Successful binding of the tracer to macrophages bearing folate receptor was demonstrated in an in vitro study. They showed higher arterial uptake of ^{18}F -FOL in atherosclerotic mouse compared with healthy controls. In a PET imaging of rabbit following intravenous administration of ^{18}F -FOL and its comparison with ^{18}F -

FDG, both tracers demonstrate similar arterial uptake of both tracers. ^{18}F -FOL does not, however, have the intense myocardial uptake like ^{18}F -FDG (Silvola et al. 2018).

Leucocyte function-associated antigen-1-based imaging

Arterial wall invasion by leucocyte is an early process in atherogenesis. To invade the arterial wall, leucocytes express leucocyte function-associated antigen-1 (LFA-1), which interacts with intercellular cell adhesion molecule expressed on the vascular endothelial lining. Targeting LFA-1 for imaging holds promise for detecting an early phase of arterial inflammation before the development of a frank plaque lesion. Meester et al. recently reported the successful synthesis of ^{111}In -DOTA-butyl amino-NorBIRT (DANBIRT), a SPECT probe that targets LFA-1 (Meester et al. 2018). Using autoradiography, histological examination, and immunohistochemical staining, the authors showed that DANBIRT localizes to the plaque areas containing LFA-1-expressing inflammatory cells and activated macrophages (Meester et al. 2018).

Conclusion and future perspective

Inflammation plays a vital role in all phases of atherosclerotic CVD. PLWH have heightened predisposition to CVD. The most evidence regarding the radionuclide imaging inflammation in the pathogenesis of CVD among PLWH has been with ^{18}F -FDG PET/CT. While ^{18}F -FDG PET/CT has several merits, it has several limitations regarding its use of vascular imaging. Several imaging probes have been synthesized and used for vascular inflammation imaging in preclinical and clinical studies. These non- ^{18}F -FDG probes hold promise for future use among PLWH.

Acknowledgments

None.

Funding

IOL is a PhD student at the time of writing this review. He receives a monthly stipend from the Nuclear Medicine

Research Infrastructure (NuMeRI) hosted at the Department of Nuclear Medicine, University of Pretoria.

No external funding was received in the conduct of this work.

Availability of data and materials

Data sharing is not applicable to this article as no datasets were generated or analyzed during the current study.

Authors' contributions

Initial drafting of the manuscript: IOL, AOA. Critical revision of manuscript: ACS, MMS. All authors read and approved the final manuscript.

Competing interests

The authors declare that they have no competing interests.

References

Abdelbaky A, Corsini E, Figueroa AL, Fontanez S, Subramanian S, Ferencik M et al (2013) Focal arterial inflammation precedes subsequent calcification in the same location: a longitudinal FDG-PET/CT study. *Circ Cardiovasc Imaging* 6:747–754

Aukrust P, Bjornsen S, Lunden B (2000) Persistently elevated levels of von Willebrand factor antigen in HIV infection. Downregulation during highly active antiretroviral therapy. *J Thromb Haemost* 84:183–187

Bernasconi E, Uhr M, Magenta L, Ranno A, Telenti A (2001) Homocysteinemia in HIV-infected patients treated with highly active antiretroviral therapy. *AIDS*. 15:1081–1082

Bleul CC, Wu L, Hoxie JA, Springer TA, Mackay CR (1997) The HIV coreceptors CXCR4 and CCR5 are differentially expressed and regulated on T lymphocytes. *Proc Natl Acad Sci U S A* 94:1925–1930

Bucerius J, Dijkgraaf I, Mottaghy FM, Schurgers LJ (2018) Target identification for the diagnosis and intervention of vulnerable atherosclerotic plaques beyond ^{18}F -fluorodeoxyglucose positron emission tomography imaging: promising tracers on the horizon. *Eur J Nucl Med Mol Imaging*. Epub ahead of print on 09 October

Bucerius J, Hyafil F, Verberne HJ, Slart RHJA, Linder O, Sciagra R et al (2016) Position paper of the Cardiovascular Committee of the European Association of nuclear medicine (EANM) on PET imaging of atherosclerosis. *Eur J Nucl Med Mol Imaging* 43:780–792

Bucerius J, Mani V, Moncrieff C, Machac J, Fuster V, Farkouh ME et al (2014) Optimizing ^{18}F -FDG PET/CT imaging of vessel wall inflammation: the impact of ^{18}F -FDG circulation time, injected dose, uptake parameters, and fasting blood glucose levels. *Eur J Nucl Med Mol Imaging* 41:369–383

Bucerius J, Schmaljohann J, Böhm I, Palmedo H, Gohlke S, Tiemann K et al (2008) Feasibility of ^{18}F fluoromethylcholine PET/CT for imaging of vessel wall alterations in humans—first results. *Eur J Nucl Med Mol Imaging* 35:815–820

Carr A, Samaras K, Burton S, Law M, Freund J, Chisholm DJ et al (1998a) A syndrome of peripheral lipodystrophy, hyperlipidaemia and insulin resistance in patients receiving HIV protease inhibitors. *AIDS*. 12:F51–F58

Carr A, Samaras K, Chisholm DJ, Cooper DA (1998b) Pathogenesis of HIV-1-protease inhibitor-associated peripheral lipodystrophy, hyperlipidaemia, and insulin resistance. *Lancet*. 351:1881–1883

Chow FC, Regan S, Zanni MV, Looby SE, Bushnell CD, Meigs JB et al (2018) Elevated ischemic stroke risk among women living with HIV infection. *AIDS*. 32:59–67

Cybulsky MI, Gimbrone MA Jr (1991) Endothelial expression of a mononuclear leukocyte adhesion molecule during atherogenesis. *Science*. 251:788–791

Cybulsky MI, Iiyama K, Li H, Zhu S, Chen M, Iiyama M et al (2001) A major role for VCAM-1, but not ICAM-1, in early atherosclerosis. *J Clin Invest* 107:1255–1262

D:A:D Study Group (2003) Combination Antiretroviral Therapy and the Risk of Myocardial Infarction. *N Engl J Med* 349:1993–2003

D:A:D Study Group (2008) Use of nucleoside reverse transcriptase inhibitors and risk of myocardial infarction in HIV-infected patients enrolled in the D:A:D study: a multi-cohort collaboration. *Lancet* 371:1417–1426

Derlin T, Habermann CR, Lengyel Z, Busch JD, Wisotzki C, Mester J et al (2011) Feasibility of ¹¹C-acetate PET/CT for imaging of fatty acid synthesis in the atherosclerotic vessel wall. *J Nucl Med* 52:1848–1854

Duprez DA, Neuhaus J, Kuller LH, Tracy R, Belloso W, De Wit S et al (2012) Inflammation, coagulation and cardiovascular disease in HIV-infected individuals. *PLoS One* 7:e44454. <https://doi.org/10.1371/journal.pone.0044454>

Durand M, Sheehy O, Bril JG, Leloir J, Tremblay C (2011) Association between HIV infection, antiretroviral therapy, and risk of acute myocardial infarction: a cohort and nested case-control study using Quebec's public health insurance database. *JAIDS*. 57:245–253

Ecker J, Liebisch G, Englmaier M, Grandl M, Robenek H, Schmitz G (2010) Induction of fatty acid synthesis is a key requirement for phagocytic differentiation of human monocyte. *Proc Natl Acad Sci U S A* 107:7812–7822

Fan J, Watanabe T (2013) Inflammatory reactions in the pathogenesis of atherosclerosis. *J Atheroscler Thromb* 10:63–71

Feng Y, Broder CC, Kennedy PE, Berger EA (1996) HIV-1 entry cofactor: functional cDNA cloning of a seven-transmembrane, G protein-coupled receptor. *Science*. 272:872–877

Figueroa AL, Abdelbaky A, Truong QA, Corsini E, MacNabb MH, Lavender ZR et al (2013) Measurement of arterial activity on routine FDG PET/CT images improves prediction of risk of future CV event. *JACC Cardiovasc Imaging* 6:1250–1259

Flinn WR, McDananiel MD, Yao JS (1984) Antithrombin III deficiency as a reflection of dynamic protein metabolism in patients undergoing vascular reconstruction. *J Vasc Surg* 1:888–895

Freiberg MS, Chang CH, Kuller LH, Skanderson M, Lowy E, Kraemer KL et al (2013) HIV infection and the risk of acute myocardial infarction. *JAMA Intern Med* 173:614–622

Gao X, Qian P, Cen D, Hong W, Peng Q, Xue M (2018) Synthesis of phosphatidylcholine in rats with oleic acid-induced pulmonary edema and effects of exogenous pulmonary surfactant on its de novo synthesis. *PLoS One* 13:e0193719

Glass TR, Ungsedhapand C, Wolbers M, Weber R, Vernazza PL, Rickenbach M et al (2006) Prevalence of risk factors for cardiovascular disease in HIV-infected patients over time: the Swiss HIV cohort study. *HIV Med.* 7:404–410

Graebe M, Pedersen SF, Borgwardt L, Højgaard L, Sillesen H, Kjaer A (2009) Molecular pathology in vulnerable carotid plaques: correlation with [18]-fluorodeoxyglucose positron emission tomography (FDG-PET). *Eur J Vasc Endovasc Surg* 37:714–721

Gupta SK, Pillarisetti K, Lysko PG (1999) Modulation of CXCR4 expression and SDF-1alpha functional activity during differentiation of human monocytes and macrophages. *J Leukoc Biol* 66:135–143

Hellberg S, Liljenbäck H, Eskola O, Morisson-Iveson V, Morrison M, Trigg W et al (2018) Positron emission tomography imaging of macrophages in atherosclerosis with ¹⁸F-GE-180, a radiotracer for translocator protein (TSPO). *Contrast Media Mol Imaging*. <https://doi.org/10.1155/2018/9186902>

Hsue PY, Ribaud HJ, Deeks SG, Bell T, Ridker PM, Fichtebaum C et al (2018) Safety and impact of low-dose methotrexate on endothelial function and inflammation in individuals with treated human immunodeficiency virus: AIDS clinical trial group study A5314. *Clin Infect Dis*. Epub ahead of print on 14 September

Hui DY (2003) Effects of HIV protease inhibitor therapy on lipid metabolism. *Prog Lipid Res* 42:81–92

Hyafil F, Pelisek J, Laitinen I, Schottelius M, Mohring M, Döring Y et al (2017) Imaging the cytokine receptor CXCR4 in atherosclerotic plaques with the radiotracer ^{68}Ga -Pentixafor for PET. *J Nucl Med* 58:499–506

Hyle EP, Mayosi BM, Middlekoop K, Mosepele M, Martey EB, Walensky RP et al (2017) The association between HIV and atherosclerotic cardiovascular disease in sub-Saharan Africa. A systematic review. *BMC Public Health* 17:954

Insull W Jr, Bartsch GE (1966) Cholesterol, triglyceride, and phospholipid content of intima, media, and atherosclerotic fatty streak in human thoracic aorta. *J Clin Invest* 45:513–523

Kato K, Schober O, Ikeda M, Schäfers M, Ishigaki T, Kies P et al (2009) Evaluation and comparison of ^{11}C -choline and calcification in aortic and common carotid arterial walls with combined PET/CT. *Eur J Nucl Med Mol Imaging* 36:1622–1628

Knudsen A, Hag AMF, Loft A, von Benzon E, Keller SH, Møller HJ et al (2015) HIV infection and arterial inflammation assessed by ^{18}F -fluorodeoxyglucose (FDG) positron emission tomography (PET): a prospective cross-sectional study. *J Nucl Cardiol* 22:372–380

Kuller LH, Tracy R, Bellosso W, De Wit S, Drummond F, Lane HC et al (2008) Inflammatory and coagulation biomarkers and mortality in patients with HIV infection. *PLoS Med* 5:e203. <https://doi.org/10.1371/journal.pmed.0050203>

Lamare F, Hinz R, Gaemperli O, Pugliese F, Mason JC, Camici PG et al (2011) Detection and quantification of large-vessel inflammation with ^{11}C -(R)-PK11195 PET/CT. *J Nucl Med* 52:33–39

Lawal I, Sathekge M (2016) F-18 FDG PET/CT imaging of cardiac and vascular inflammation and infection. *Br Med Bull* 120:55–74

Lawal IO, Ankrah AO, Popoola GO, Lengana T, Sathekge MM (2018) Arterial inflammation in young patients with human immunodeficiency virus infection: a cross-sectional study using F-18 FDG PET/CT. *J Nucl Cardiol*. Epub ahead of print on 07 February. <https://doi.org/10.1007/s12350-018-1207-x>

Lee HJ, Barback CV, Hoh CK, Qin Z, Kader K, Hall DJ et al (2017) Fluorescence-based molecular imaging of porcine urinary bladder sentinel lymph nodes. *J Nucl Med* 58:547–553

Lee R, Kim J, Paeng JC, Byun JW, Cheon GJ, Lee DS et al (2018) Measurement of ^{68}Ga -DOTATOC uptake in the thoracic aorta and its correlation with cardiovascular risk. *Nucl Med Mol Imaging* 52:279–286

Li X, Heber D, Leike T, Beitzke D, Lu X, Zhang X et al (2017) [⁶⁸Ga]Pentixafor-PET/MRI for the detection of chemokine receptor 4 expression in atherosclerotic plaques. *Eur J Nucl Med Mol Imaging*. Epub ahead of print on September 21. <https://doi.org/10.1007/s00259-017-3831-0>

Libby P (2006) Inflammation and cardiovascular disease mechanisms. *Am J Clin Nutr* 83(suppl):456S–460S

Lijfering WM, Ten Kate MK, Sprenger HG, Van der Meer J (2006) Absolute risk of venous and arterial thrombosis in HIV-infected patients and effects of combination anti-retroviral therapy. *J Thromb Haemost* 4:1928–1930

Liss MA, Stroup SP, Cand ZQ, Hoh C, Hall DJ, Vera DR et al (2014) Robotic-assisted fluorescence sentinel lymph node mapping using multi-nodal image-guidance in an animal model. *Urology*. 84:982

Lo J, Lu MT, Ihenachor EJ, Wei J, Looby SE, Fitch KV et al (2015) Effects of statin therapy on coronary artery plaque volume and high risk plaque morphology in HIV-infected patients with subclinical atherosclerosis: a randomized double-blind placebo-controlled trial. *Lancet HIV* 2:e52–e63

Luehmann HP, Pressly ED, Detering L, Wang C, Pierce R, Woodard PK et al (2014) PET/CT imaging of chemokine receptor CCR5 in vascular injury model using targeted nanoparticles. *J Nucl Med* 55:629–634

Majluf-Cruz A, Silva-Estrada M, Sánchez-Barboza R, Montiel-Manzano G, Treviño-Pérez S, Santoscoy-Gómez M et al (2004) Venous thrombosis among patients with AIDS. *Clin Appl Thromb Hemost* 10:19–25

Malmberg C, Ripa RS, Johnbeck CB, Knigge U, Langer SW, Mortensen J et al (2015) ⁶⁴Cu-DOTATATE for noninvasive assessment of atherosclerosis in large arteries and its correlation with risk factors: head-to-head comparison with ⁶⁸Ga-DOTATOC in 60 patients. *J Nucl Med* 56:1895–1900

Mary-Krause M, Cotte L, Simon A, Partisani M (2003) Costagliola D, and the clinical epidemiology group from the French hospital database. *AIDS*. 17:2479–2486

Mavroudis CA, Majumder B, Loizides S, Christophides T, Johnson M, Rakhit RD (2013) Coronary artery disease and HIV; getting to the HAART of the matter. *Int J Cardiol* 167:1143–1153

McMurray HF, Parthasarathy S, Steinberg D (1993) Oxidatively modified low density lipoprotein is a chemoattractant for human T lymphocytes. *J Clin Invest* 92:1004–1008

Meester EJ, Krenning BJ, de Blois RH, Norenberg JP, de Jong M, Bernsen MR et al (2018) Imaging of atherosclerosis, targeting LFA-1 on inflammatory cells with ¹¹¹In-DANBIRT. *J Nucl Cardiol*. Epub ahead of print on 13 March

Morlat P, Roussillon C, Henard S, Salmon D, Bonnet F, Cacoub P et al (2014) Causes of death among HIV-infected patients in France in 2010 (national survey): trends since 2000. *AIDS*. 28:1181–1191

Mosepele M, Molefe-Baikai-Molefe OJ, Grinspoon SK, Triant VA (2018) Benefits and risks of statin therapy in HIV-infected population. *Curr Infect Dis Rep* 20:20

Musselwhite LW, Sheikh V, Norton TD, Rupert A, Porter BO, Penzak SR et al (2011) Markers of endothelial dysfunction, coagulation and tissue fibrosis independently predict venous thromboembolism in HIV. *AIDS*. 25:787–795

Obel N, Farkas DK, Kronborg G, Larsen CS, Pedersen G, Riis A et al (2010) Abacavir and risk of myocardial infarction in HIV-infected patients on highly active antiretroviral therapy: a population-based nationwide cohort study. *HIV Med* 11:130–136

Ridker PM, Everett BM, Thuren T, MacFadyen JG, Chang WH, Ballantyne C et al (2017) Antiinflammatory therapy with Canakinumab for atherosclerotic disease. *N Engl J Med* 377:1119–1131

Rominger A, Saam T, Wolpers S, Cyran CC, Schmidt M, Foerster S et al (2009) ¹⁸F-FDG PET/CT identifies patients at risk for future vascular events in an otherwise asymptomatic cohort with neoplastic disease. *J Nucl Med* 50:1611–1620

Rudd JHF, Myers KS, Bansilal S, Machac J, Pinto CA, Tong C et al (2008) Atherosclerosis inflammation imaging with ¹⁸F-FDG PET: carotid, iliac, and femoral uptake reproducibility, quantification methods, and recommendations. *J Nucl Med* 49:871–878

Rudd JHF, Warburton EA, Fryer TD, Jones HA, Clark JC, Antoun N et al (2002) Imaging atherosclerotic plaque inflammation with [¹⁸F]-Fluorodeoxyglucose positron emission tomography. *Circulation*. 105:2708–2711

Sene D, Piette JC, Cacoub P (2008) Antiphospholipid antibodies, antiphospholipid syndrome and infections. *Autoimmune Rev* 7:272–277

Shah ASV, Stelzle D, Lee KK, Beck EJ, Alam S, Clifford S et al (2018) Global burden of atherosclerotic cardiovascular disease in people living with the human immunodeficiency virus: a systematic review and meta-analysis. *Circulation*. 138:1100–1112

Silvola JMU, Li XG, Virta J, Marjamäki P, Liljenbäck H, Hytönen JP et al (2018) Aluminium fluoride-18 labeled folate enables in vivo detection of atherosclerotic plaque inflammation by positron emission tomography. *Sci Rep* 8:9720

Subramanian S, Tawakol A, Burdo TH, Abbara S, Wei J, Vijayakumar J et al (2012) Arterial inflammation in patients with HIV. *JAMA*. 308:379–386

Tarkin JM, Joshi FR, Evans NR, Chowdhury MM, Figg NL, Shah AV et al (2017) Detection of atherosclerotic inflammation by ⁶⁸Ga-DOTATATE PET compared to [¹⁸F]FDG PET imaging. *J Am Coll Cardiol* 69:1774–1791

Tawakol A, Ishai A, Li D, Pakx RAP, Hur S, Kaiser Y et al (2017) Association of Arterial and Lymph Node Inflammation with distinct inflammatory pathways in human immunodeficiency virus infection. *JAMA Cardiol* 2:163–171

Tawakol A, Migrino RQ, Bashian GG, Bedri S, Vermylen D, Cury RC et al (2006) In vivo ¹⁸F-Fluorodeoxyglucose positron emission tomography imaging provides a noninvasive measure of carotid plaque inflammation in patients. *J Am Coll Cardiol* 48:1818–1824

UNAIDS (2018) Global HIV & AIDS statistics. Fact sheet. Available on <https://www.unaids.org/resources/fact-sheet>. Accessed 27 Oct 2018

Vigne J, Thackeray J, Essers J, Makowski M, Varasteh Z, Curaj A et al (2018) Current and emerging preclinical approaches for imaging-based characterization of atherosclerosis. *Mol Imaging Biol*. Epub ahead of print on 24 September

Walenkamp AME, Lapa C, Herrmann K, Wester HJ (2017) CXCR4 ligands: the next big hit? *J Nucl Med* 58:77S–82S

Wei L, Pertryk J, Gaudet C, Kamkar M, Gan W, Duan Y et al (2018) Development of an inflammation imaging tracer, ¹¹¹In-DOTA-DAPTA, targeting chemokine receptor CCR5 and preliminary evaluation in an ApoE^{-/-} atherosclerosis mouse model. *J Nucl Cardiol*. Epub ahead of print on 07 February

Weinberg D, Thackeray JT, Daum G, Sohns JM, Kropf S, Wester HJ et al (2018) Clinical molecular imaging of chemokine receptor CXCR4 expression in atherosclerotic plaque using

⁶⁸Ga-Pentixafor PET: correlation with cardiovascular risk factors and calcified plaque burden. *J Nucl Med* 59:266–272

Xia W, Hilgenbrink AR, Matteson EL, Lockwood MB, Cheng JX, Low PS (2009) A functional folate receptor is induced during macrophage activation and can be used to target drugs to activated macrophages. *Blood*. 113:438–446

Yamashita T, Kawashima S, Ozaki M, Namiki M, Inoue N, Hirata K et al (2002) Propagermanium reduces atherosclerosis in apolipoprotein E knockout mice via inhibition of macrophage infiltration. *Artrioscler Thromb Vasc Biol* 22:969–974

Yarasheski KE, Laciny E, Overton ET, Reeds DN, Harrod M, Baldwin S et al (2012) ¹⁸FDG PET-CT imaging detects arterial inflammation and early atherosclerosis in HIV-infected adults with cardiovascular disease risk factors. *J Inflamm* 9:22. <https://doi.org/10.1186/1476-9255-9-26>

Zanni MV, Toribio M, Robbins GK, Burdo TH, Lu MT, Ishai AE et al (2016) Effects of antiretroviral therapy on immune function and arterial inflammation in treatment-naïve patients with human immunodeficiency virus infection. *JAMA Cardiol* 1:474–480

Zanni MV, Toribio M, Wilks MQ, Lu MT, Burdo TH, Walker J et al (2017) Application of a novel CD206+ macrophage-specific arterial imaging strategy in HIV-infected individuals. *J Infect Dis* 215:1264–1269

Chapter 3

Molecular imaging of cardiovascular inflammation and infection in people living with HIV infection

Ismaheel O. Lawal^{1,2}, Anton C. Stoltz³, Mike M Sathekge^{1,2}

1. Department of Nuclear Medicine, University of Pretoria, Pretoria 0001, South Africa.
2. Nuclear Medicine Research Infrastructure (NuMeRI), Steve Biko Academic Hospital, Pretoria 0001, South Africa.
3. Infectious Disease Unit, Department of Internal Medicine, University of Pretoria & Steve Biko Academic Hospital, Pretoria 0001, South Africa.

Clin Transl Imaging. 2020;8(3):141-155

Abstract

Widespread use of effective antiretroviral therapy (ART) in people living with human immunodeficiency virus (PLHIV) infection has changed the prognosis of the disease from a fatal and debilitating one to a chronic manageable illness. ART leads to immune restoration, but immune functional levels seen in HIV-uninfected people are never achieved. The dynamics of immune suppression, chronic immune activation, and immune senescence predispose PLHIV to certain inflammatory and infectious conditions of the cardiovascular system. Atherosclerotic cardiovascular disease is a chronic inflammatory condition that is a rising cause of mortality and morbidity among PLHIV. Certain risk factors prevalent among PLHIV, such as intravenous drug abuse, use of ART, and susceptibility, to tuberculous disease even at near-normal immune functional levels predispose them to inflammation and infections of the different components of the heart including the pericardium, epicardium, and endocardium. Molecular imaging using radionuclide techniques has been shown to have excellent clinical utility in the evaluation of inflammation and infection. The strengths of molecular imaging techniques lie in their sensitivity for early disease detection before morphological changes occur and in therapy response assessment before significant reparative changes have occurred. Molecular imaging techniques are now becoming more widespread in clinical application with increasing availability and utilization in developing countries where the most significant burden of HIV infection is felt. This review aimed to present an update on the evidence supporting the role of molecular imaging modalities with radionuclide techniques for imaging of cardiovascular inflammation and infection focusing on atherosclerotic cardiovascular disease, pericarditis, myocarditis, and endocarditis in PLHIV.

Keywords

Atherosclerosis · Tuberculous pericarditis · Vascular inflammation · ^{18}F -FDG PET/CT · HIV infection · Infective endocarditis

Introduction

Infection by the human immunodeficiency virus (HIV) remains a significant cause of mortality and morbidity globally [1]. Infection by HIV causes rapid depletion of the host immune system as the virus targets immune cells expressing the CD 4 molecule [2]. Early depletion of the gut-associated lymphoid tissue leads to systemic translocation of gut microbes causing chronic immune activation [3]. Anti-retroviral therapy (ART) is very effective in inhibiting viral replication. The effectiveness of ART is manifested in the life expectancy of PLHIV which is now approaching that of the HIV-uninfected people [4, 5]. Despite the improvement in the immune system with ART, people living with HIV (PLHIV) never achieve complete immune recovery even with complete viral suppression [6]. The cytotoxic function of CD8+ T lymphocytes, for example (a subset of lymphocytes not directly affected by HIV), never returns to normal even with complete viral suppression [7]. PLHIV, therefore, are at increased risk of acquiring infections seen in HIV-uninfected people as well as opportunistic infections that result from relative immunosuppression. PLHIV successfully treated with ART and achieved suppressed viremia have circulating cytokines that reflect persistent immune activation and dysfunction [8]. Chronic immune activation in PLHIV has been implicated as a predisposing factor to a group of non-infectious disorders which are emerging as significant causes of mortality and morbidity. These chronic metabolic non-infectious conditions include atherosclerotic cardiovascular diseases (ASCVD); accelerated aging; liver disease, bone, and metabolic disorders; non-AIDS defining cancers and neurocognitive dysfunction [9, 10]. PLHIV are, therefore, at increased risk of infection due to immune dysfunction and non-infectious inflammatory conditions such as ASCVD due to chronic immune activation. In this review, we aimed to present an update on the evidence supporting the use of molecular imaging techniques in the evaluation of cardiovascular inflammation and infection. We will focus on ASCVD, pericarditis, myocarditis, and endocarditis. ¹⁸F-Fluorodeoxy-d-glucose positron emission tomography with computed tomography (¹⁸F-FDG PET/CT) has been the most reported molecular imaging technique in the evaluation of cardiovascular inflammation and infection. It will form the main thrust of this review.

Atherosclerotic cardiovascular disease

Inflammation is critical to the formation and progression of ASCVD [11]. The earliest event in atheroma formation is vascular intima injury caused by factors including smoking, hypertension, and hyperglycemia. Vascular intima injury causes the accumulation of atherogenic plasma-derived cholesterol-rich lipids in the vascular intima as well as upregulation of cell adhesion molecules such as vascular cell adhesion molecule-1 (VCAM-1), and intercellular cell adhesion molecule-1 (ICAM-1), which favor recruitment of monocytes and T lymphocytes into the vessel wall [12–14]. Atherogenic lipid molecules are oxidized within the vascular to form oxidized pro-inflammatory lipids [12]. Monocytes mature to become macrophages in the vessel intima. Macrophages engulf the atherogenic oxidized lipids to become foam cells. Vascular smooth muscles also accumulate the atherogenic lipids, become activated, and secrete chemoattractants and chemokines that further attract circulating immune cells to the site of atheroma formation [12]. The matured atheromatous plaque typically contains lipid-rich necrotic core covered by a fibrous cap made up of a mixture of smooth muscle cells and supporting extracellular matrix. The base of the lesion often contains foam cells and T lymphocytes. Inflammation also plays a crucial role in plaque rupture, the catastrophic complication of atherosclerosis. Macrophages produce matrix metalloproteinases that can digest the fibrous cap leading plaque rupture. T cells produce interferon which inhibits the smooth muscle proliferation causing weakening of the fibrous cap [15]. HIV infection has been identified as an additional risk factor for ASCVD. PLHIV is twice at risk of ASCVD compared with HIV-uninfected individuals. The global burden of ASCVD among PLHIV has tripled in the last two decades [16]. The mechanisms by which HIV infection increases the risk of ASCVD include direct viral invasion of the vessel wall causing arterial inflammation; chronic immune activation due to HIV infection; ART-induced metabolic disturbances such as lipid dysregulation, insulin resistance, and diabetes mellitus; and the preponderance of the traditional cardiovascular risk factors among PLHIV [17–20].

In HIV infection, there is persistent viral replication even in individuals with completely suppressed viremia. This persistent viral replication not only leads to a progressive decline in the CD4+ T-cell population but also causes immune activation and chronic systemic inflammation. Uncontrolled viral replication seen in ART-naïve patients is associated with vascular endothelial dysfunction, the precursor of ASCVD [21]. Effective ART with suppressed viremia reduces but

does not eliminate immune activation or the elevated risk of acquiring ASCVD [17, 22]. Pro-atherogenic soluble factors in PLHIV encourage foam cell formation by monocyte through the reduction of cholesterol efflux from them [23]. ART, especially with protease inhibitor, is associated with proatherogenic lipid metabolism dysregulation [24].

Inflammation is crucial to the formation, progression, and rupture of the atherosclerotic plaque. Activated inflammatory cells accentuate their glucose use to cope with the high energy demand of the inflammatory process. ^{18}F -FDG, an analog of glucose, can, therefore, be used for PET/CT imaging of arterial inflammation in ASCVD. In the arterial wall, the intensity of ^{18}F -FDG uptake correlates with the level of macrophage invasion [25, 26]. The intensity of ^{18}F -FDG uptake is higher in symptomatic plaque compared with asymptomatic plaque and uptake in asymptomatic patients predicts the future risk of vascular events [27–29]. The utility ^{18}F -FDG PET/CT for imaging subclinical ASCVD in PLHIV has been shown in different studies [30]. Arterial ^{18}F -FDG accumulation is significantly higher in chronic HIV-infected individuals than age, gender, and Framingham risk score-matched controls but comparable to the level of uptake seen in the arteries of older patients with established atherosclerotic disease [31]. This finding suggests that the level of arterial inflammation in PLHIV is as high as the level in older patients with established ASCVD [31].

ART improves life expectancy in PLHIV but does not eliminate the risk of ASCVD. In a cohort of HIV-infected individuals who obtained ^{18}F -FDG PET/CT before commencing ART, effective ART did not lead to a significant reduction in arterial ^{18}F -FDG uptake after 6 months of treatment [32]. Persistent elevated arterial ^{18}F -FDG uptake suggests residual inflammation despite effective ART. Statin therapy targeting arterial inflammation is protective against ASCVD regardless of its lipid-lowering effect. In the SATURN-HIV trial, statin therapy with rosvastatin led to a significant reduction in soluble markers of monocyte activation (sCD14 and sCD163) without significant change in circulating monocyte level demonstrating the additional benefit of statin therapy in PLHIV on regular ART [33]. Quantification of arterial ^{18}F -FDG uptake before and after therapy provides a direct means of determining the effectiveness of therapeutic agents targeting inflammation in ASCVD risk reduction strategy [34]. A study comparing arterial ^{18}F -FDG uptake as a surrogate marker of inflammation between HIV-infected and HIV-uninfected patients found no significant difference in arterial ^{18}F -FDG uptake between the two groups [35]. In a sub-group analysis, however, there was significantly higher arterial

wall ^{18}F -FDG uptake in statin-naïve HIV-infected patients compared with statin-naïve HIV-uninfected controls. These results demonstrate the residual arterial inflammation in HIV-infected people despite regular ART use.

Many other agents beyond statins have been explored for their anti-inflammatory property in ASCVD risk reduction strategy [17]. The CANTOS trial recently reported a reduction in inflammation associated with a dose-dependent reduction in recurrent major cardiovascular events in HIV-uninfected individuals treated with canakinumab, a monoclonal antibody targeting interleukin-1 β (IL-1 β) [36]. Hsue and colleagues have reported the utility of ^{18}F -FDG PET/CT in evaluating the anti-inflammatory effect of canakinumab in HIV-infected individuals with suppressed viremia on ART and treated with a single dose of canakinumab. At 8 weeks post-treatment, there was a significant reduction in arterial ^{18}F -FDG uptake [37]. ^{18}F -FDG has, therefore, emerged as a useful non-invasive biomarker for direct monitoring of arterial inflammation in the development and evaluation of drugs targeting inflammatory pathways in ASCVD.

ASCVD has a very long preclinical phase with atherogenesis starting long before clinical manifestation [38]. Our group recently demonstrated higher arterial ^{18}F -FDG uptake in young PLHIV who otherwise had no or low-risk factors for ASCVD compared with age- and gender-matched controls [39]. Our results showed that HIV and its treatment are independent risk factors for ASCVD and that the disease process starts quite early in life among PLHIV. Demonstration of arterial inflammation at a very young age among PLHIV support the results from earlier studies reporting younger age at clinical presentation of ASCVD among PLHIV compared with the general population of HIV-uninfected people [40].

A few studies have reported non-significant differences in arterial ^{18}F -FDG uptake between PLHIV and HIV-uninfected individuals [32, 41–43]. These negative reports may be a result of non-standardized imaging protocol [41], the technical challenge militating against accurate lesion comparison in test–retest study design [42], or small patient population [32, 43]. A significant challenge with ^{18}F -FDG PET/CT imaging of vascular inflammation lies in its inherent limited spatial resolution causing a significant underestimation of quantified vascular ^{18}F -FDG. The average thickness of the arterial wall is less than twice the spatial resolution of most PET/CT cameras in current clinical use which causes significant underestimation due to partial volume effect [44, 45]. There is an additional need to subtract signals contributed by

blood-pool activity from within the vascular lumen. To achieve the latter, target-to-background ratio (TBR) computed by obtaining the mean of multiple SUVmax measurements in the arterial wall of interest and dividing it by the SUV obtained from the lumen of an adjacent vein. TBR has a good correlation with actual arterial ^{18}F -FDG uptake as shown in a kinetic modelling study [46]. There is also a good correlation between TBR taken from different vascular territory in an individual as well as good intra- and inter-observer agreements [47]. To improve the performance of ^{18}F -FDG PET/CT for imaging of vascular inflammation in ASCD/D, the Cardiovascular Committee of the European Association of Nuclear Medicine (EANM) recently published a set of guidelines on patient preparation, image acquisition, and reporting of ^{18}F -FDG PET/CT [48]. When observed, these set of criteria improves quantified arterial ^{18}F -FDG uptake measured by SUVmax and TBR [49]. Figure 1 shows the impact of observing the recommendations by the cardiovascular committee of EANM on arterial ^{18}F -FDG uptake and background blood-pool activity clearance.

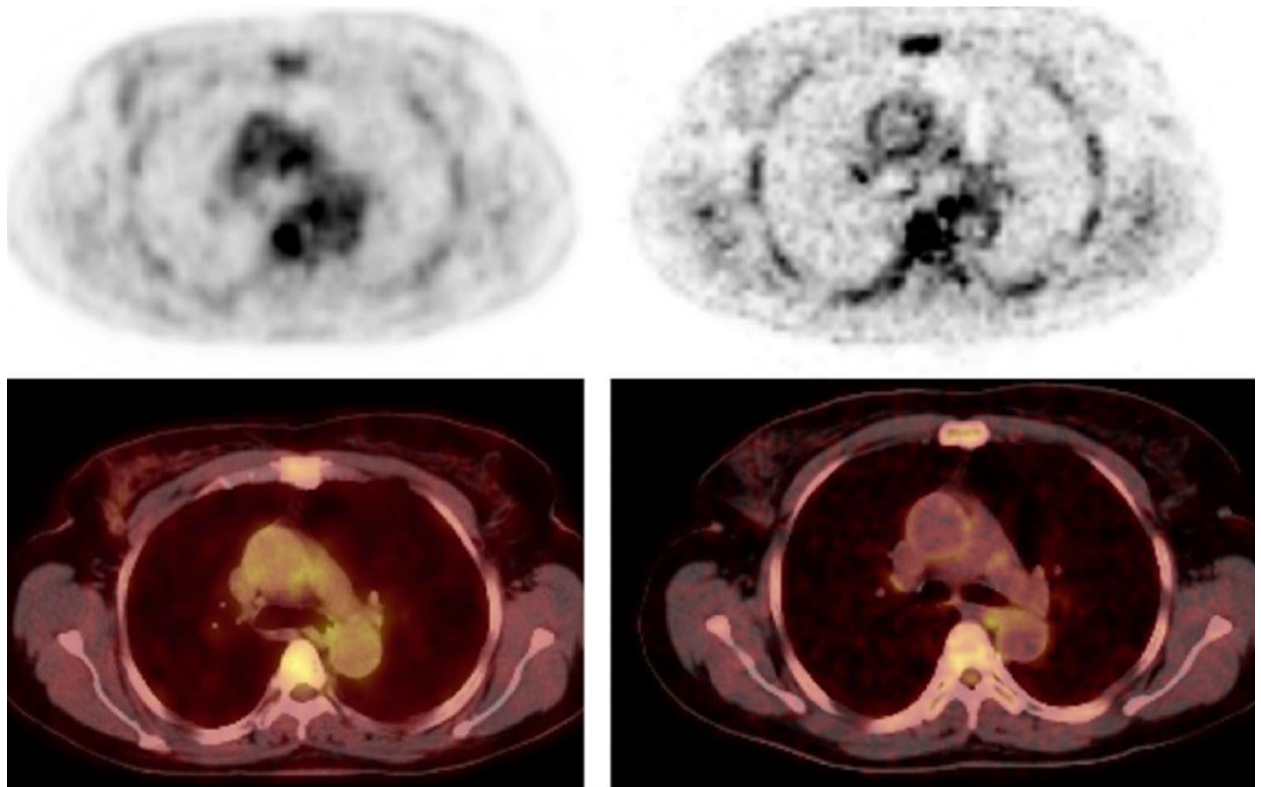


Fig 1 A 54-year-old female had dual-time points ^{18}F -FDG PET/CT imaging. Early imaging acquired at 60 min post-tracer injection using the routine oncologic PET parameters shows high blood-pool background activity (right images). Delayed imaging acquired at 124 min post-tracer injecting using PET parameters dedicated for vascular inflammation imaging showed good background activity clearance with improvement in arterial wall ^{18}F -FDG uptake (left images). Dual-time point imaging was acquired in this patient to show the improvement of arterial

^{18}F -FDG uptake and background activity clearance obtained when uptake time is delayed, and the acquisition parameters are optimized for vascular inflammation imaging

Several targets, other than glucose utilization, can be explored for arterial inflammation imaging in PLHIV [50]. Arterial ^{18}F -FDG uptake measures metabolic activity in the tissues of the vessel wall including smooth muscles, fibroblasts, and inflammatory cells. Molecular probes targeting markers expressed specifically by inflammatory cells may be more accurate in characterizing arterial inflammation. Macrophages express CD206 molecules, the molecular target for radiolabeled tilmanocept. $^{99\text{m}}\text{Tc}$ -Tilmanocept is approved for sentinel lymph mapping of solid human tumors, especially early breast cancer and intermediate-thickness malignant melanoma. $^{99\text{m}}\text{Tc}$ -Tilmanocept injected subcutaneously accumulates more in the aortas of HIV-infected patients compared with HIV-uninfected individuals with similar Framingham risk score [51]. This higher accumulation of $^{99\text{m}}\text{Tc}$ -tilmanocept reflects arterial inflammation in HIV-infected individuals compared with uninfected individuals. This study utilized $^{99\text{m}}\text{Tc}$ -labeled tilmanocept administered by subcutaneous injection for SPECT/CT imaging. Radiolabelling of tilmanocept with PET radionuclide such as gallium-68 has been described [52, 53]. Intravenously administered tilmanocept labelled with a PET radionuclide may offer a more effective technique for characterizing arterial inflammation in PLHIV.

In summary, ^{18}F -FDG PET/CT is a useful imaging tool for measuring arterial inflammation as a risk for ASCVD in PLHIV. Its use as a non-invasive technique for direct monitoring of changes in arterial inflammation in response to anti-inflammatory therapy is likely to expand, as investigations into this form of treatment become more widespread. The PET system significantly under-estimates arterial ^{18}F -FDG uptake due to the limited diameter of most vessels. This limitation emphasizes the need for the application of standardized imaging parameters which significantly improve PET quantification of arterial ^{18}F -FDG uptake.

Pericarditis

Pericarditis is a common complication seen in PLHIV worldwide [54]. The pericardial disease has a variable manifestation from asymptomatic small pericardial effusion to cardiac tamponade [55]. In developed countries, the cause of pericardial effusion is often idiopathic [55, 56]. In tuberculosis-endemic regions of the world such as Africa, *Mycobacterium tuberculosis* is responsible for 86–100% of pericarditis in PLHIV [57]. Immune suppression seen in HIV

infection causes impairment in cellular immunity leading to a heightened risk of acquisition of new and reactivation of previous tuberculosis (TB) [58]. There is a 10% lifetime risk of TB disease in individuals without HIV infection compared with a 10% annual risk of TB disease in PLHIV [59, 60]. The annual risk of TB disease in advanced immunosuppression of HIV infection increases to 30% [61]. Other infectious causes of pericarditis in PLHIV include bacteria (such as *Staphylococcus aureus*, *Streptococcus pneumoniae*, *Listeria monocytogenes*, *Proteus* species, *Chlamydia trachomatis*, *Klebsiella* species, and *Pseudomonas aeruginosa*); viruses (such as HIV, herpes simplex I/II, and cytomegalovirus); fungi (*Histoplasma capsulatum*, *Cryptococcus neoformans*, and *Candida* species); and protozoa (such as *Toxoplasma gondii*) [56].

The lungs are the commonest organs of primary TB disease. HIV infection is a significant risk factor for the extrapulmonary spread of TB [62]. TB spreads to involve the pericardium homogeneously, from chest nodes contiguous to the pericardium, or via direct spread from infected foci in the lungs or pleura. The hematogenous route is the most common route of spread to the pericardium in PLHIV [63]. TB pericarditis progresses through four stages including (1) dry stage associated with chest pain, pericardial friction rub, and widespread ST elevation without effusion; (2) effusive stage of moderate to large effusion with signs and symptoms of heart failure or pericardial tamponade; (3) adsorptive phase seen as thickened pericardium on imaging with associated thick fibrinous fluid around the heart; and (4) constrictive phase characterized by signs, symptoms, and imaging features of constrictive pericarditis without residual pericardial fluid [54]. The effusive phase is the commonest stage at which patients present at the hospital for care [64]. Figure 2 shows the images of a patient with restrictive cardiac disease caused by pericardial calcification from a previous episode of TB pericarditis.

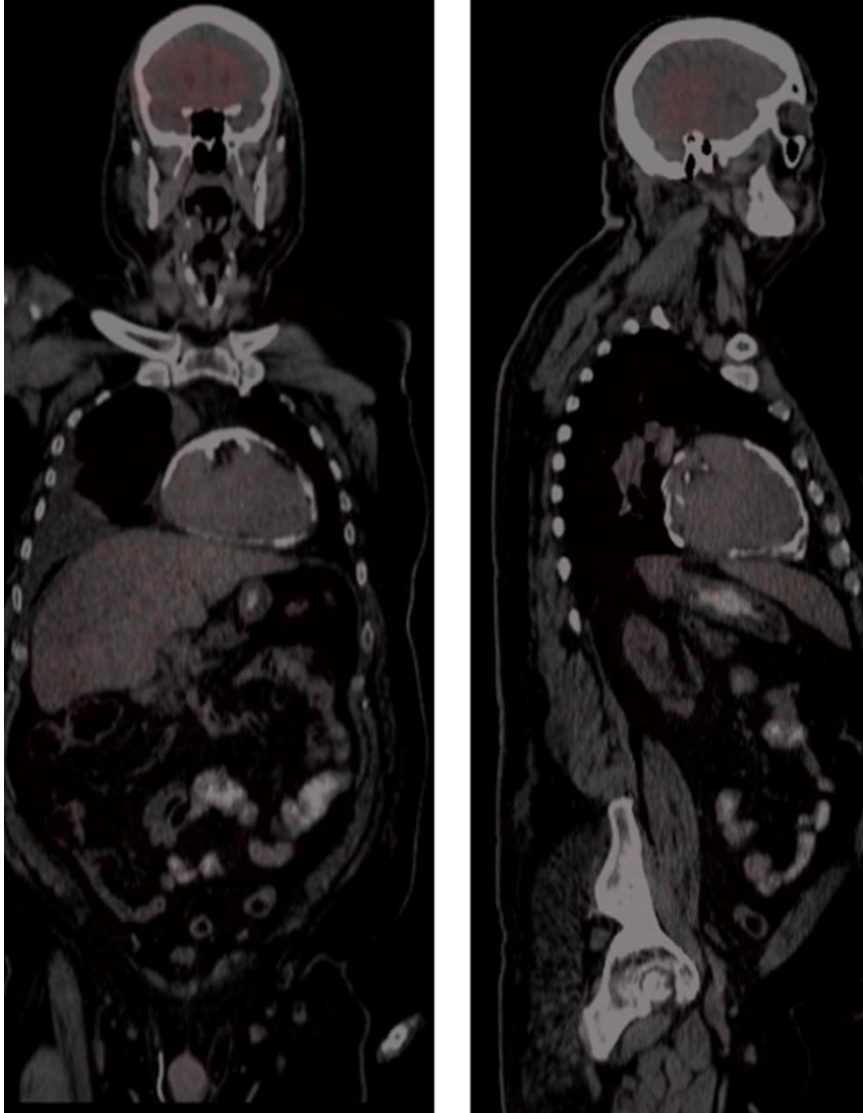


Fig 2 A 62-year-old male with symptoms of heart failure and right pleural effusion. Adequate assessment of cardiac function could not be performed on echocardiography due to a poor acoustic window. ^{18}F -FDG PET/CT done shows dense pericardial calcification with no associated significant metabolic activity confirming the late sequelae of a previous episode of tuberculous pericarditis. These images emphasize the utility of ^{18}F -FDG PET as a tool to differentiate between an active tuberculous pericarditis requiring anti-tuberculous medication with anti-inflammatory therapy using corticosteroid versus the sequelae of a previous infection requiring a different approach to therapy such as pericardial decortication.

The definitive diagnosis of TB pericarditis rests on demonstrating the tubercle bacilli in pericardial fluid or pericardial tissue biopsy sample. Alternatively, histological examination of the pericardial biopsy specimen looking for the typical caseous necrosis due to TB may help establish the diagnosis. The currently available techniques for microscopy and culture to demonstrate acid and alcohol fast tubercle bacilli have disappointingly low sensitivity [63].

Culture, with better sensitivity, takes 2–6 weeks to confirm a positive microbial growth. Due to this low yield of the available tests for definitive diagnosis, the majority of patients are treated empirically [64]. Ancillary tests using imaging and biochemical evaluations have proven useful in the management of TB pericarditis [65].

^{18}F -FDG PET/CT is a useful supportive imaging modality for the diagnosis of pericarditis [66]. ^{18}F -FDG accumulates in the inflamed pericardium in a manner proportional to the level of inflammation (Fig. 3). Tuberculosis causes intense inflammation leading to a high level of ^{18}F -FDG uptake in the pericardium of patients with acute TB pericarditis. In a study comparing patterns of ^{18}F -FDG PET/CT findings in patients with acute TB pericarditis versus idiopathic pericarditis, Dong and colleagues found significantly higher ^{18}F -FDG uptake in the pericardium of patients with acute TB pericarditis versus idiopathic pericarditis (mean SUVmax of pericardium: 13.5 for TB pericarditis versus 3.0 for idiopathic pericarditis, $p = 0.002$) [67]. In TB pericarditis, the pericardium was thicker (5.1 mm versus 3.4 mm, $p = 0.004$) and there was associated lymphadenopathy which demonstrated significantly higher ^{18}F -FDG uptake (mean SUVmax of lymph nodes: 5.3 versus 2.8 for TB pericarditis and idiopathic pericarditis, respectively, $p < 0.001$) compared with patients with idiopathic pericarditis. This study showed the potential utility of ^{18}F -FDG PET/CT in differentiating between the two common causes of pericarditis with distinctively different treatments. Also, the study showed associated mediastinal and supraclavicular lymph node involvement with intense ^{18}F -FDG uptake in TB pericarditis. Biopsy of these nodes for histological and/or microbiological assessment for TB involvement may provide an easier way to access tissue for disease confirmation especially since the analysis of pericardial fluid or pericardial biopsy specimen may fail to confirm the presence of the disease [63].



Fig 3 A 21-year-old HIV-infected male on antiretroviral therapy for 11 months with clinical symptoms suggestive of tuberculous disease (new-onset weight loss, fever, and night sweat) without associated cough. ^{18}F -FDG PET/CT was obtained to evaluate for extra-pulmonary tuberculosis. Images show intense ^{18}F -FDG uptake in thickened pericardium as well as in right supraclavicular nodes and conglomerate of anterior mediastinal nodes (arrows). Histological examination of the biopsy specimen of the right supraclavicular node confirmed tuberculosis. Symptoms resolved on treatment for extra-pulmonary tuberculosis (tuberculous pericarditis and lymphadenitis). In this case, ^{18}F -FDG PET/CT findings support the clinical suspicion of extra pulmonary TB, TB pericarditis in this case. Imaging findings also help guide biopsy for histological/microbiological confirmation from a peripheral site and avoiding a more invasive pericardial biopsy with its attendant complications

Among the infectious causes of pericarditis, TB appears to be the most severe with a mortality of up to 40% even with effective treatment in symptomatic PLHIV [68]. The intense ^{18}F -FDG uptake seen in TB pericarditis is not specific to it. While TB is responsible for the majority of cases of pericarditis in PLHIV especially in TB-endemic regions of the world, infectious, inflammatory non-infectious, and neoplastic conditions which cause trapping of ^{18}F -FDG in the pericardium are responsible for a minority of cases [69]. Neoplastic conditions that involve the pericardium, such as Kaposi sarcoma and lymphoma, also cause intense ^{18}F -FDG uptake in the involved pericardium and associated lymphadenopathy [70]. These conditions, while less common causes of pericarditis than TB, need to be excluded. A neoplastic condition causing pericarditis may have associated mass lesion on imaging [70]. ^{18}F -FDG PET/CT imaging offers supportive clues in the diagnosis of pericarditis, including prominent metabolically active mediastinal and supraclavicular nodes easily accessible for biopsy [71], and whole-body imaging that allows for detection of disease at other sites, especially characteristic lung lesions of pulmonary TB.

Anti-tuberculous treatment (ATT) is the mainstay of treatment of TB. A subset of patients has residual TB disease after completing a standard course of ATT [72, 73]. The clinical utility of ^{18}F -FDG PET/CT for assessing disease severity [74, 75], predicts response to ATTT

[76–78], enabling evaluation of therapy response in the management of TB that have been widely reported [79–81]. Successful ATT leads to a corresponding reduction in PET signal. In multiple case reports, there is a normalization of the ^{18}F -FDG PET signal in the pericardium in response to ATT and steroid therapy in patients treated for TB pericarditis [71, 82].

In summary, ^{18}F -FDG PET/CT is useful in the diagnosis of pericarditis. Pattern of disease involvement seen on ^{18}F -FDG PET/CT may help differentiate between TB pericarditis and idiopathic pericarditis, two common causes of pericarditis. ^{18}F -FDG PET signal returns to normal after successful ATT. This makes ^{18}F -FDG PET/CT useful for therapy response assessment. There are several etiological factors responsible for pericarditis in PLHIV, ^{18}F -FDG PET/CT imaging can, unfortunately, not discriminate between these causes accurately enough to obviate the need for tissue diagnosis/ microbiological confirmation.

Myocarditis

Myocarditis is characterized by inflammation of the heart muscle causing lymphocyte infiltration and necrosis of myocytes [83]. In the pre-ART era, myocarditis was seen in 52% of HIV-infected patients in an autopsy series [84]. The successful roll-out of ART has led to a significant reduction in opportunistic infection-related myocarditis. HIV infects the myocytes in patchy distributions [85]. In addition to HIV, several other opportunistic viruses, fungi, bacteria, and protozoa are responsible for myocarditis in PLHIV [86]. On histological assessment, there appears to be no difference in the morphology of myocarditis caused by different organisms or myocarditis in HIV-infected and HIV-uninfected people [87]. In patients with TB pericarditis, there is associated TB myocarditis in 53% of them, making *Mycobacterium tuberculosis* an important cause of myopericarditis in PLHIV [88].

Prompt and accurate diagnosis of myocarditis is challenging because symptoms and laboratory biomarkers are non-specific. Definitive diagnosis rests on demonstrating typical appearance on histological evaluation of endomyocardial biopsy (EMB) specimen. EMB is rarely done in the diagnostic evaluation of patients with suspected myocarditis. In a large study of 22,299 patients hospitalized with myocarditis, EMB was performed in 798 patients (3.6%) [89]. After adjusting for baseline characteristics and comorbidities, EMB was significantly associated with higher in-hospital mortality; longer hospital stay; and higher incidence of cardiac tamponade, ventricular tachycardia, acute renal failure, and cardiogenic shock [89]. The longer

hospital-stay and higher in-hospital mortality reported in this study may be due to selection bias where patients with more severe disease had EMB compared with less sick patients who did not. The sensitivity of EMB in the diagnostic evaluation of myocarditis is low due to the patchy distribution of the disease. Imaging, therefore, plays a vital role in the diagnosis of the disease.

Cardiac magnetic resonance (CMR) is the diagnostic imaging of choice for the evaluation of myocarditis. In the acute setting, CMR assesses the hallmarks of acute inflammation including edema on T2-weighted imaging, hyperemia on early gadolinium enhancement, and myocytes necrosis on delayed gadolinium enhancement [90]. The use of each of these imaging features is not sufficiently sensitive for the diagnosis of acute myocarditis. The Lake Louise criteria (LLC) combine the three CMR features for the diagnosis of acute myocarditis. The imaging features used in LLC, while useful in differentiating healthy heart from diseased myocardium, are not specific for acute myocarditis. LLC has a lower diagnostic sensitivity for chronic myocarditis and acute myocarditis complicated by heart failure [91]. CMR is susceptible to image artifacts, and several methodological and technical problems may be encountered during image acquisition that may impact on its diagnostic performance [92]. Given these limitations of CMR, complementary imaging may be necessary for the evaluation of patients with suspected myocarditis.

^{18}F -FDG PET/CT is a useful imaging modality in inflammation imaging. It is, however, important to emphasize here a limitation of ^{18}F -FDG PET imaging of cardiac inflammation an infection, which is the intense physiologic uptake of ^{18}F -FDG by the myocardium. The myocardium uses different metabolic substrates including glucose at different diseased and health states. It, therefore, traps ^{18}F -FDG significantly. Intense uptake of ^{18}F -FDG by the myocardium makes the study uninterpretable when imaging is performed for infection or inflammation indications. There is, therefore, a need for myocardial suppression procedure before ^{18}F -FDG PET imaging of the heart. The most common method for myocardial suppression of glucose utilization (and by extension ^{18}F -FDG utilization) is prolonged fasting for up to 16 h and dietary modification (high fat, low carbohydrate, and protein permitted diet) 1 day before the study [93]. Pharmacologic intervention using unfractionated heparin may also be explored for myocardial suppression of glucose utilization. Recently, Clément et al. [94] reported that a 1-week ketogenic diet provided a further decrease in myocardial ^{18}F -FDG uptake and increase lesion detectability in an animal model of autoimmune myocarditis. This approach may

have limited clinical applicability especially in the symptomatic patients where a prompt diagnosis is desired.

In a longitudinal study of a murine model of autoimmune myocarditis, Werner et al. showed a high ^{18}F -FDG PET signal in the acute phase of myocarditis which showed a good correlation with the level of macrophages present at the site of myocardial inflammation [95]. ^{18}F -FDG PET signal decreased at the subacute phase of the disease. This preclinical study showed that ^{18}F -FDG uptake in acute myocarditis is proportional to the level of inflammation in the affected myocardium. There are limited studies in the literature that have reported the role of ^{18}F -FDG PET/CT in the evaluation of myocarditis. Studies on ^{18}F -FDG PET/CT imaging in PLHIV are even rarer. Pathological changes seen in myocarditis are similar between HIV-infected and HIV-uninfected people [87]. Experience reported on the use of ^{18}F -FDG PET/CT in HIV-uninfected people may, therefore, be extrapolated to PLHIV. In a group of patients with different forms of myocarditis including acute and chronic forms of the disease and using EMB as the diagnostic gold standard, Ozawa et al. [96] reported a perfect sensitivity, specificity, positive predictive value, and negative predictive value of 100% each for ^{18}F -FDG PET/CT in the detection of myocarditis if performed within the first 14 days of onset of symptoms. The diagnostic performance of ^{18}F -FDG PET/CT dropped if imaging was performed beyond this time. These findings are in agreement with the preclinical study reporting the highest intensity of ^{18}F -FDG PET signal in the acute phase of myocarditis with a signal reduction in the subacute phase of the disease [95]. Others have reported cases of myocarditis where ^{18}F -FDG PET/CT imaging contributed to the diagnosis of the disease [97–99]. Following successful treatment or resolution of myocarditis, ^{18}F -FDG PET signals return to normal [100]. This shows that ^{18}F -FDG PET/CT may be useful as a tool for therapy response assessment.

The application of hybrid imaging with PET/MR is gaining popularity in clinical usage. The excellent soft tissue resolution and the well-characterized features of myocarditis available from CMR combined with the metabolic information available from ^{18}F -FDG PET may offer superior diagnostic performance than either modality alone. Evidence is emerging, supporting the use of hybrid ^{18}F -FDG PET/MR in the evaluation of patients with myocarditis [90, 101]. Initial cases reported on the utility of ^{18}F -FDG PET/MR in the evaluation of patients with myocarditis have provided encouraging results with good concordance between the two imaging modalities [102–104]. In a prospective comparison of ^{18}F -FDG PET and CMR in 55 patients

with suspected myocarditis, 23 patients had CMR features suggestive of myocarditis while 18 patients had pathologic ^{18}F -FDG uptake [105]. Six patients with pathologic CMR findings did not have corresponding ^{18}F -FDG uptake while only one patient had pathologic ^{18}F -FDG uptake without corresponding pathologic CMR finding. There was at least a good spatial agreement between pathologic findings on CMR finding versus pathologic ^{18}F -FDG uptake. Using CMR findings as the reference gold standard, ^{18}F -FDG PET had a sensitivity of 74%, a specificity of 97%, and a diagnostic accuracy of 87% [105].

Despite rigorous preparation for myocardial suppression, some patients may still have physiologic ^{18}F -FDG uptake in the myocardium compromising image interpretation [105]. This has led to an attempt at investigating other radionuclide probes that target inflammation but have no physiologic uptake in the normal myocardium for use in molecular imaging of cardiac inflammation and infection. ^{11}C -methionine is trapped by macrophages and can be used for inflammation imaging [106]. In a murine model of autoimmune myocarditis, Maya and colleagues show that the level of ^{11}C -methionine correlates well with the level of macrophages in lesions [107]. There was a good correlation between the signal intensity of ^{11}C -methionine and ^{18}F -FDG. Exploration of this and other radiotracers without physiologic myocardial uptake (especially peptides labelled to radionuclide with wider availability than ^{11}C) is warranted for clinical translation in radionuclide imaging of myocarditis.

In summary, molecular imaging with ^{18}F -FDG PET/CT may be helpful in the diagnosis of myocarditis especially in the acute phase of the disease. With the increasing availability of PET/MR in routine clinical practice, this hybrid imaging technique may provide a better diagnostic accuracy in the assessment of myocarditis than either technique used alone. The need for myocardial suppression to prevent the physiologic uptake of ^{18}F -FDG in the heart muscle is a limitation to the use of ^{18}F -FDG PET/CT in the evaluation of myocarditis.

Infective endocarditis

Infective endocarditis (IE) is a relatively rare disease but one associated with high morbidity and mortality. There has been a steady decline in the incidence of IE among PLHIV in the ART era [108–110]. HIV itself has not been consistently shown to be an independent risk factor for IE. Certain factors prevalent among PLHIV increase their chances of acquiring infection of the native heart tissues or that of cardiac-related devices. In the developed countries, intravenous

drug use is the single most important factor predisposing to IE among PLHIV with a higher incidence of IE seen in injection drug users (IDUs) who are HIV-infected compared with IDUs who are HIV negative [111]. Intravenous drug use is a less common mode of transmission of HIV in Sub-Saharan Africa compared with developed countries. Studies performed in developing countries where HIV prevalence is high have not shown HIV to be an independent risk factor for IE. In a cohort of 92 patients evaluated for probable IE in South Africa, only one patient was HIV positive [112]. In another study from the Democratic Republic of Congo, only 1.2% of 83 consecutive HIV-infected patients with heart disease had IE [113]. In the developing countries, the main risk factors for IE are rheumatic valvular heart disease, congenital heart disease, the presence of prosthetic valves, and history of infective endocarditis [112]. Skin abscess and bacteremia, which are common among PLHIV, may be additional risk factors for IE in them [114, 115].

The diagnosis of IE is not different between HIV-infected and HIV-uninfected patients. The diagnosis of IE is according to the modified Duke criteria which are based on suggestive clinical findings, echocardiography, and positive blood culture to isolate the causative organism [116]. The clinical presentation of IE does not appear to be different between HIV-infected and HIV-uninfected people [117, 118]. PLHIV are more likely to have IE which involves right-sided heart valves or a combination of right-sided and left-sided heart valves in contrast to HIV-uninfected people who have predominantly left-sided valvular involvement [117, 118]. Nonbacterial thrombotic endocarditis (also known as marantic endocarditis) has been described in patients with advanced HIV infection [119]. Marantic endocarditis is characterized by friable vegetations on the heart valves without infection and a high likelihood of distant embolization [119]. The absence of bacteremia and, consequently, a negative blood culture may impact on the diagnostic yield of the Duke criteria for the diagnosis of endocarditis in this setting. Despite this concern, no significant difference was reported in the diagnostic performance of the Duke criteria in HIV-infected IDUs compared with HIV-uninfected IDUs [120]. Among PLHIV, low CD4 counts < 50 cells/mm³ and high viral load (HIV RNA > 100,000 copies/mL), which connote severe immune suppression and high viremia, are predictive of poor IE treatment outcome [121].

In its most recent guidelines, the European Society of Cardiology included abnormal tracer uptake on radiolabelled leucocyte single-photon emission tomography and computed

tomography (SPECT/CT) or ^{18}F -FDG PET/CT as major criteria in its modification of the Duke criteria for the diagnosis of IE in patients with suspected prosthetic valve endocarditis [116]. Both radiolabelled leucocyte SPECT/CT and ^{18}F -FDG PET/CT are useful adjuncts to echocardiography and blood culture in the diagnosis of prosthetic valve endocarditis (PVE), but less so in native valve endocarditis (NVE). To our knowledge, no studies have been done exclusively in PLHIV on the use of radionuclide techniques in the diagnosis of IE. Lessons learned from studies recruiting patients regardless of their HIV serostatus can safely be applied to the HIV-infected population. Comprehensive reviews of the diagnostic performances of radiolabelled leucocyte SPECT/CT and ^{18}F -FDG PET/CT have been recently published [122, 123]. In the most recent meta-analysis, the pooled sensitivity of radiolabelled leucocytes scintigraphy and ^{18}F -FDG PET/CT in patients with IE were 80% (95% CI 67–94) and 71% (95% CI 56–87), respectively [122]. The respective pooled specificity for radiolabelled leucocytes scintigraphy and ^{18}F -FDG PET/CT in patients with suspected IE were 100% (95% CI 98–101) and 89% (95% CI 84–95). In patients with suspected cardiac implantable electronic device related infection, the pooled sensitivity, and specificity were 85% (95% CI 77–93) and 91% (95% CI 87–96) for ^{18}F -FDG PET/CT, respectively [122].

The application of radiolabelled leucocytes SPECT/CT is premised on leucocyte migration to the site of infection. This imaging technique provides a highly specific means of imaging cardiac and cardiac device-related infections as radiolabelled leucocytes do not accumulate to a significant extent at the site of sterile inflammation seen in the early postoperative period and as a physiologic reaction induced by prosthetic materials. Radiolabelling of leucocytes is technically demanding, requires highly skilled technicians, and involved the handling of blood with the attendant risk of staff exposure to blood-borne pathogens. In radiolabelled leucocytes SPECT/CT, imaging is acquired at 2 or 3-time-points over 24 h for $^{99\text{m}}\text{Tc}$ -HMPAO-labeled leucocytes and up to 48 h for ^{111}In -oxine-labeled leucocytes scintigraphy.

^{18}F -FDG PET/CT is a more commonly used radionuclide technique for IE imaging [124]. It does not involve blood handling, and imaging is completed within 2 hours. The better resolution of the PET system may make ^{18}F -FDG PET/CT more sensitive for IE compared with radiolabelled leucocytes SPECT/CT. The most recent meta-analysis has, however, not confirmed this assumption [122]. ^{18}F -FDG accumulates at the site of sterile inflammation, a drawback

that may limit the utility of ^{18}F -FDG PET/CT for IE imaging within 3 months after surgery. Prosthetic cardiac devices induce sterile inflammation causing increased physiologic ^{18}F -FDG uptake around them [125]. A recent study did not find a significant reduction in physiologic ^{18}F -FDG uptake around the prosthetic heart valve over 1-year postoperatively [126]. The study, however, proposed normality criteria to guide image interpretation.

Rheumatic heart disease (RHD) has since ceased to be of a public health concern in the developed countries but continues to be a leading cause of acquired heart disease contributing significantly to cardiac mortality and morbidity in developing countries [127, 128]. Rheumatic heart disease results from poorly treated group A Streptococcal pharyngitis in childhood that leads to autoimmune response characterized by damage of the heart valves and myocardium. RHD has a high predilection for the mitral valve causing mitral regurgitation and less commonly, mitral stenosis. Most recent studies in Africa show a low incidence of RHD among PLHIV [129-131], but when present, may serve as a risk factor for IE [112]. ^{18}F -FDG PET/CT is useful for unraveling the cause of fever in immunodeficiency states [132, 133]. Fever is the most frequent symptom of IE [116, 124]. In immunosuppressed patients presenting with fever of unknown origin where the cause of fever remains unknown after standard diagnostic work-up, ^{18}F -FDG PET/CT helps identify IE occurring on the background of RHD, Fig. 4 [134]. A comparative study has reported the diagnostic performance of ^{18}F -FDG PET/CT in 19 patients with acute RHD, 17 patients with chronic RHD, and 12 healthy controls. Diffuse ^{18}F -FDG in the myocardium was seen in all but five patients with acute RHD [135]. The significance of this diffuse myocardial uptake is unknown, as no details regarding image interpretation were presented in the study. Further study regarding the role of ^{18}F -FDG PET/CT in RHD is, therefore, needed.

In summary, molecular imaging using SPECT and PET techniques is increasingly being used for the diagnosis work-up of patients with suspected IE due to its accuracy in patients in whom diagnosis cannot be confirmed using the Duke criteria. Availability, especially in the developing countries, remains a limitation militating against a more widespread use of molecular imaging in the evaluation of endocarditis among PLHIV.

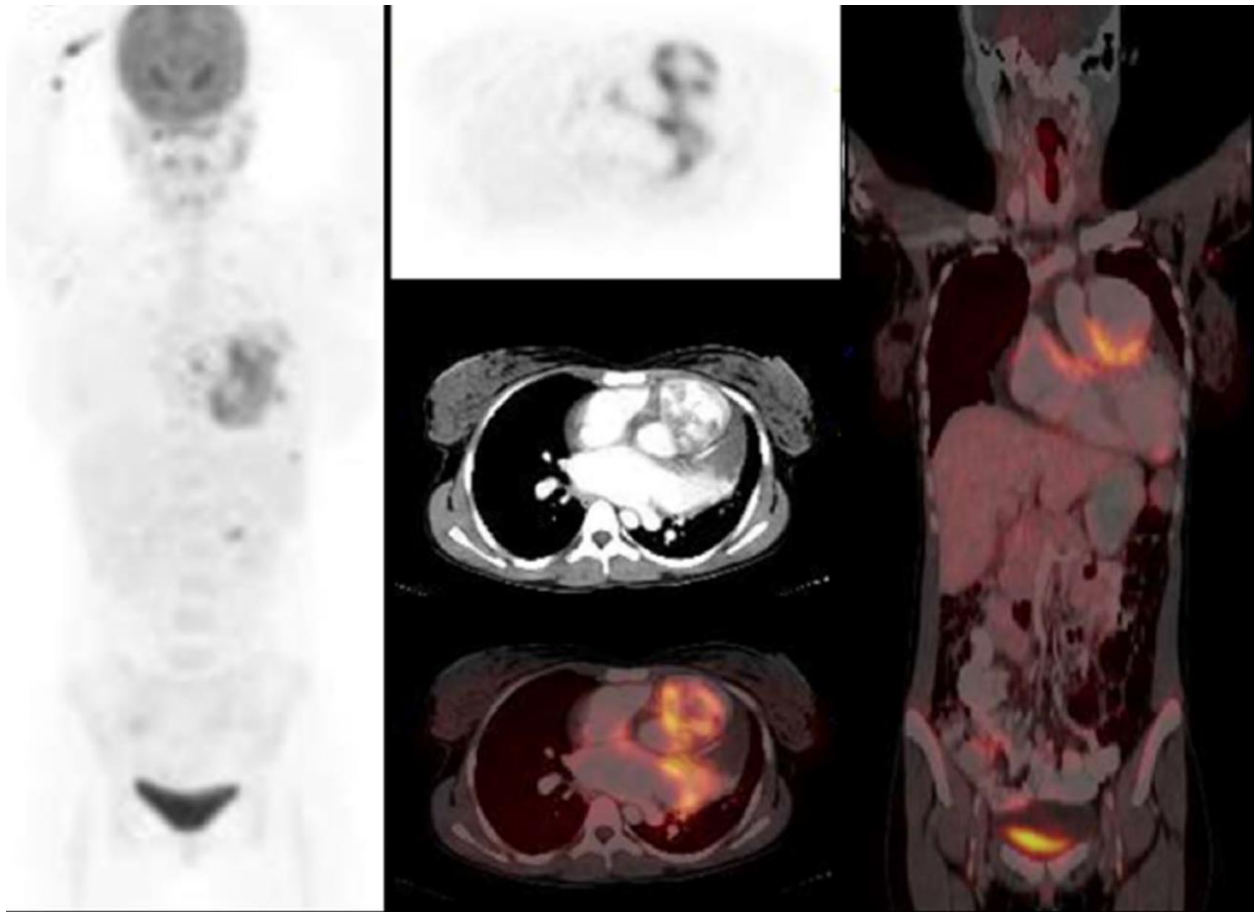


Fig 4 Images of a newly diagnosed HIV-infected female who had ^{18}F -FDG PET/CT to identify the cause of fever of unknown origin. Images showed intense ^{18}F -FDG uptake in the mitral valve and surrounding myocardium. The patient subsequently succumbed to her disease. Post-mortem analysis confirmed infective endocarditis on the background of rheumatic heart disease. These images demonstrate the potential utility of ^{18}F -FDG PET/CT in the evaluation of endocarditis occurring on the background of rheumatic heart disease

Conclusion

Molecular imaging using radionuclide techniques is increasingly showing higher utilization for characterizing and diagnosing cardiovascular inflammation and infection in PLHIV. Molecular imaging techniques, especially with ^{18}F -FDG PET/CT, are useful for risk prediction, disease quantification, and for measuring the impact of intervention in subclinical atherosclerotic cardiovascular disease among PLHIV. The ability to risk-stratify patients may be helpful in the future to select patients who may benefit from primary prophylaxis against ASCVD.

Inflammation is becoming a critical therapy target in ASCVD. The ability of molecular imaging to directly quantify lesion or arterial inflammation makes it a suitable tool for evaluating the effectiveness of new therapeutic agents targeting inflammation in ASCVD. PET and SPECT

imaging techniques are essential tools in the evaluation of cardiac infection especially in suspected infective endocarditis where the diagnosis remains inconclusive after standard diagnostic work-up. PET and SPECT techniques are of clinical value to guide tissue biopsy for histological or microbiological confirmation of cardiac inflammation and infection especially since these conditions may have patchy distribution leading to sampling error when biopsy is done blindly without guidance to the sites of disease involvement. The prompt return to normalcy of metabolic changes before morphological restoration makes molecular techniques using radionuclide modalities for therapy response assessment preventing over or under treatment and associated consequences. More studies are necessary to define better the roles of molecular imaging techniques in cardiovascular inflammation and infection among PLHIV. This call is likely to be answered soon as SPECT and PET techniques become increasingly available in developing countries where the greater proportion of PLHIV resides.

Author contributions IO Lawal: literature search, literature review, content planning, writing, and editing. AC Stoltz: content planning, editing, and critical review. MM Sathekge: literature review, content planning, writing, editing, and critical review.

Funding No external funding was received in the course of this work.

Compliance with ethical standards

Conflict of interest The authors declare that they have no conflict of interest.

Ethical approval This expert review does not contain any studies with human subjects performed by any of the authors.

References

1. UNAIDS (2019) Global HIV & AIDS statistics—2019 fact sheet. <https://www.unaids.org/en/resources/fact-sheet> . Accessed 9 Feb 2020
2. Simon V, Ho DD, Abdool Karim Q (2006) HIV/AIDS epidemiology, pathogenesis, prevention, and treatment. *Lancet* 368:489– 504. [https://doi.org/10.1016/S0140-6736\(06\)69157-5](https://doi.org/10.1016/S0140-6736(06)69157-5)
3. Cassol E, Malfeld S, Mahasha P, van der Merwe S, Cassol S, Seebregts C et al (2010) Persistent microbial translocation and immune activation in HIV-1-infected South Africans receiving combination antiretroviral therapy. *J Infect Dis* 202:723–733. <https://doi.org/10.1086/655229>
4. The Collaboration of Observational HIV Epidemiological Research Europe (COHERE) in Euro-Coord, Lewden C, Bouteloup V, De Wit S, Sabin C, Mocroft A et al (2012) All-cause mortality in treated HIV-infected adults with CD4 \geq 500/mm³ compared with the general population: evidence from a large European observational cohort collaboration. *Int J Epidemiol* 41:433–445. <https://doi.org/10.1093/ije/dyr164>
5. Sabin CA (2013) Do people with HIV infection have a normal life expectancy in the era of combination antiretroviral therapy? *BMC Med* 11:251. <https://doi.org/10.1186/1741-7015-11-251>
6. Yang X, Su B, Zhang X, Liu Y, Wu H, Zhang T (2020) Incomplete immune reconstitution in HIV/AIDS patients on antiretroviral therapy: challenges of immunological non-responders. *J Leukoc Bio*. <https://doi.org/10.1002/JLB.4MR1019-189R>
7. Perdomo-Celis F, Velilla PA, Taborda NA, Rugeles MT (2019) An altered cytotoxic program of CD8⁺ T-cells in HIV-infected patients despite HAART-induced viral suppression. *PLoS ONE* 14:e0210540. <https://doi.org/10.1371/journal.pone.0210540>
8. Nabatanzi R, Bayigga L, Cose S, Jones SR, Joloba M, Canderan G et al (2019) Monocyte dysfunction, activation and inflammation after long-term antiretroviral therapy in an African cohort. *Clin Infect Dis* 220:1414–1419. <https://doi.org/10.1093/infdis/jiz320>
9. Deeks SG (2011) HIV infection, inflammation, immunosenescence, and Aging. *Annu Rev Med* 62:141–155. <https://doi.org/10.1146/annurev-med-042909-093756>

10. Deeks SG (2009) HIV infection, antiretroviral treatment, ageing, and non-AIDS related morbidity. *BMJ* 3338:a3172. <https://doi.org/10.1136/bmj.a3172>
11. Ross R (1999) Atherosclerosis an inflammatory disease. *N Engl J Med* 340:115–126
12. Insull W (2009) The pathology of atherosclerosis: plaque development and plaque responses to medical treatment. *Am J Med* 122(Suppl):S3–S14. <https://doi.org/10.1016/j.amjmed.2008.10.013>
13. Li H, Cybulsky MI, Gimbrone MA Jr, Lippy P (1993) An atherogenic diet rapidly induces VCAM-1, a cytokine-regulatable mononuclear leukocyte adhesion molecule, in rabbit aortic endothelium. *Arterioscler Thromb* 13:197–204. <https://doi.org/10.1161/01.atv.13.2.197>
14. Cybulsky MI, Iiyama K, Li H, Zhu S, Chen M, Iiyama M et al (2001) A major role for VCAM-1, but not ICAM-1, in early atherosclerosis. *J Clin Invest* 107:1255–1262. <https://doi.org/10.1172/JCI11871>
15. Fan J, Watanabe T (2013) Inflammatory reactions in the pathogenesis of atherosclerosis. *J Atheroscler Thromb* 10:63–71. <https://doi.org/10.5551/jat.10.63>
16. Shah ASV, Stelzle D, Lee KK, Beck EJ, Alam S, Clifford S et al (2018) Global burden of atherosclerotic cardiovascular disease in people living with HIV. *Circulation* 138:1100–1112. <https://doi.org/10.1161/CIRCULATIONAHA.117.033369>
17. Titanji B, Gavegnano C, Hsue P, Schinazi R, Marconi VC (2020) Targeting inflammation to reduce atherosclerotic cardiovascular risk in people with HIV infection. *J Am Heart Assoc* 9:e014873. <https://doi.org/10.1161/JAHA.119.014873>
18. Hemkens LG, Bucher HC (2014) HIV infection and cardiovascular disease. *Eur Heart J* 35:1373–1381. <https://doi.org/10.1093/eurheartj/ehu528>
19. Nguyen KA, Peer N, de Villiers A, Mukasa B, Matsha TE, Mills EJ et al (2017) Metabolic syndrome in people living with human immunodeficiency virus: an assessment of the prevalence and the agreement between diagnostic criteria. *Inj J Endocrinol* 2017:1613657. <https://doi.org/10.1155/2017/1613657>
20. Njuguna B, Kiplagat J, Bloomfield GS, Pastakia SD, Vedanthan R, Koethe JR (2018) Prevalence, risk factors, and pathophysiology of dysglycemia among people living with HIV in Sub-Saharan Africa. *J Diabetes Res* 2018:6916497. <https://doi.org/10.1155/2018/6916497>

21. Torriani FJ, Komarow L, Parker RA, Cotter BR, Currier JS, Dubé MP et al (5152s) Endothelial function in human immunodeficiency virus-infected antiretroviral-naïve subjects before and after starting potent antiretroviral therapy: The ACTG (AIDS Clinical Trials Group) study 5152s. *J Am Coll Cardiol* 52:569–576. <https://doi.org/10.1016/j.jacc.2008.04.049>
22. Nabatanzi R, Bayigga L, Cose S, Jones SR, Joloba M, Canderan G et al (2019) Monocyte dysfunction, activation, and inflammation after long-term antiretroviral therapy in an African cohort. *J Infect Dis* 220:1414–1419. <https://doi.org/10.1093/infdis/jiz320>
23. Maisa A, Hearps AC, Angelovich TA, Pereira CF, Zhou J, Shi MDY et al (2015) Monocytes from HIV-infected individuals show impaired cholesterol efflux and increased foam cell formation after transendothelial migration. *AIDS* 29:1445–1457. <https://doi.org/10.1097/QAD.0000000000000739>
24. Hui DY (2003) Effects of HIV protease inhibitor therapy on lipid metabolism. *Prog Lipid Res* 42:81–92. [https://doi.org/10.1016/s0163-7827\(02\)00046-2](https://doi.org/10.1016/s0163-7827(02)00046-2)
25. Tawakol A, Migrino RQ, Bashian GG, Bedri S, Vermylen D, Cury RC et al (2006) In vivo ¹⁸F-fluorodeoxyglucose positron emission tomography imaging provides a noninvasive measure of carotid plaque inflammation in patients. *J Am Coll Cardiol* 48:1818–1824. <https://doi.org/10.1016/j.jacc.2006.05.076>
26. Graebe M, Pedersen SF, Borgwardt L, Højgaard L, Sillesen H, Kjaer A (2009) Molecular pathology in vulnerable carotid plaques: correlation with [18]-fluorodeoxyglucose positron emission tomography (FDG-PET). *Eur J Vasc Endovasc Surg* 37:714–721. <https://doi.org/10.1016/j.ejvs.2008.11.018>
27. Rudd JHF, Warburton EA, Fryer TD, Jones HA, Clark JC, Antoun N et al (2002) Imaging atherosclerotic plaque inflammation with [¹⁸F]-fluorodeoxyglucose positron emission tomography. *Circulation* 105:2708–2711. <https://doi.org/10.1161/01.cir.0000020548.60110.76>
28. Rominger A, Saam T, Wolpers S, Cyran CC, Schmidt M, Foerster S et al (2009) ¹⁸F-FDG PET/CT identifies patients at risk for future vascular events in an otherwise asymptomatic cohort with neoplastic disease. *J Nucl Med* 50:1611–1620. <https://doi.org/10.2967/jnumed.109.065151>

30. Figueroa AL, Abdelbaky A, Truong QA, Corsini E, MacNabb MH, Lavender ZR et al (2013) Measurement of arterial activity on routine FDG PET/CT images improves prediction of risk of future CV event. *JACC Cardiovasc Imaging* 6:1250–1259. <https://doi.org/10.1016/j.jcmg.2013.08.006>
31. Schoepf IC, Buechel RR, Kovari H, Hammoud DA, Tarr PE (2019) Subclinical atherosclerosis imaging in people living with HIV. *J Clin Med* 8:1125. <https://doi.org/10.3390/jcm8081125>
32. Subramanian S, Tawakol A, Burdo TH, Abbara S, Wei J, Vijayakumar J et al (2012) Arterial inflammation in patients with HIV. *JAMA* 308:379–386. <https://doi.org/10.1001/jama.2012.6698>
33. Zanni MV, Toribio M, Robbins GK, Burdo TH, Lu MT, Ishai AE et al (2016) Effects of antiretroviral therapy on immune function and arterial inflammation in treatment-naïve patients with human immunodeficiency virus infection. *JAMA Cardiol* 1:474–480. <https://doi.org/10.1001/jamacardio.2016.0846>
34. Funderburg NT, Jiang Y, Debanne SM, Storer N, Danielle L, Clagett B et al (2014) Rosuvastatin treatment reduces markers of monocyte activation in HIV-infected subjects on antiretroviral therapy. *Clin Infect Dis* 58:588–595. <https://doi.org/10.1093/cid/cit748>
35. Pirro M, Simental-Mendía LE, Bianconi V, Watts GF, Banach M, Sahebkar A (2019) Effect of statin therapy on arterial inflammation based on ¹⁸F-FDG PET/CT: a systematic review and meta-analysis of interventional studies. *J Clin Med* 8:118. <https://doi.org/10.3390/jcm8010118>
36. Tawakol A, Ishai A, Li D, Pakx RAP, Hur S, Kaiser Y et al (2017) Association of arterial and lymph node inflammation with distinct inflammatory pathways in human immunodeficiency virus infection. *JAMA Cardiol* 2:163–171. <https://doi.org/10.1001/jamacardio.2016.4728>
37. Ridker PM, Everett BM, Thuren T, MacFadyen JG, Chang WH, Ballantyne C et al (2017) Antiinflammatory therapy with canakinumab for atherosclerotic disease. *N Engl J Med* 377:1119–1131. <https://doi.org/10.1056/NEJMoa1707914>
38. Hsue PY, Li D, Ma Y, Ishai A, Manion M, Nahrendorf M et al (2018) IL-1 β inhibition reduces atherosclerotic inflammation in HIV infection. *J Am Coll Cardiol* 72:2809–2810. <https://doi.org/10.1016/j.jacc.2018.09.038>

39. Tuzcu EM, Kapadia SR, Tutar E, Ziada KM, Hobbs RE, McCarthy PM et al (2001) High prevalence of coronary atherosclerosis in asymptomatic teenagers and young adults: evidence from intravascular ultrasound. *Circulation* 103:2705–2710. <https://doi.org/10.1161/01.cir.103.22.2705>
40. Lawal IO, Ankrah AO, Popoola GO, Lengana T, Sathekge MM (2019) Arterial inflammation in young patients with human immunodeficiency virus infection: A cross-sectional study using F-18 FDG PET/CT. *J Nucl Cardiol* 26:1258–1265. <https://doi.org/10.1007/s12350-018-1207-x>
41. Boccara F, Lang S, Meuleman C, Ederhy S, Mary-Krause M, Costagliola D et al (2013) HIV and coronary heart disease: time for a better understanding. *J Am Coll Cardiol* 61:511–523. <https://doi.org/10.1016/j.jacc.2012.06.063>
42. Knudsen A, Hag AMF, Loft A, von Benzon E, Keller SH, Møller HJ et al (2015) HIV infection and arterial inflammation assessed by ¹⁸F-fluorodeoxyglucose (FDG) positron emission tomography (PET): a prospective cross-sectional study. *J Nucl Cardiol* 22:372–380. <https://doi.org/10.1007/s12350-014-0032-0>
43. Lo J, Lu MT, Ihenachor EJ, Wei J, Looby SE, Fitch KV et al (2015) Effects of statin therapy on coronary artery plaque volume and high risk plaque morphology in HIV-infected patients with subclinical atherosclerosis: a randomized double-blind placebo-controlled trial. *Lancet HIV* 2:e52–e63. [https://doi.org/10.1016/S2352-3018\(14\)00032-0](https://doi.org/10.1016/S2352-3018(14)00032-0)
44. Yarasheski KE, Laciny E, Overton ET, Reeds DN, Harrod M, Baldwin S et al (2012) ¹⁸FDG PET-CT imaging detects arterial inflammation and early atherosclerosis in HIV-infected adults with cardiovascular disease risk factors. *J Inflamm* 9:22. <https://doi.org/10.1186/1476-9255-9-26>
45. Burg S, Dupas A, Stute S, Dieudonné A, Huet P, Le Guludec D et al (2013) Partial volume effect estimation and correction in the aortic vascular wall in PET imaging. *Phys Med Biol* 58:7527–7542. <https://doi.org/10.1088/0031-9155/58/21/7527>
46. Huet P, Burg S, Le Guludec D, Hyafil F, Buvat I (2015) Variability and uncertainty of ¹⁸F-FDG PET imaging protocols for assessing inflammation in atherosclerosis: suggestions for improvement. *J Nucl Med* 56:552–559. <https://doi.org/10.2967/jnumed.114.142596>

47. Toczek J, Wu J, Hillmer AT, Han J, Esterlis I, Cosgrove KP et al (2020) Accuracy of arterial [¹⁸F]-Fluorodeoxyglucose uptake quantification: A kinetic modeling study. *J Nucl Cardiol*. <https://doi.org/10.1007/s12350-020-02055-x> (Epub ahead of print on 10 February 2020)
48. Rudd JHF, Myers KS, Bansilal S, Machac J, Pinto CA, Tong C et al (2008) Atherosclerosis inflammation imaging with ¹⁸F-FDG PET: carotid, iliac, and femoral uptake reproducibility, quantification methods, and recommendations. *J Nucl Med* 49:871–878. <https://doi.org/10.2967/jnumed.107.050294>
49. Bucerius J, Hyafil F, Verberne HJ, Slart RHJA, Lindner O, Sciagra R et al (2016) Position paper of the Cardiovascular Committee of the European Association of Nuclear medicine (EANM) on PET imaging of atherosclerosis. *Eur J Nucl Med Mol Imaging* 43:780–792. <https://doi.org/10.1007/s00259-015-3259-3>
50. Lawal IO, Mokoala KG, Popoola GO, Lengana T, Ankrah AO, Stoltz AC et al (2019) Impact of optimized PET imaging conditions on ¹⁸F-FDG uptake quantification in patients with apparently normal aortas. *J Nucl Cardiol*. <https://doi.org/10.1007/s12350-019-01833-6> (Epub ahead of print on 06 August 2019)
51. Lawal IO, Ankrah AO, Stoltz AC, Sathekge MM (2019) Radionuclide imaging of inflammation in atherosclerotic vascular disease among people living with HIV infection: current practice and future perspective. *Eur J Hybrid Imaging* 3:5. <https://doi.org/10.1186/s41824-019-0053-7>
52. Zanni MV, Toribio M, Wilks MQ, Lu MT, Burdo TH, Walker J et al (2017) Application of a novel CD206+ macrophage-specific arterial imaging strategy in HIV-infected individuals. *J Infect Dis* 215:1264–1269. <https://doi.org/10.1093/infdis/jix095>
53. Stroup SP, Kane CJ, Farchschchi-Heydari S, James CM, Davis CH, Wallace AM et al (2012) Preoperative sentinel lymph node mapping of the prostate using PET/CT fusion imaging and Ga-68-labeled tilmanocept in an animal model. *Clin Exp Metastasis* 29:673–680. <https://doi.org/10.1007/s10585-012-9498-9>
54. Qin Z, Hoh CK, Hall DJ, Vera DR (2015) A tri-modal molecular imaging agent for sentinel lymph node mapping. *Nucl Med Biol* 42:917–922. <https://doi.org/10.1016/j.nucmedbio.2015.07.011>

55. Ntsekhe M, Mayosi BM (2013) Tuberculous pericarditis with and without HIV. *Heart Fail Rev* 18:367–373. <https://doi.org/10.1007/s10741-012-9310-6>
56. Heidenreich PA, Eisenberg MJ, Kee LL, Somelofski CA, Hollander H, Schiller NB et al (1995) Pericardial effusion in AIDS: incidence and survival. *Circulation* 92:3229–3234. <https://doi.org/10.1161/01.CIR.92.11.3229>
57. Thienemann F, Sliwa K, Rockstroh JK (2013) HIV and the heart: the impact of antiretroviral therapy: a global perspective. *Eur Heart J* 34:3538–3546. <https://doi.org/10.1093/eurheartj/ehs388>
58. Ntsekhe M, Hakim J (2005) Impact of human immunodeficiency virus infection on cardiovascular disease in Africa. *Circulation* 112:3602–3607. <https://doi.org/10.1161/CIRCULATIONAHA.105.549220>
59. Pawlowski A, Jansson M, Sköld M, Rottenberg ME, Källenius G (2012) Tuberculosis and HIV co-infection. *PLoS Pathog* 8:e1002464. <https://doi.org/10.1371/journal.ppat.1002464>
60. Selwyn PA, Hartel D, Lewis VA, Schoenbaum EE, Vermund SH et al (1989) A prospective study of the risk of tuberculosis among intravenous drug users with human immunodeficiency virus infection. *N Engl J Med* 320:545–550. <https://doi.org/10.1056/NEJM198903023200901>
61. Aaron L, Saadoun D, Calatroni I, Launay O, Mémain N, Vincent V et al (2004) Tuberculosis in HIV-infected patients: a comprehensive review. *Clin Microbiol Infect* 10:388–398. <https://doi.org/10.1111/j.1469-0691.2004.00758.x>
62. Maartens G, Wilkinson RJ (2007) Tuberculosis. *Lancet* 370:2030–2043. [https://doi.org/10.1016/S1406-6736\(07\)61262-8](https://doi.org/10.1016/S1406-6736(07)61262-8)
63. Gounden S, Perumal R, Magula NP (2018) Extrapulmonary tuberculosis in the setting of HIV hyperendemicity at a tertiary hospital in Durban, South Africa. *South Afr J Infect Dis* 33:57–64. <https://doi.org/10.1080/23120053.2017.1403207>
64. Isiguzo G, De Bruyn E, Howlett P, Ntsekhe M (2020) Diagnosis and management of tuberculous pericarditis: what is new? *Curr Cardiol Rep* 22:2. <https://doi.org/10.1007/s11886-020-1254-1>
65. Mayosi BM, Wiysonge CS, Ntsekhe M, Volmink JA, Gumedze F, Maartens G et al (2006) Clinical characteristics and initial management of patients with tuberculous

- pericarditis in the HIV era: the investigation of the management of pericarditis in Africa (IMPI Africa) registry. *BMC Infect Dis* 6:2. <https://doi.org/10.1186/1471-2334-6-2>
66. Alajaji W, Xu B, Sripariwuth A, Menon V, Kumar A, Schleicher M et al (2018) Noninvasive multimodality imaging for the diagnosis of constrictive pericarditis: a contemporary review. *Circ Cardiovasc Imaging* 11:e007878. <https://doi.org/10.1161/CIRCIMAGING.118.007878>
67. Lawal I, Sathekge M (2016) F-18 FDG PET/CT imaging of cardiac and vascular inflammation and infection. *Bri Med Bullet* 120:55–74. <https://doi.org/10.1093/bmb/ldw035>
68. Dong A, Dong H, Wang Y, Cheng C, Zuo C, Lu J (2013) ¹⁸F-FDG PET/CT in differentiating acute tuberculous from idiopathic pericarditis: preliminary study. *Clin Nucl Med* 38:e160–e165. <https://doi.org/10.1097/RLU.0b013e31827a2537>
69. Mayosi BM, Wiysonge CS, Ntsekhe M, Gumede F, Volmink JA, Maartens G et al (2008) Mortality in patients treated for tuberculous pericarditis in Sub-Saharan Africa. *S Afr Med J* 98:36–40
70. Kim MS, Kim EK, Choi JY, Oh JK, Chang SA (2019) Clinical utility of [¹⁸F]FDG-PET/CT in pericardial disease. *Curr Cardiol Rep* 21:107. <https://doi.org/10.1007/s11886-019-1193-x>
71. James OG, Christensen JD, Wong TZ, Borges-Neto S, Kowek LM (2011) Utility of FDG PET/CT in inflammatory cardiovascular disease. *Radiographics* 31:1271–1286. <https://doi.org/10.1148/rg.31510522>
72. Testempassi E, Kubota K, Morooka M, Ito K, Masuda-Miyata Y, Yamashita H et al (2010) Constrictive tuberculous pericarditis diagnosed using ¹⁸F-fluorodeoxyglucose positron emission tomography: a report of two cases. *Ann Nucl Med* 24:421–425. <https://doi.org/10.1007/s12149-010-0365-y>
73. Lawal I, Fourie B, Mathebula M, Moagi I, Lengana T, Moeketsi N et al (2019) FDG-PET/CT as a non-invasive biomarker for assessing adequacy of treatment and predicting relapse in patients treated for pulmonary tuberculosis. *J Nucl Med*. <https://doi.org/10.2967/jnumed.119.233783> (Epub ahead of print on August 26, 2019)

74. Malherbe ST, Shenai S, Ronacher K, Loxton AG, Dolganov G, Kriel M et al (2016) Persisting positron tomography lesion activity and *Mycobacterium tuberculosis* mRNA after tuberculosis cure. *Nat Med* 22:1094–1100. <https://doi.org/10.1038/nm.4177>
75. Malherbe ST, Chen RY, Dupont P, Kant I, Kriel M, Loxton AG et al (2020) Quantitative ¹⁸F-FDG PET-CT scan characteristics correlate with tuberculosis treatment response. *EJNMMI Res* 10:8. <https://doi.org/10.1186/s13550-020-0591-9>
76. Malherbe ST, Dupont P, Kant I, Ahlers P, Kriel M, Loxton AG et al (2018) A semi-automatic technique to quantify complex tuberculous lung lesions on ¹⁸F-fluorodeoxyglucose positron emission tomography/computerized tomography images. *EJNMMI Res* 8:55. <https://doi.org/10.1186/s13550-018-0411-7>
77. Ankrah AO, van der Werf TS, de Vries EF, Dierckx RA, Sathekge MM, Glaudemans AW (2016) PET/CT imaging of *Mycobacterium tuberculosis* infection. *Clin Transl Imaging* 4:131–144. <https://doi.org/10.1007/s40336-016-0164-0>
78. Sathekge M, Maes A, Kgomo M, Stoltz A, Van de Wiele C (2011) Use of ¹⁸F-FDG PET to predict response to first-line tuberculostatics in HIV-associated tuberculosis. *J Nucl Med* 52:880–885. <https://doi.org/10.2967/jnumed.110.083709>
79. Sathekge M, Maes A, D'Asseler Y, Vorster M, Gongxeka H, Van de Wiele C (2012) Tuberculous lymphadenitis: FDG PET and CT findings in responsive and nonresponsive disease. *Eur J Nucl Med Mol Imaging* 39:1184–1190. <https://doi.org/10.1007/s00259-012-2115-y>
80. Lawal I, Zeevaart J, Ebenhan T, Ankrah A, Vorster M, Kruger HG, Govender T et al (2017) Metabolic imaging of infection. *J Nucl Med* 58:1727–1732. <https://doi.org/10.2967/jnumed.117.191635>
81. Sathekge MM, Ankrah AO, Lawal I, Vorster M (2018) Monitoring response to therapy. *Semin Nucl Med* 48:166–181. <https://doi.org/10.1053/j.semnuclmed.2017.10.004>
82. Dureja S, Sen IB, Acharya S (2014) Potential role of F-18 FDG PET-CT as an imaging biomarker for the noninvasive evaluation in uncomplicated skeletal tuberculosis: a prospective clinical observational study. *Eur Spine J* 23:2449–2454. <https://doi.org/10.1007/s00586-014-3483-8>

83. Ozmen O, Koksai D, Ozcan A, Tatci E, Gokcek A (2014) Decreased metabolic uptake in tuberculous pericarditis indicating response to antituberculous therapy on FDG PET/CT. *Clin Nucl Med* 39:917–919. <https://doi.org/10.1097/RLU.0000000000000044> 3
84. Pham TV, Torres M (2015) Human immunodeficiency virus infection-related heart disease. *Emerg Med Clin N Am* 33:613–622. <https://doi.org/10.1016/j.em.2015.04.009>
85. Anderson DW, Virmani R, Reilly JM, O’Leary T, Cunnion RE, Robinowitz M et al (1988) Prevalent myocarditis at necropsy in the acquired immunodeficiency syndrome. *J Am Coll Cardiol* 11:792–799. [https://doi.org/10.1016/0735-1097\(88\)90213-6](https://doi.org/10.1016/0735-1097(88)90213-6)
86. Barbaro G (2001) Cardiovascular manifestations of HIV infection. *J R Soc Med* 94:348–390. <https://doi.org/10.1177/014107680109400804>
87. Bruno R, Socchi P, Filice G (2003) Overview on the incidence and the characteristics of HIV-related opportunistic infections and neoplasms of the heart: impact of highly active antiretroviral therapy. *AIDS* 17(Suppl 1):S83–S87. <https://doi.org/10.1097/00002030-200304001-00012>
88. Herskowitz A, Wu TC, Willoughby SB, Vlahov D, Ansari AA, Beschoner WE et al (1994) Myocarditis and cardiotropic viral infection associated with severe left ventricular dysfunction in late-stage infection with human immunodeficiency virus. *J Am Coll Cardiol* 24:1025–1032. [https://doi.org/10.1016/0735-1097\(94\)90865-6](https://doi.org/10.1016/0735-1097(94)90865-6)
89. Syed FF, Ntsekhe M, Gumedze F, Badri M, Mayosi BM (2014) Myopericarditis in tuberculous pericardial effusion: prevalence, predictors and outcome. *Heart* 100:135–139. <https://doi.org/10.1136/heart.jnl-2013-30478.6>
90. Elbadawi A, Elgendy IY, Ha LD, Mentias A, Ogunbayo GO, Tahir MW et al (2018) National trends and outcomes of endomyocardial biopsy for patients with myocarditis: from the National inpatient sample database. *J Cardiac Fail* 24:337–341. <https://doi.org/10.1016/j.cardfail.2018.03.013>
91. Chen W, Jeudy J (2019) Assessment of myocarditis: cardiac MR, PET/CT, or PET/MR? *Curr Cardiol Rep* 21:76. <https://doi.org/10.1007/s11886-019-1158-0>
92. Lurz P, Luecke C, Eitel I, Föhrenbach F, Frank C, Grothoff M et al (2016) Comprehensive cardiac magnetic resonance imaging in patients with suspected myocarditis: the MyoRacer Trial. *J Am Coll Cardiol* 67:1800–1811. <https://doi.org/10.1016/j.jacc.2016.02.013>

93. Friedrich MG, Sechtem U, Schulz-Menger J, Holmvang G, Alakija P, Cooper LT et al (2009) Cardiovascular magnetic resonance in myocarditis: a JACC White Paper. *J Am Coll Cardiol* 53:1475–1487. <https://doi.org/10.1016/j.jacc.2009.02.007>
94. Chareonthaitawee P, Beanlands RS, Chen W, Dorbala S, Miller EJ, Murthy VL et al (2017) Joint SNMMI-ASNC expert consensus document on the role of ¹⁸F-FDG PET/CT in cardiac sarcoid detection and therapy monitoring. *J Nucl Med* 58:1341–1353. <https://doi.org/10.2967/jnumed.117.196287>
95. Clément A, Boutley H, Poussier S, Pieson J, Lhuillier M, Kolodziej A et al (2018) A 1-week extension of a ketogenic diet provides a further decrease in myocardial ¹⁸F-FDG uptake and a high detectability of myocarditis with FDG-PET. *J Nucl Cardiol*. <https://doi.org/10.1007/s12350-018-1404-7> (Epub ahead of print on August 20, 2018)
96. Werner RA, Wakabayashi H, Bauer J, Schütz C, Zechmeister C, Hayakawa N et al (2019) Longitudinal ¹⁸F-FDG PET imaging in a model of autoimmune myocarditis. *Eur Heart J Cardiovasc Imaging* 20:467–474. <https://doi.org/10.1093/ehjci/jeu119>
97. Ozawa K, Funabashi N, Daimon M, Takaoka H, Takano H, Uehara M et al (2013) Determination of optimum periods between onset of suspected acute myocarditis and ¹⁸F-fluorodeoxyglucose positron emission tomography in the diagnosis of inflammatory left ventricular myocardium. *Int J Cardiol* 169:196–200. <https://doi.org/10.1016/j.ijcard.2013.08.098>
98. Takano H, Nakagawa K, Ishio N, Daimon M, Daimon M, Kobayashi Y et al (2008) Active myocarditis in a patient with chronic active Epstein-Barr virus infection. *Int J Cardiol* 130:e11–13. <https://doi.org/10.1016/j.ijcard.2007.07.040>
99. Tanimura M, Dohi K, Imanaka-Yoshida K, Omori T, Moriwaki K, Nakamori S et al (2017) Fulminant myocarditis with prolonged active lymphocytic infiltration after hemodynamic recovery. *Int Heart J* 58:294–297. <https://doi.org/10.1536/ihj.16-225>
100. Piriou N, Sassier J, Pallardy A, Serfaty JM, Trochu JN (2015) Utility of cardiac FDG-PET imaging coupled to magnetic resonance for the management of an acute myocarditis with noninformative endomyocardial biopsy. *Eur Heart J Cardiovasc Imaging* 16:574. <https://doi.org/10.1093/ehjci/jeu319>

101. Moeriwaki K, Dohi K, Omori T, Tanimura M, Sugiura E, Nakamori S et al (2017) A survival case of fulminant right-side dominant eosinophilic myocarditis. *Int Heart J* 58:459–462. <https://doi.org/10.1536/ihj.16-338>
102. Rischpler C, Woodard PK (2019) PET/MR imaging in cardiovascular imaging. *PET Clin* 14:233–244. <https://doi.org/10.1016/j.cpet.2018.12.005>
103. Abgral R, Dweck MR, Trivieri MG, Robson PM, Karakatsanis N, Mani V et al (2017) Clinical utility of combined FDG-PET/MR to assess myocardial disease. *JACC Cardiovasc Imaging* 10:594–597. <https://doi.org/10.1016/j.jcmg.2016.02.029>
104. von Olshausen G, Hyafil F, Langwieser N, Laugwitz KL, Schwaiger M, Ibrahim T (2014) Detection of acute inflammatory myocarditis in Epstein Barr virus infection using hybrid ¹⁸F-fluoro-deoxyglucose-positron emission tomography/magnetic resonance imaging. *Circulation* 130:925–926. <https://doi.org/10.1161/CIRCULATION.114.011000>
105. Nensa F, Poeppel TD, Krings P, Schlosser T (2014) Multiparametric assessment of myocarditis using simultaneous positron emission tomography/magnetic resonance imaging. *Eur Heart J* 35:2173. <https://doi.org/10.1093/eurheartj/ehu086>
106. Nensa F, Kloth J, Tezgah E, Poeppel TD, Heusch P, Goebel J et al (2018) Feasibility of FDG-PET in myocarditis: comparison to CMR using integrated PET/MRI. *J Nucl Cardiol* 25:785–794. <https://doi.org/10.1007/s12350-016-0616-y>
107. Oka S, Okudaira H, Ono M, Schuster DM, Goodman MM, Kawai K et al (2014) Differences in transport mechanisms of trans-1-amino-3-[¹⁸F]fluorocyclobutanecarboxylic acid in inflammation, prostate cancer, and glioma cells: comparison with L-[methyl-¹¹C]methionine and 2-deoxy-2-[¹⁸F]fluoro-D-glucose. *Mol Imaging Biol* 16:322–329. <https://doi.org/10.1007/s11307-013-0693-0>
108. Maya Y, Werner RA, Schütz C, Wakabayashi H, Samnick S, Lapa C et al (2016) ¹¹C-methionine PET of myocardial inflammation in a rat model of experimental autoimmune myocarditis. *J Nucl Med* 57:1985–1990. <https://doi.org/10.2967/jnumed.116.174045>
109. Muñoz-Moreno MF, Ryan P, Alvaro-Meca A, Valencia J, Tamayo E, Resino S (2019) National temporal trend analysis of infective endocarditis among patients infected

- with HIV in Spain (1997–2014): a retrospective study. *J Clin Med* 8:1167. <https://doi.org/10.3390/jcm8081167>
110. Bor DH, Woolhandler S, Nardin R, Bruschi J, Himmelstein DU (2013) Infective endocarditis in the U.S., 1998–2009: a nationwide study. *PLoS ONE* 8:e60033. <https://doi.org/10.1371/journal.pone.0060033>
 111. Polanco A, Itagaki S, Chiang Y, Chikwe J (2014) Changing prevalence, profile, and outcomes of patients with HIV undergoing cardiac surgery in the United States. *Am Heart J* 167:363–368. <https://doi.org/10.1016/j.ahj.2013.09.021>
 112. Wilson LE, Thomas DL, Astemborski J, Freedman TL, Vlahov D (2002) Prospective study of infective endocarditis among injection drug users. *J Infect Dis* 185:1761–1766. <https://doi.org/10.1086/340827>
 113. Koegelenberg CF, Doubell AF, Orth H, Reuter H (2003) Infective endocarditis in the Western Cape Province of South Africa: a three-year prospective study. *QJM* 93:217–225. <https://doi.org/10.1093/qjmed/hcg028>
 114. Longo-Mbenza B, Tondoungu K, Muvova D, Phuati MB, Seghers KV, Kestelot H (1995) A clinical study of cardiac manifestations related to acquired immunodeficiency syndrome (AIDS) in Kinshasa [in French]. *Arch Mal Coeur Vaiss* 88:1437–1443
 115. Spijkerman IJB, van Ameijden EJC, Mientges GHC, Coutinho RA, van den Hoek A (1996) Human immunodeficiency virus infection and other risk factors for skin abscess and endocarditis among injection drug users. *J Clin Epidemiol* 49:1149–1154
 116. Furuno JP, Johnson JK, Schweizer ML, Uche A, Stine OC, Shurland SM et al (2011) Community-associated methicillin resistant *Staphylococcus aureus* bacteremia and endocarditis among HIV patients: a cohort study. *BMC Infect Dis* 11:298. <https://doi.org/10.1186/1471-2334-11-298>
 117. Habib G, Lancellotti P, Antunes MJ, Bongiorni MG, Casalta JP, Zotti FD et al (2015) 2015 ESC guidelines for the management of infective endocarditis. *Eur Heart J* 36:3075–3123. <https://doi.org/10.1093/eurheartj/ehv319>
 118. Nel SH, Naidoo DP (2014) An echocardiographic study of infective endocarditis, with special reference to patients with HIV. *Cardiovasc J Afr* 25:50–57. <https://doi.org/10.5830/CVJA-2013-084>

119. Tsabedze N, Vachiat A, Zachariah D, Manga P (2018) A new face of cardiac emergencies: human immunodeficiency virus related cardiac disease. *Cardiol Clin* 36:161–170. <https://doi.org/10.1016/j.ccl.2017.09.005>
120. Cammarosano C, Lewis W (1985) Cardiac lesions in acquired immune deficiency syndrome (AIDS). *J Am Coll Cardiol*. [https://doi.org/10.1016/S0735-1097\(85\)80397-1](https://doi.org/10.1016/S0735-1097(85)80397-1)
121. Cecchi E, Imazio M, Tidu M, Forno D, De Rosa FG, Dal Conte I et al (2007) Infective endocarditis in drug addicts: role of HIV infection and the diagnostic accuracy of Duke criteria. *J Cardiovasc Med* 8:169–175. <https://doi.org/10.2459/01.JCM.0000260824.14596.86>
122. Gebo KA, Burkey MD, Lucas GM, Moore RD, Wilson LE (2006) Incidence of, risk factors for, clinical presentation, and 1-year outcomes of infective endocarditis in an urban HIV cohort. *J Acquir Immune Defic Syndr* 43:426–432. <https://doi.org/10.1097/01.qai.0000243120.67529.78>
123. Cantoni V, Sollini M, Green R, Berchiolli R, Lazzeri E, Mannarino T et al (2018) Comprehensive meta-analysis on [¹⁸F]FDG PET/CT and radiolabeled leucocyte SPECT-SPECT/CT imaging in infectious endocarditis and cardiovascular electronic device infections. *Clin Transl Imaging* 6:3–18. <https://doi.org/10.1007/s40336-018-0265-z>
124. Gomes A, Glaudemans AWJM, Touw DJ, van Melle JP, Willems TP, Maass AH et al (2017) Diagnostic value of imaging in infective endocarditis: a systematic review. *Lancet Infect Dis* 17:e1–e14. [https://doi.org/10.1016/S1473-3099\(16\)30141-4](https://doi.org/10.1016/S1473-3099(16)30141-4)
125. Habib G, Erba PA, Iung B, Donal E, Cosyns B, Leroche C et al (2019) Clinical presentation, aetiology and outcome of infective endocarditis. Results of the ESC-EORP EURO-ENDO (European infective endocarditis) registry: a prospective cohort study. *Eur Heart J* 40:3222–3233. <https://doi.org/10.1093/eurheartj/ehz620>
126. Mathieu C, Mikail N, Benali K, Iung B, Duval X, Nataf P et al (2017) Characterization of ¹⁸F-fluorodeoxyglucose uptake pattern in noninfected prosthetic heart valves. *Circ Cardiovasc Imaging* 10:e005585. <https://doi.org/10.1161/CIRCIMAGING.116.005585>
127. Roque A, Pizzi MN, Fernández-Hidalgo N, Permanyer E, Cuellar-Calabria H, Romero-Farina G et al (2020) Morphometabolic post-surgical patterns of non-infected

- prosthetic heart valves by [¹⁸F]FDG PET/CTA: “normality” is a possible diagnosis. *Eur Heart J Cardiovasc Imaging* 21:24–33. <https://doi.org/10.1093/ehjci/jez222>
128. Essop MR, Nkomo VT (2005) Rheumatic and nonrheumatic valvular heart disease: epidemiology, management, and prevention in Africa. *Circulation* 112:3584–3591. <https://doi.org/10.1161/CIRCULATIONAHA.105.539775>
129. Curry C, Zuhlke L, Mocumbi A, Kennedy N (2018) Acquired heart disease in low-income and middle-income countries. *Arch Dis Child* 103:73–77. <https://doi.org/10.1136/archdischild-2016-312521>
130. Manafe N, Ngale A, Biquiza N, Zimba I, Majid N, Mocumbi AO (2019) Need for active cardiovascular screening in HIV-infected children under antiretroviral therapy in Africa. *Cardiovasc Diagn Ther* 9:68–72. <https://doi.org/10.21037/cdt.2018.09.18>
131. Hovis IW, Namuyonga J, Kisitu GP, Ndagire E, Okello E, Longenecker CT et al (2019) Decreased prevalence of rheumatic heart disease confirmed among HIV-positive youth. *Pediatr Infect Dis J* 38:406–409. <https://doi.org/10.1097/INF.00000000000002161>
132. Gleason B, Mirembe G, Namuyonga J, Okello E, Lwabi P, Lubega I et al (2016) Prevalence of latent rheumatic heart disease among HIV-infected children in Kampala, Uganda. *J Acquir Immune Defic Syndr* 71:196–199. <https://doi.org/10.1097/PHH.00000000000000419>
133. Martin C, Castaigne C, Tondeur M, Flamen P, De Wit S (2013) Role and interpretation of fluorodeoxyglucose-positron emission tomography/computed tomography in HIV-infected patients with fever of unknown origin: a prospective study. *HIV Med* 14:455–462. <https://doi.org/10.1111/hiv.12030>
134. Lawal IO, Popoola GO, Lengana T, Ankrah AO, Ebenhan T, Sathekge MM (2019) Diagnostic utility of ¹⁸F-FDG PET/CT in fever of unknown origin among patients with end-stage renal disease treated with renal replacement therapy. *Hell J Nucl Med* 22:70–75. <https://doi.org/10.1967/s002449910962>
135. Sathekge M, Stoltz A, Gheysens O (2015) Rheumatic fever: a forgotten but still existing cause of fever of unknown origin detected on FDG PET/CT. *Clin Nucl Med* 40:250–252. <https://doi.org/10.1097/RLU.00000000000000619>

136. Nagesh CM, Saxena A, Patel C, Karunanithi S, Nadig M, Malhotra A (2015) The role of ^{18}F fluorodeoxyglucose positron emission tomography (^{18}F -FDG-PET) in children with rheumatic carditis and chronic rheumatic heart disease. *Nucl Med Rev Cent East Eur* 18:25–28. <https://doi.org/10.5603/NMR.2015.0006>

Chapter 4

Arterial inflammation in young patients with human immunodeficiency virus infection: A cross-sectional study using ^{18}F -FDG PET/CT

Ismaheel O. Lawal, MD,^a Alfred O. Ankrah, MD,^{a,b} Gbenga O. Popoola, MD,^c Thabo Lengana, MD,^a and Mike M. Sathekge, MD, PhD^a

- a. Department of Nuclear Medicine, University of Pretoria and Steve Biko Academic Hospital, Pretoria, South Africa
- b. Department of Nuclear Medicine and Molecular Imaging, University Medical Center Groningen, University of Groningen, Groningen, The Netherlands
- c. Department of Epidemiology and Community Health, University of Ilorin, Ilorin, Nigeria

J Nucl Cardiol. 2019;26(4):1258-1265.

Abstract

Background. HIV infection is associated with the risk of development of atherosclerosis at a younger age. We compared arterial inflammation in HIV-infected and HIV-uninfected patients with otherwise low-risk factors for cardiovascular disease (CVD) using ^{18}F -FDG PET/CT.

Methods. 242 patients aged 18–40 years with low-risk factors for CVD consisting of 121 HIV-infected patients and 121 HIV-uninfected age- and gender-matched controls were studied, mean age = 34.95 ± 5.46 years. We calculated and compared the target-to-background ratio of ^{18}F -FDG uptake in ascending aorta of HIV-infected and non-infected patients.

Results. Median CD4 count and viral load were 375.5 cells/mm³ (range 2-1094) and 6391.00 copies/mL (range 24-1,348,622), respectively. There was slightly higher but significant overlap in the TBR between HIV-infected group compared with control (1.22, 0.87-2.02 vs. 1.12, 0.38-1.40, $P < 0.001$). TBR was neither affected by CD4 count levels nor the presence or absence of detectable viremia. We also found no significant difference in TBR between male and female patients with HIV infection. We found a weak positive correlation between TBR and CD4 count, TBR and duration of HIV infection, and a very weak negative correlation between TBR and viral load. There was no significant difference in TBR between patients on HAART and those not yet commenced on therapy.

Conclusion. Marginally higher TBR with a significant overlap exist in HIV-infected patients compared with control. Arterial ^{18}F -FDG uptake is not affected by the CD 4 count, viral load, gender, or duration of HIV infection.

Key Words

^{18}F -FDG, PET/CT, HIV, inflammation, cardiovascular disease

Abbreviations

HAART	Highly active antiretroviral therapy
CD 4	Cluster of differentiation 4
CT	Computed tomography
CVD	Cardiovascular disease
FDG	Fluorodeoxyglucose
HIV	Human immunodeficiency virus
Hs-CRP	High-sensitivity C-reactive protein
PET	Positron emission tomography
SUV	Standardized uptake value
TBR	Target-to-background ratio

INTRODUCTION

Successful rollout of highly active antiretroviral therapy (HAART) in most regions of the world has led to a significant reduction in human immunodeficiency virus (HIV)-related mortality.¹ This reduction in mortality is partly due to the decrease in the incidence HIV-associated infections, as well as HIV-defining cancers. Consequently, HIV infection is now recognized as a chronic medical condition.² Many observational studies have shown higher rates of cardiovascular diseases (CVD) among HIV-infected individuals compared with HIV-uninfected populations.^{3,4} The pathophysiological basis of this increased risk is not entirely understood at present. Chronic immune activation in long-standing HIV infection is suspected to be the cause of arterial inflammation seen in HIV patients.

Fluorine-18 fluorodeoxyglucose positron emission tomography/computed tomography (¹⁸F-FDG PET/CT) has been used in the evaluation of several inflammatory conditions of the cardiovascular system.⁵⁻⁷ Using arterial ¹⁸F-FDG uptake as a surrogate for vascular inflammation, a few studies have reported a higher incidence of vascular inflammation in HIV-infected cohorts compared to HIV-uninfected control groups.^{8,9} These studies are limited by their modest patient populations. More importantly, all these studies were done in older patient populations with the average age greater than 50 years. HIV-associated CVD is, however, known to occur earlier, below the age of 50 years.¹⁰ This may suggest that vascular inflammation, an early process in the pathogenesis of CVD, is present at even a younger age among HIV patients. The aim of this study was, therefore, to compare arterial inflammation in young HIV-infected with HIV-uninfected individuals with otherwise low or no risk for CVD using ¹⁸F-FDG PET/CT.

METHODS

Patients

We reviewed the scans of HIV patients imaged between September 2015 and June 2017 referred for oncological or inflammatory indications. We included patients aged between 18 and 40 years with no abnormality (finding suggestive of malignancy or inflammation/infection). Our exclusion criteria were patients with the following:

- Systemic hypertension (Systolic pressure >140 mmHg, Diastolic pressure > 90 mmHg) documented.

- A history of type I or type II diabetes mellitus with/without use of oral antidiabetic agent or insulin.
- A history of acute or chronic renal failure.
- Vascular calcification noted on the CT component of the PET/CT study.
- A history cerebrovascular or cardiac/cardiovascular disease.
- Suspected or confirmed vasculitis.
- Smokers (at least one stick of cigarette per day).
- A history of peripheral vascular disease.
- Impaired lipid profile (Total cholesterol \leq 5 mmol/L, low-density lipoprotein (LDL) cholesterol \leq 3 mmol/L, high-density lipoprotein (HDL) cholesterol $>$ 1 mmol/L and Triglyceride $<$ 1.7 mmol/L).
- Statins use.

One hundred and twenty-one HIV-positive patients met our inclusion and exclusion criteria. We searched the electronic database of the hospital to identify HIV-negative patients who had ^{18}F -FDG PET/CT scans from September 2015 and June 2017. We sought for patients with no abnormality detected on their images (inflammation/infection or malignancy), who met all the inclusion and exclusion criteria which we used for the HIV-positive patients. We selected patients from this group to be used as controls. A total of 274 HIV-negative individuals satisfied these criteria. An age- and gender-matched control was identified from the pool of the HIV negative patients for each of the HIV-positive subjects. In total, 242 patients consisting of 121 HIV-positive patients and 121 HIV-negative patients (matched controls) were studied.

For each of the HIV-positive patients, the duration since diagnosis of HIV infection, whether or not the patient was on ART, CD 4 count, and viral load tested within four weeks of ^{18}F -FDG PET/CT were recorded.

FDG PET/CT Imaging

Imaging was done as previously reported.¹¹ Briefly, all patients fasted for a minimum of six hours. Blood sugar before imaging was $<$ 11.0 mmol/L in all patients. The activity of ^{18}F -FDG administered was weight-based, and calculated using the formula: Activity administered = [(body weight in Kg \div 10)+1] x 37 Mega Becquerel (MBq). Imaging was acquired on a Biograph 40 Truepoint PET/CT scanner (Siemens Medical Solution, Illinois, USA). Intravenous contrast,

100 mL Omnipaque 350 (GE Healthcare, Wisconsin, USA) was given after a scan delay time of 80 seconds. CT parameters were adjusted for patients' weight (120KeV, 40-150 mAs) with a section width of 5 mm and pitch of 0.8. Vertex to midhigh PET imaging was acquired in 3D mode at 3 minutes per bed position. Computed tomography data were used for attenuation correction. Image reconstruction was done with the ordered subset expectation maximization iterative reconstruction algorithm (4 iterations, 8 subsets). A Gaussian filter was applied at 5.0 mm full width at half maximum (FWHM).

Image Analysis

All images were analyzed by a single investigator who was blinded to the HIV status of the patients. Image analysis was done on a dedicated workstation equipped with a Syngo software (Siemens medical solutions, Illinois, USA). Image analysis was done as previously reported by Subramanian et al.⁸ Briefly, the investigator drew five circular regions of interest enclosing the arterial wall at 5 mm intervals on the ascending aorta and recorded the maximum standardized uptake values (SUVmax). The mean of the SUVmax measurements of each patient was calculated to obtain the mean SUVmax aorta. Background activity was obtained by drawing five circular regions of interest within the lumen of the superior vena cava (SVC) to obtain SUV at the same levels as for the aorta. The mean of the SUV measurement taken within the SVC was then calculated and used as the background. We calculated target-to-background ratio (TBR) using the formula: $TBR = \text{mean aortic SUV} \div \text{mean SVC SUV}$. TBR was used as a measure of arterial inflammation.

Statistical Analysis

Descriptive statistics of the demographic and clinical characteristics of the study population were done. The independent samples *t* test was used to test for difference in TBR between the HIV-infected group and the control group and also to test if TBR was significantly different between HIV-infected patients with detectable viremia and those whose viral load was below the detectable limit. In addition, a sub-group analysis was done using independent samples *t* test to determine if there was a significant difference between male and female patients. Analysis of variance (ANOVA) was used to test if TBR is significantly different between the HIV-infected

group and control as well as between those HIV-positive patients already on ART and those not yet on ART. The HIV-infected group was sub-categorized in sub-classes based on the CD4 count. Kruskal–Wallis test was used to test for significant difference in TBR between the various groups. Spearman correlation was used to evaluate for correlations between any of CD4 count, viral load, or duration of HIV infection and TBR. The statistical significance level was set at a *P* value of < 0.05. Statistical analysis was done using IBM SPSS Statistics version 21.0 (IBM Corp., Armonk, New York, USA).

RESULTS

Clinical characteristics of the study population are shown in Table 1. A total of 242 patients consisting of 121 HIV-infected patients and 121 HIV-uninfected controls were included, females = 190, males = 52. The mean age of patients was 34.95 ± 5.46 years. At the time of ^{18}F -FDG PET/CT imaging, 81.80% of the HIV-infected patients were already on ART. The group's median CD4 count was 375.50 cells/mm³ with the median time since HIV diagnosis of 42 months. Out of 121 HIV-infected patients, 58 patients had lower than detectable viral loads. In 63 patients with detectable viremia, the median viral load was 6391.00 copies/mL.

Table 1 Characteristics of the study population

Variables	Frequency	Percent
Age (years)		
Mean \pm SD	34.95 \pm 5.46	
Range	18 – 40	
Gender		
Male	52	21.5
Female	190	78.5
ART status		
On ART	99	81.8
Not on ART	22	18.2
CD4 count (cells/mm³)		
Median (Range)	375.50 (2.00 – 1094.00)	
Viral load (copies/mL)		
Median (Range)	6391.00 (24.00 – 1,348,622.00)	
Duration of HIV infection (months)		
Median (Range)	42.00 (1.00 – 156.00)	

SD: Standard deviation; **ART:** Antiretroviral therapy; **CD4:** Cluster of differentiation 4; **HIV:** Human immunodeficiency virus

We found marginally higher, but with a significant overlap in the TBR of the HIV-infected patients compared with control (1.22 ± 0.20 vs 1.12 ± 0.14 , $P < 0.001$), Figure 1. Table 2 shows the distribution of TBR between the HIV-infected patients and the control. No statistically significant difference was seen in the TBR at different CD4 count levels (Table 3). We performed a sub-group analysis to determine the effect of gender on TBR (Table 4). There was higher TBR among males with HIV infection compared to non-infection cohorts ($P = 0.002$). Similarly, HIV-infected females show higher TBR compared to the females in the control group ($P = 0.001$). Among the HIV-infected patients, no significant difference was demonstrated between males and females ($P = 0.727$). Representative images are shown in Figures 2 and 3.

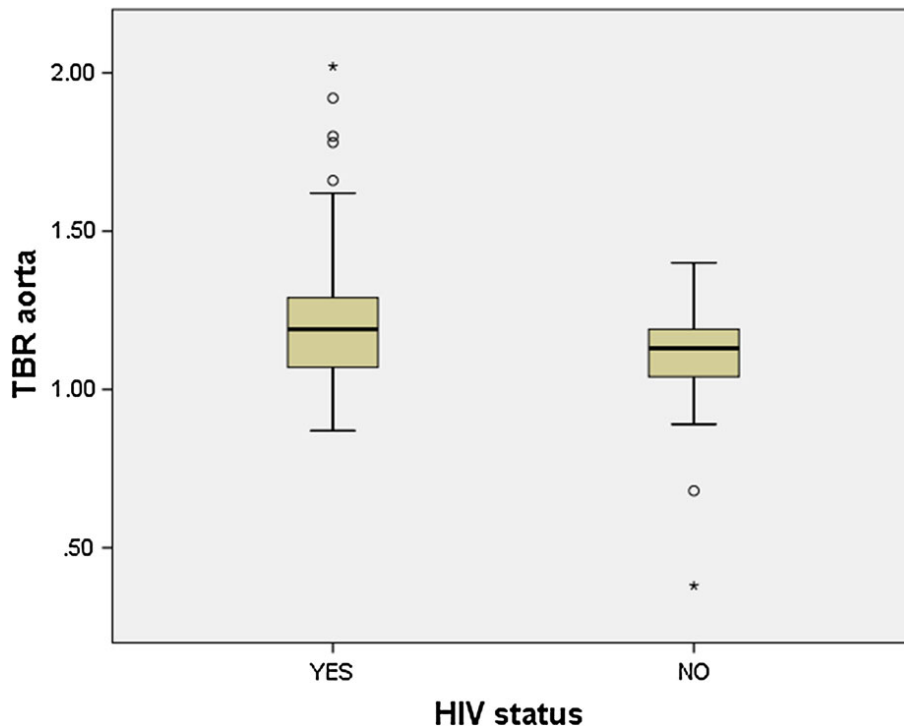


Fig 1 Box plot showing the distribution of TBR in the HIV-infected group and control

Table 2 Comparison of TBR between HIV-infected patients and control group

Variable	HIV-infected	Control	t	p value
TBR				
Mean ± SD	1.22 ± 0.20	1.12 ± 0.14	4.515	<0.001*
Range	0.87 – 2.02	0.38 – 1.40		

t: Independent samples t-test; U: Mann Whitney U test; *: p value < 0.05 (statistically significant); **TBR**: Target-to-background ratio

Table 3: Relationship between TBR and CD4 count level

Variable	CD4 Count				K
	< 200	200 - 350	350 - 500	> 500	
TBR					
Median	1.18	1.23	1.13	1.20	6.707
(Range)	(0.87–2.02)	(1.02-1.78)	(1.01-1.49)	(0.94-1.80)	

K: Kruskal Wallis test; *: p value < 0.05 (statistically significant); TBR: Target-to-background ratio; CD4: Cluster of differentiation 4

Table 4 Sub-group analysis showing the effect of gender on TBR

TBR	HIV-Infected	Control	t	p value
	Mean ± SD	Mean ± SD		
Males				
Mean ± SD	1.24 ± 0.24	1.04 ± 0.18	3.190	0.002*
Females				
Mean ± SD	1.22 ± 0.19	1.15 ± 0.12	3.314	0.001*
<i>t (p value)</i>	<i>0.350 (0.727)</i>	<i>-3.402</i>		<i>(0.001*)</i>

t: Independent samples t-test, *: p value < 0.05 (statistically significant)

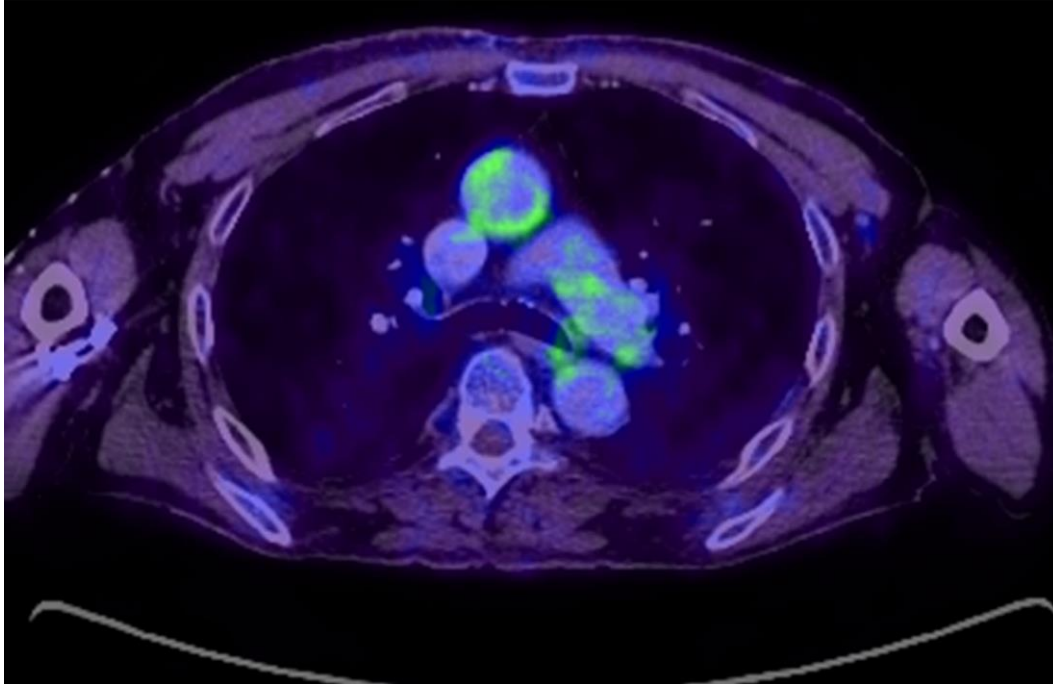


Fig 2 Axial slice of fused PET/CT image of an HIV-infected patient showing increased ¹⁸F-FDG uptake in the wall of the ascending aorta

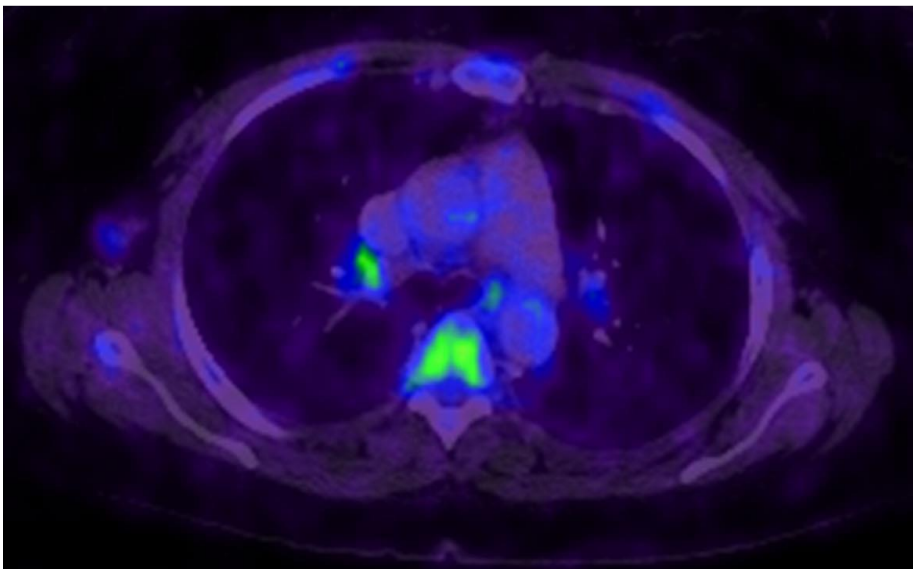


Fig 3 Axial slice of fused PET/CT image of an HIV-negative patient with no significantly increased ¹⁸F-FDG uptake in the wall of the ascending aorta

The viral load in HIV patients did not seem to influence the TBR as both groups (patients with detectable viral load and those with undetectable viral loads) did not show any significant difference in TBR, $P = 0.367$ (Table 5). Table 6 shows a Spearman correlation demonstrating a very weak positive correlation between TBR vs duration of HIV infection, viral load, and CD4 count level. A weak negative correlation was found between TBR and viral load. None of these numerical correlations, however, reached a statistically significant level.

Table 5 The effect of viral load on TBR

Variable	Viral Load		t	p value
	Detectable	LDL		
TBR				
Mean ± SD	1.27 ± 0.29	1.22 ± 0.18	0.908	0.367

t: Independent samples t-test; **LDL**: Lower than detectable limit; **TBR**: Target-to-background ratio

Table 6 Correlation between TBR versus duration of HIV infection, CD4 count and viral load of HIV-infected patients

Variable	TBR	
	r	p value
Duration of HIV (months)	0.088	0.407
CD4 COUNT	0.113	0.238
VIRAL LOAD	-0.138	0.502

r: Spearman correlation coefficient; *: p value <0.05; **HIV**: Human immunodeficiency virus; **TBR**: Target-to-background ratio; **CD4**: Cluster of differentiation 4

We tested whether there was a difference in the TBR among HIV-infected patients on ART, HIV-infected patients not yet on ART, and control group using ANOVA, a significant difference in TBR was found among the three groups, $P < 0.001$ (Table 7). A post hoc analysis revealed that while a difference exists in TBR between the HIV-infected group and control, there was no difference between the two HIV-infected groups (i.e., those patients on ART vs those patients not yet commenced on ART).

Table 7 Effect of ART use on TBR

	On ART	Not on ART	Controls	F	p value
Variable	Mean ± SD	Mean ± SD	Mean ± SD		
TBR	1.27 ± 0.19 ^a	1.21 ± 0.22 ^a	1.12 ± 0.14 ^b	10.308	<0.001*

NB: Different alphabets indicate significant difference using LSD (Least Significant Difference) **post hoc test F:** ANOVA (Analysis of Variance); *: *p* value <0.05; **ART:** Anti-retroviral therapy; **TBR:** Target-to-background ratio

DISCUSSION

Traditionally, individuals below age 40 years are not considered for routine screening for CVD. In this study, with the largest population so far published on the utility of ¹⁸F-FDG PET/CT in the evaluation of arterial inflammation in HIV patients, we found a marginally higher TBR in HIV-infected patients compared to their age- and gender-matched controls. There was, however, a significant overlap in the TBR between the two groups. Subramanian et al⁸ compared aortic TBR of 27 patients with well-controlled HIV infection with two groups of HIV-uninfected controls. TBR was higher in the HIV-infected group compared with HIV-negative group, but comparable to that in the group of patients with established atherosclerotic disease. This suggests that HIV infection may be associated with the same level of vascular inflammation as present in the vessels of those patients with established atherosclerotic disease. Another study with a smaller patient population found slightly higher aortic TBR in HIV-infected patients compared with HIV-negative patients, but the difference was not significant.⁹ Knudsen et al failed to demonstrate any significant difference in aortic TBR between HIV-infected and HIV-negative patients.¹²

¹⁸F-FDG uptake in the arterial wall is a reflection of vascular invasion by activated macrophages. Activated macrophages increase their use of glucose to meet the increased metabolic demand for energy. A study has shown that arterial uptake of ¹⁸F-FDG correlates well with the level of activated macrophage invasion.¹³ Statins have an anti-inflammatory effect on vascular inflammation. However, a study which randomized 40 HIV-infected patients to 1 year of atorvastatin (19 patients) and a placebo (21 patients) did not find any significant difference in changes between the groups after 1 year.¹⁴ In the context of vascular infection or inflammation,

in other settings such as vasculitis, a reduction in PET signal following therapeutic intervention is associated with response to treatment.^{6,15}

We found no significant effect of viral load on TBR. Similarly, CD4 count level did not influence the aortic TBR in our study. Our finding is consistent with the finding of a previous finding in a study by Zanni and colleagues. Zanni et al did not find any significant difference in TBR before, and six months after starting ART.¹⁶ We demonstrated statistically significant differences in TBR among HIV-infected patients on ART, HIV-infected patients not yet on ART and HIV-uninfected control. A post hoc analysis, however, showed that this difference exists between the HIV-infected patients (whether on ART or not) and the HIV-uninfected control. There was no difference in TBR between the two HIV-infected sub-groups. This may suggest that HAART did not appear to affect TBR. The duration of HIV infection also did not appear to significantly influence aortic TBR. These findings may suggest that the risk for vascular inflammation as measured by TBR once established in HIV patients is not modified by the use of HAART. Larger prospective studies are needed to validate this.

Most studies evaluating the utility of ¹⁸F-FDG PET in the detection of vascular inflammation have used longer uptake time (time from ¹⁸F-FDG injection to the start of PET/CT imaging) of about 3 hours.^{8,9,12,14} This retrospective study included patients imaged using standard oncologic/infection protocol where imaging is started earlier at 60 minutes' post-¹⁸F-FDG injection. The likely implication for this is that there could be a lower ¹⁸F-FDG uptake in the arterial wall and high background activity at the time of imaging. We speculate that a later imaging at 2.5 hours or beyond may even demonstrate a more significant difference in the arterial ¹⁸F-FDG uptake between the HIV-infected group and the HIV-uninfected control. Bucerius and colleagues described a higher arterial ¹⁸F-FDG uptake in patients imaged after a longer uptake time (> 145 minutes) compared to patients who were scanned earlier (≥ 97 to ≤ 111 minutes).¹⁷ In their study, while meanTBRmax showed a progressively increasing trend with uptake time, the SUVmax of ¹⁸F-FDG uptake in the aorta decreased with delayed imaging suggesting that improvement in meanTBRmax seen in the study was as a result of better background clearance on late imaging.

Patients included in this study were routinely imaged with intravenous contrast administered. Intravenous contrast, especially within large vessels such as the aorta, may cause up-scaling of PET data on the attenuated corrected images leading to erroneously higher

SUVmax values. Since patients in both groups had intravenous contrast administered for imaging, the effect of over-correction of PET data may not impact significantly on the TBR.

Limitations

Our study has some limitations. The first limitation is its retrospective design. Another drawback is the lack of follow-up to identify which of these young patients eventually developed a frank CVD. Again, imaging in this study was not optimized for arterial ^{18}F -FDG uptake evaluation as it has been described in other studies. A longer uptake time may show higher TBR in HIV-infection patients compared with the control group. Patients included in this study were imaged for inflammation or malignancy. None of these patients showed abnormal ^{18}F -FDG accumulation suggestive of the presence of malignancy or infection/inflammation. The absence of abnormal ^{18}F -FDG accumulation, however, does not entirely rule out the fact that circulating cytokines may have influenced arterial uptake of ^{18}F -FDG uptake in these patients. It is unknown the extent to which this could have impacted on our results.

CONCLUSION

Marginally higher TBR with significant overlap exists in HIV-infected patients compared with controls. Arterial ^{18}F -FDG uptake is not affected by the CD 4 count, viral load, duration of HIV infection, the use of and duration of HAART, and gender.

NEW KNOWLEDGE GAINED

The previous studies have demonstrated higher TBR in older HIV-infected patients in a few studies with modest patient populations compared with HIV-negative population. These studies included patients who have other risk factors for cardiovascular diseases. Our study, on the contrary, focuses on young HIV patients with no or low-risk factors of cardiovascular disease. We demonstrate a marginally increase TBR risk in this group that is unaffected by factors that usually modify HIV-associated conditions.

Acknowledgements

The authors thank the members of staff of the department of Nuclear Medicine, University of Pretoria and Steve Biko Academic Hospital.

Disclosures

Ismaheel O. Lawal, Alfred O. Ankrah, Gbenga O. Popoola, Thabo Lengana, and Mike M. Sathekge declares that they have no conflict of interest.

References

1. Wang H, Wolock TM, Carter A, Nguyen G, Kyu HH, Gakidou E, et al. Estimates of global, regional, and national incidence, prevalence, and mortality of HIV, 1980-2015: the Global of Disease Study 2015. *Lancet HIV*. 2016;3:e361-87.
2. Deeks SG, Lewin SR, Havlir DV. The end of AIDS: HIV infection as a chronic disease. *Lancet*. 2013;382:1525-33.
3. Lang S, Mary-Krause M, Cotte L, Gilquin J, Partisani M, Simon A, et al. Increased risk of myocardial infarction in HIV-infected patients in France, relative to the general population. *AIDS*. 2010;24:1228-30.
4. Islam FM, Wu J, Jansson J, Wilson DP. Relative risk of cardiovascular disease among people living with HIV: a systematic review and meta-analysis. *HIV Med*. 2012;13:453-68.
5. Hammad B, Evans NR, Rudd JHF, Tawakol A. Molecular imaging of atherosclerosis with integrated PET imaging. *J Nucl Cardiol*. 2017;24:938-43.
6. Lawal I, Sathekge M. F-18 FDG PET/CT imaging of cardiac and vascular inflammation and infection. *Br Med Bull*. 2016;120:55-74.
7. Ahmadian A, Pawar S, Govender P, Berman J, Ruberg FL, Miller EJ. The response of FDG uptake to immunosuppressive treatment of FDG PET/CT imaging for cardiac sarcoidosis. *J Nucl Cardiol*. 2017;24:413-24.
8. Subramanian S, Tawakol A, Burdo TH, Abbara S, Wei J, Vijayakumar J, et al. Arterial Inflammation in Patients With HIV. *JAMA*. 2012;308:379-86.
9. Yarasheski KE, Laciny E, Overton ET, Reeds DN, Harrod M, Baldwin S, et al. ¹⁸F-FDG PET-CT imaging detects arterial inflammation and early atherosclerosis in HIV-infected adults with cardiovascular risk factors. *Inflammation*. 2012;9:26. Doi:10.1186/1476-9255-9-26.
10. Boccara F, Lang S, Meuleman C, Ederhy S, Mary-Krause M, Costagliola D, et al. HIV and coronary artery disease: time for better understanding. *J Am Coll Cardiol*. 2013;61:511-23.
11. Lawal I, Lengana T, Ololade K, Boshomane T, Reyneke F, Modiselle M, et al. ¹⁸F-FDG PET/CT in the detection of asymptomatic malignant melanoma recurrence. *Nuklearmedizin*. 2017;56:83-9.

12. Knudsen A, Hag AMF, Loft A, von Benzon E, Keller SH, MØller HJ, et al. HIV infection and arterial inflammation assessed by ¹⁸F-fluorodeoxyglucose (FDG) positron emission tomography (PET): A prospective cross-sectional study. *J Nucl Cardiol*. 2015;25:372-80.
13. Tawakol A, Migrino RQ, Bashian GG, Bedri S, Vermylen D, Cury RC, et al. In vivo ¹⁸F-fluorodeoxyglucose positron emission tomography imaging provides a noninvasive measure of carotid plaque inflammation in patients. *J Am Coll Cardiol*. 2006;48:1818-24.
14. Lo J, Lu MT, Ihenachor EJ, Wei J, Looby SE, Fitch KV, et al. Effects of Statin Therapy on Coronary Artery Plaque Volume and High Risk Plaque Morphology in HIV-Infected Patients with Subclinical Atherosclerosis: a Randomized Double-Blind Placebo-Controlled Trial. *Lancet HIV*. 2015;2:e52-63.
15. Lawal I, Zeevaart JR, Ebenhan T, Ankrah A, Vorster M, Kruger H, et al. Metabolic Imaging of Infection. *J Nucl Med*. 2017. [article in press].
16. Zanni MV, Toribio M, Robbins GK, Burdo TH, Lu MT, Ishai AE, et al. Effects of Antiretroviral Therapy on Immune Function and Arterial Inflammation in Treatment-Naïve Patients with Human Immunodeficiency Virus Infection. *JAMA Cardiol*. 2016;1:474-80.
17. Bucerius J, Mani V, Moncrieff C, Machac J, Fuster V, Farkouh ME, et al. Optimizing ¹⁸F-FDG PET/CT imaging of vessel wall inflammation: the impact of ¹⁸F-FDG circulation time, injected dose, uptake parameters, and fasting blood glucose levels. *Eur J Nucl Med Mol Imaging*. 2014;41:369-83.

Chapter 5

Impact of optimized PET imaging conditions on ^{18}F -FDG uptake quantification in patients with apparently normal aortas

Ismaheel O. Lawal, MD,^a Kgomotso G. Mokoala, MD,^a Gbenga O. Popoola, MD,^b Thabo Lengana, MD,^a Alfred O. Ankrah, MD,^{a,c} Anton C. Stoltz, MD, PhD,^d and Mike M. Sathekge, MD, PhD^a

- a. Department of Nuclear Medicine, University of Pretoria and Steve Biko Academic Hospital, Pretoria, South Africa
- b. Department of Epidemiology and Community Health, University of Ilorin, Ilorin, Nigeria
- c. Department of Nuclear Medicine and Molecular Imaging, University Medical Center, Groningen, University of Groningen, Groningen, The Netherlands
- d. Infectious Disease Unit, Department of Internal Medicine, University of Pretoria and Steve Biko Academic Hospital, Pretoria, South Africa

J Nucl Cardiol. Published online ahead of print on 06 August 2019

Abstract

Background. The cardiovascular committee of the European Association of Nuclear Medicine (EANM) recently published recommendations on imaging conditions to be observed during ^{18}F -FDG PET imaging of vascular inflammation. This study aimed to evaluate the impact of applying these optimized imaging conditions on PET quantification of arterial ^{18}F -FDG uptake.

Methods and Results. Fifty-seven patients were prospectively recruited to undergo an early ^{18}F -FDG PET/CT imaging at 60 minutes and repeat delayed imaging at ≥ 120 minutes post tracer injection. Routine oncologic ^{18}F -FDGPET protocol was observed for early imaging, while delayed imaging parameters were optimized for vascular inflammation imaging as recommended by the EANM. Aortic SUVmax of the ascending aorta and SUVmean from the lumen of the superior vena cava (SVC SUVmean) were obtained on early and delayed imaging. Target-to-background ratio (TBR) was obtained for the early and delayed imaging. Aortic SUVmax increased by a mean of 70%, while SVC SUVmean decreased by a mean of 52% between early and delayed imaging ($P < 0.001$). TBR increased by 122% following delayed imaging. TBR increased, while SVC SUVmean declined across all time-points from 120 to > 180 minutes. Aortic SUVmax significantly increased at imaging time-points between 120 and 180 minutes. No significant improvement in aortic SUVmax was seen at imaging time-points beyond 180 minutes.

Conclusions. ^{18}F -FDGPET imaging conditions optimized for vascular inflammation imaging lead to an improved quantification through an increase in the quantified vascular tracer uptake and decrease in blood-pool background activity.

Key Words

^{18}F -FDG, PET/CT, vascular inflammation, atherosclerosis, TBR

Abbreviations

CT	Computed tomography
EANM	European Association of Nuclear Medicine
¹⁸ F-FDG	Fluorine-18 fluorodeoxyglucose
MBq	Mega Becquerel
PET	Positron emission tomography
ROI	Region of interest
SVC	Superior vena cava
SUVmax	Maximum standardized uptake value
SUVmean	Mean standardized uptake value
TBR	Target-to-background ratio

INTRODUCTION

Atherosclerotic cardiovascular disease remains a significant cause of death globally.¹ Inflammation plays an essential role in the formation, progression, and complication of vascular atheromatous lesions.² Radionuclide methods are a viable tool for imaging of vascular inflammation.³ Fluorine-18 Fluorodeoxyglucose (¹⁸F-FDG) positron emission tomography with computed tomography (PET/CT) is the most used radionuclide technique for vascular and cardiac inflammation and infection imaging.⁴ ¹⁸F-FDG accumulates more in vessels of individuals at higher risk of cardiovascular disease.⁵ In patients with established vascular atheroma, a higher level of ¹⁸F-FDG uptake has been reported in symptomatic as compared with asymptomatic plaque. In asymptomatic plaque, the level of ¹⁸F-FDG accumulation in the vascular lesions predicts future risk of vascular event.^{6,7}

Despite the widespread use of ¹⁸F-FDG PET/CT for vascular inflammation imaging for research purposes, many limitations militating against the accurate quantification of arterial ¹⁸F-FDG uptake remain. The mean thickness of the arterial wall is often less than twice the spatial resolution of most clinical PET cameras, subjecting ¹⁸F-FDG quantification to significant partial volume averaging.^{8,9} Target-to-background ratio (TBR), a ratio of arterial ¹⁸F-FDG uptake to blood-pool background activity, is the most commonly used parameter for quantifying arterial ¹⁸F-FDG uptake. Delayed imaging beyond the typical 60-minute uptake time observed in oncologic PET imaging is often required to achieve an optimum arterial ¹⁸F-FDG uptake and blood-pool background clearance.^{10,11} Wide variability exists regarding the uptake time and other imaging parameters observed in reported studies.⁸ Many studies have reported TBR obtained from routine PET imaging done for other indications.^{5,7,12}

Given this wide variability, the cardiovascular committee of the European Association of Nuclear Medicine (EANM) made a set of technical recommendations on imaging conditions that should be observed in PET imaging of atherosclerotic vascular inflammation.¹³ One of the key elements of these recommendations is an uptake time of 120 minutes, significantly longer than the 60-minute uptake time for routine oncologic ¹⁸F-FDG PET imaging. To date and to our knowledge, no study has been done to show that these recommended parameters, when observed, produce a better quantification of arterial ¹⁸F-FDG. The aim of our study was, therefore, to evaluate the impact of optimized PET conditions on vascular uptake of ¹⁸F-FDG quantification in vascular inflammation imaging.

METHODS

Patients

Patients referred to the Department of Nuclear Medicine at Steve Biko Academic Hospital for various indications between August and December 2018 were prospectively recruited to undergo two sets of ^{18}F -FDG PET/CT imaging. We recruited adults who had no pathology on their ^{18}F -FDG PET/CT imaging and whose blood sugar level was $\leq 7\text{mmol/L}$ at the time of intravenous injection of ^{18}F -FDG. Our exclusion criteria included use of anti-inflammatory therapy, active inflammation, or malignancy and renal failure (glomerular filtration rate $< 60\text{mL/min/m}^2$). All patients signed informed consent to participate in the study. The research ethics committee of the faculty of health sciences, University of Pretoria approved the study.

Early PET/CT Imaging

Early imaging was done as per our routine departmental ^{18}F -FDG PET/CT imaging protocol for oncologic and inflammation/infection imaging. Briefly, all patients observed a minimum of 6 hours of fasting. Fasting blood sugar was obtained in all patients using a portable glucometer. The activity of ^{18}F -FDG administered was calculated using the formula: $[(\text{body weight in kg} \div 10) + 1] \times 37 \text{ MBq}$ corresponding to 3-4 MBq recommended in the EANM position paper.¹³ After an uptake period of 60 minutes (median = 64, range = 60 to 69), a vertex to mid-thigh non-contrasted CT followed by PET imaging was performed using a hybrid Biograph Truepoint PET/CT camera (Siemens Medical Solution, IL, USA). CT parameters were as follows: tube voltage = 120 KeV, tube current = 40 mAs, sectional width = 5 mm and pitch = 0.8, matrix = 512 x 512. CT data were used for attenuation correction and anatomic co-localization. PET imaging was done in 3D mode at 3 minutes per bed position. PET images were reconstructed using ordered subset expectation maximization (OSEM) iterative reconstruction algorithm (8 iterations) with a Gaussian filter applied at 5.0mm full width at half maximum.

Delayed PET/CT Imaging

Patients who had no evident pathology either due to infection or malignancy and who consented to participate in the study underwent delayed PET/CT imaging at ≥ 120 minutes post ^{18}F -FDG injection. CT imaging with similar parameters to those of the early PET/CT imaging was repeated for the delayed imaging. For the delayed PET imaging, two-bed positions over the chest

were acquired at 8 minutes per bed position. No post-filtering was applied, and image reconstruction was performed with OSEM (120 iterations).

Statistical Analysis

Categorical data are presented as proportions/percentages. Continuous variables are presented as mean \pm SD and/or median (range). We categorized patients into groups based on the time of the delayed imaging. We compared baseline clinical characteristics between patients' groups using Fisher's Exact χ^2 test and Analysis of variance (ANOVA). We used the Paired-Samples *t* test to compare early and late variables. We used the Pearson Correlation to check for correlation between the late parameters and the time the delayed imaging was acquired. We used Spearman Correlation to test for correlation between change in TBR, aortic SUVmax, and SVC SUVmean vs the time the delayed imaging was obtained. We then evaluated the changes in TBR, aortic SUVmax, and SVC SUVmean with delayed imaging time using Paired-Samples *t* test. We used simple and multiple linear regression to check if any of age, male gender, hypertension, smoking, or fasting blood sugar level could predict any of the quantitative parameters on the early and delayed imaging. We set statistical significance at a *P* value of < 0.05 . We performed statistical analysis using SPSS statistics version 21.0 (IBM Corp., Armonk, NW, USA).

RESULTS

Among 64 eligible patients, 7 patients were excluded due to use of anti-inflammatory therapy ($n = 3$), presence of renal failure ($n = 2$), and refusal of patients to participate in the study ($n = 2$). A total of 57 patients were eventually included with a mean age of 45.93 ± 15.07 years. There were 33 females, and 23 were smokers. Twenty-one percent of patients were hypertensive, while 18 patients had well-controlled type II diabetes mellitus with a mean fasting blood sugar of 5.84 mmol/L for the whole group. All patients had normal-appearing arteries (aorta and other arteries) on CT with no foci of calcification. Table 1 shows the detail baseline characteristics of the patients included in this study.

Table 1 Baseline characteristics of the study participants

Variable	Frequency (N = 57)	Percent
Age (years)		
Mean \pm SD	45.93 \pm 15.07	
Sex		
Male	24	42.11
Female	33	57.89
Hypertension		
Yes	12	21.05
No	45	78.95
Diabetes mellitus		
Yes	10	17.54
No	47	82.46
Smoking		
Yes	23	40.35
No	34	59.65
Indications for ¹⁸F-FDG PET/CT		
Evaluation for possible occult cancer	3	5.26
Re-staging post cancer therapy	27	47.37
Suspected cancer recurrence	15	26.32
Suspected fever of unknown origin	12	21.05
Fasting blood sugar (mmol/L)		
Mean \pm SD	5.84 \pm 0.73	
Range	4.40 – 7.00	
Time of delayed imaging		
Mean \pm SD	142.74 \pm 28.94	
Range	120.0 – 245.0	

Impact of Delayed Imaging on Quantitative Parameters

The mean time between intravenous ¹⁸F-FDG injection and the start of delayed imaging was 142.74 minutes (range 120.00-245.00). In 14 patients, delayed imaging was acquired at 120 minutes. Delayed imaging was acquired between 121 and 150 minutes in 29 patients, between 151 and 180 minutes in seven patients, and >180 minutes in another seven patients. Baseline clinical characteristics were not significantly different among patients' groups by delayed imaging time (Table 2). Aortic SUVmax of the ascending aorta rose on the delayed imaging

compared with the early imaging in all patients with a mean rise of 70%, $P < 0.001$ (Figure 1A). Conversely, there was a significant drop in SVC SUV_{mean} in the delayed imaging compared with the early imaging with a mean decrease of 52%, $P < 0.001$ (Figure 1B). Delayed imaging showed a significant rise in TBR of 122% compared with the early imaging, $P < 0.001$ (Figure 1C). Table 3 shows the average aortic SUV_{max}, venous SUV_{mean}, and TBR on the early and delayed imaging.

Table 2 Comparison in the baseline characteristics of patients categorized according to the time of delayed imaging

Variable	Time of imaging				Total n (%)	χ^2	p value
	120 n (%)	121 – 150 n (%)	151 – 180 n (%)	> 180 n (%)			
Age							
Mean \pm SD	50.79 \pm 13.53	45.48 \pm 16.47	39.71 \pm 13.63	44.29 \pm 12.93		0.913 ^F	0.441
Gender							
Male	6(42.9)	13(44.8)	2(28.6)	3(42.9)	24(42.1)	0.699	0.952
Female	8(57.1)	16(55.2)	5(71.4)	4(57.1)	33(57.9)		
Hypertension							
Yes	3(21.4)	6(20.7)	2(28.6)	1(14.3)	12(21.1)	0.667	0.961
No	11(78.6)	23(79.3)	5(71.4)	6(85.7)	45(78.9)		
Smoking							
Yes	6(42.9)	13(44.8)	2(28.6)	2(28.6)	23(40.4)	1.062	0.871
No	8(57.1)	16(55.2)	5(71.4)	5(71.4)	34(59.6)		
FBS							
Mean \pm SD	5.86 \pm 0.72	5.66 \pm 0.71	6.20 \pm 0.40	6.21 \pm 0.95		1.844 ^F	0.150

χ^2 : Fisher's Exact Chi square test; **F**: Analysis of variance (ANOVA); **FBS**: Fasting blood sugar

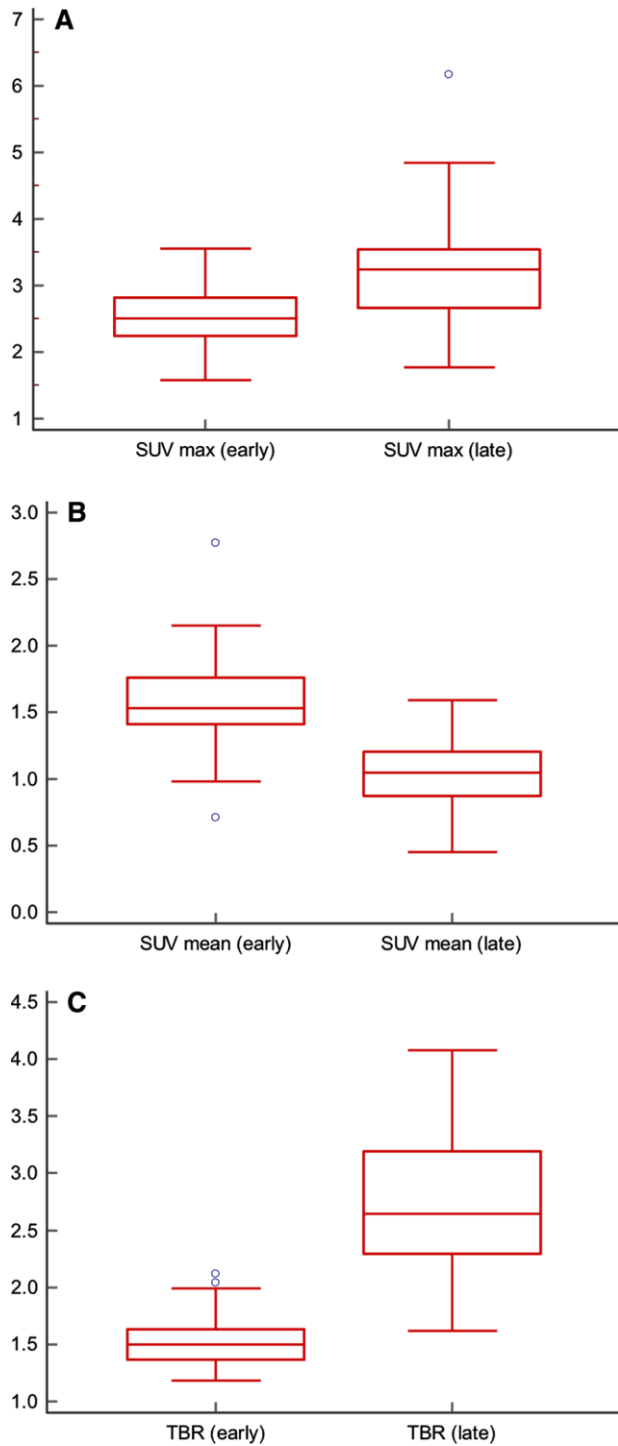


Fig 1 Box plots showing significant differences in (A) aortic SUVmax, (B) SVC SUVmean, and (C) aortic TBR between the early and delayed ^{18}F -FDG PET imaging. Aortic SUVmax increased by a mean of 70%; venous TBR decreased by a mean of 52% and TBR increased by a mean of 122% between early and delayed imaging, $P < 0.001$ in all cases.

Table 3 Changes in aortic SUVmax, SVC SUVmean, and aortic TBR between early and delayed ¹⁸F-FDG PET imaging

Variable	Timing	Duration (minutes)		Mean difference	95% Confidence interval		t	p value
		Mean ± SD	Range		Lower	Upper		
Aortic TBR	Early	1.53 ± 0.20	1.18 – 2.12	1.22	1.06	1.37	15.737	<0.001*
	Late	2.75 ± 0.59	1.62 – 4.08					
SVC SUVmean	Early	1.57 ± 0.33	0.71 – 2.77	-0.52	-0.58	-0.46	-17.894	<0.001*
	Late	1.04 ± 0.25	0.45 – 1.59					
Aortic SUVmax	Early	2.52 ± 0.43	1.58 – 3.56	0.70	0.54	0.86	8.802	<0.001*
	Late	3.22 ± 0.75	1.77 – 6.17					

t: Paired Samples T test; *: p value <0.01

Correlation Between the Time of Delayed Imaging and the Change in Quantitative Parameters

Delayed imaging was acquired over a range of time in the participants, 120 to 245 minutes. We found a weak negative correlation between the SVC SUVmean_late and the time of delayed imaging (Pearson correlation coefficient = - 0.298, $P = .025$). Similarly, we found a moderate positive correlation between TBR_late and the time of delayed imaging (Pearson correlation coefficient = 0.526, $P < 0.001$). Aortic SUVmax_late was not significantly correlated with the time of delayed imaging.

Consequently, SUVmean decreases, while TBR increases with further delay in the time of delayed imaging beyond 120 minutes. The change in SUVmax with further delay in imaging time did not reach statistical significance. Table 4 shows the relationship between the time of delayed imaging and the TBR_late, SVC SUVmean_late, and aortic SUVmax_late. Figures 2a and b show the typical image of an early and delayed ¹⁸F-FDG PET/CT imaging.

Table 4 Correlation between quantified parameters and the time of delayed imaging.

Variables	Time of delayed imaging	
	r_p	p value
TBR_late	0.526	<0.001*
SVC SUVmean_late	-0.298	0.025*
Aortic SUVmax_late	0.136	0.314
Change in parameters	r_s	
TBR	0.307	0.003*
SVC SUVmean	-0.271	0.043*
Aortic SUVmax	-0.144	0.284

r_p : Pearson Correlation Coefficient; r_s : Spearman Correlation coefficient; *: p value < 0.05

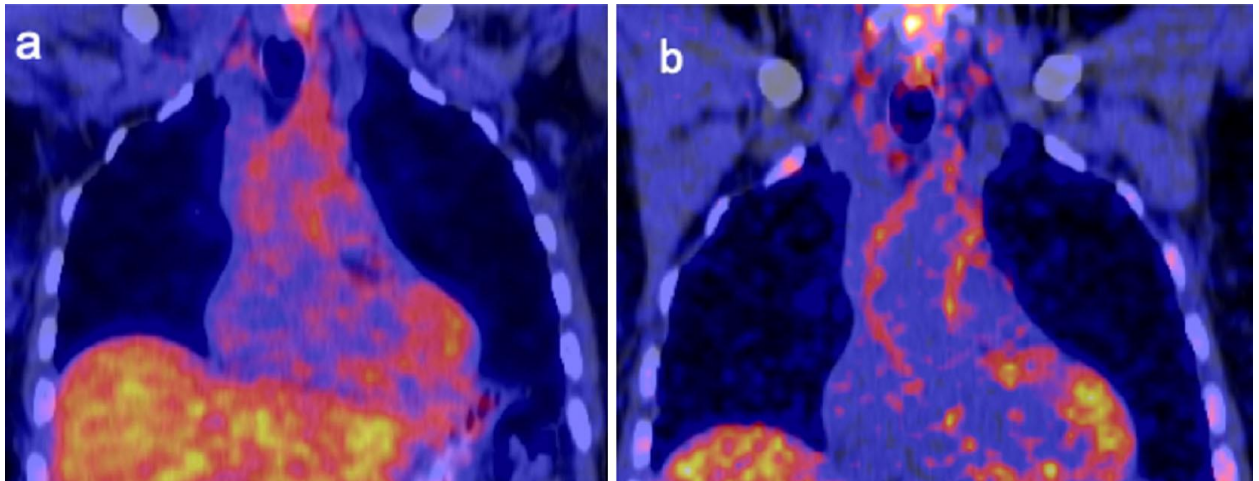


Fig 2 Coronal fused ^{18}F -FDG PET/CT imaged of a typical patient. The early image (A) shows tracer localization to the ascending aorta wall, but with high blood-pool background activity. Delayed image (B) shows an increase in the intensity of tracer localized to the aortic wall with a much-improved clearance of background blood-pool activity.

In a sub-group analysis evaluating the impact of the time of delayed imaging on changes TBR, aortic SUVmax, and SVC SUVmean, we found a progressive improvement in TBR obtained on the delayed imaging at different time-points from 120 minutes to > 180 minutes ($P < 0.001$). SVC SUVmean also showed a progressive decline across all imaging time-points from 120 to beyond 180 minutes ($P < 0.005$). Aortic SUVmax significantly increased progressively from 120 minutes up till 180 minutes of imaging time-point. The improvement in aortic SUVmax beyond 180-minute imaging time-point did not reach a statistical significance. Table 5

shows the detailed changes in TBR, aortic SUVmax, and SVC SUVmean with the time of delayed imaging. Figure 3 is a graphical representation of the changes in then different quantitative parameters with increasing time of imaging.

Table 5 Changes in TBR, aortic SUVmax and SVC SUVmean with the time of delayed imaging

Time of delay	n	Early Mean ± SD	Late Mean ± SD	t	p-value
TBR					
120 minutes	14	1.54 ± 0.18	2.68 ± 0.58	-8.585	<0.001*
121 – 150 minutes	29	1.53 ± 0.21	2.53 ± 0.43	-11.110	<0.001*
151 – 180 minutes	7	1.36 ± 0.07	3.06 ± 0.66	-6.795	<0.001*
> 180 minutes	7	1.68 ± 0.22	3.47 ± 0.43	-11.132	<0.001*
SVC SUVmean					
120 minutes	14	1.60 ± 0.18	1.10 ± 0.18	10.542	<0.001*
121 – 150 minutes	29	1.57 ± 0.31	1.09 ± 0.24	13.745	<0.001*
151 – 180 minutes	7	1.59 ± 0.55	0.94 ± 0.32	6.147	0.001*
> 180 minutes	7	1.45 ± 0.40	0.85 ± 0.28	5.004	0.002*
Aortic SUVmax					
120 minutes	14	2.55 ± 0.27	3.34 ± 0.54	-6.467	<0.001*
121 – 150 minutes	29	2.55 ± 0.46	3.15 ± 0.55	-6.288	<0.001*
151 – 180 minutes	7	2.34 ± 0.58	3.01 ± 1.02	-3.381	0.015*
> 180 minutes	7	2.54 ± 0.46	3.50 ± 1.39	-2.271	0.064

t: Paired Samples T test; *: p value <0.05

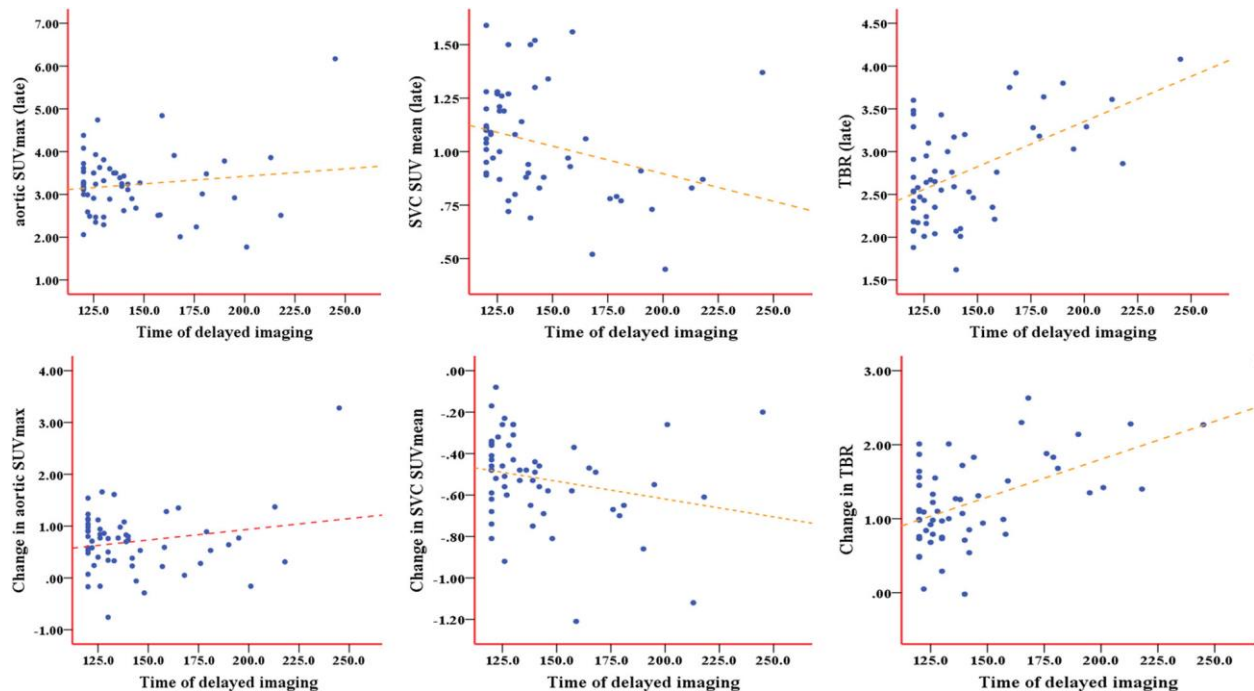


Fig 3 Scatter plots showing the changes of the time of delayed imaging on (top row from right to left) the TBR_late, SVC SUVmean_late, and aortic SUVmax_late. Scatter plots on the bottom row show the changes in (from right to left) the TBR, SVC SUVmean, and aortic SUVmax with the increasing time at which the delayed images were acquired

Predictors of Quantitative Parameters

Among the factors (age, male gender, systemic hypertension, smoking history, and fasting blood sugar) tested for their abilities to predict the quantitative parameters on both the early and delayed imaging, history of hypertension was the most consistent in predicting aortic SUVmax and SVC SUVmean on the early and delayed imaging, $P > 0.05$. None of the factors tested was a significant predictor of TBR either on the early or delayed imaging. Table 6 shows the performance of the different factors tested in their abilities to predict the quantitative parameters on both the early and delayed imaging.

Table 6 Predictors of arterial SUVmax, SUV SUVmean and TBR on early and delayed imaging

Variables	Simple linear regression		Multiple linear regression	
	b (95% CI)	<i>p</i> value	Adjusted b (95% CI)	<i>p</i> value
TBR early				
Age	-0.004 (-0.007 – 0.000)	0.038*		
Gender (male)	0.024 (-0.087 – 0.134)	0.670		
Hypertension	-0.058 (-0.191 – 0.075)	0.385		
Smoking	0.019 (-0.092 – 0.131)	0.728		
FBS	-0.046 (-0.120 - 0.029)	0.223		
TBR late				
Age	-0.006 (-0.016 – 0.005)	0.287		
Gender (male)	-0.073 (-0.393 – 0.246)	0.647		
Hypertension	-0.003 (-0.402 – 0.395)	0.987		
Smoking	-0.248 (-0.562 – 0.067)	0.121		
FBS	0.062 (-0.156 – 0.280)	0.573		
SVC SUVmean (early)				
Age	0.008 (0.002 – 0.013)	0.007*	0.004 (-0.002 – 0.009)	0.117
Gender (male)	-0.223 (-0.390 - -0.056)	0.010*	-0.173 (-0.335 - -0.011)	0.037*
Hypertension	0.377 (0.187 – 0.566)	<0.001*	0.299 (0.100 – 0.498)	0.004*
Smoking	-0.175 (-0.347 - -0.002)	0.047*	-0.027 (-0.194 – 0.140)	0.747
FBS	0.070 (-0.049 – 0.189)	0.243		
SVC SUVmean (late)				
Age	0.005 (0.001 – 0.010)	0.027*	0.003 (-0.002 – 0.007)	0.229
Gender (male)	-0.129 (-0.262 – 0.004)	0.057		
Hypertension	0.300 (0.150 – 0.451)	<0.001*	0.268 (0.109 – 0.427)	0.001*
Smoking	-0.080 (-0.217 – 0.057)	0.246		
FBS	0.017 (-0.077 – 0.111)	0.717		
Aortic SUVmax (early)				
Age	0.007 (-0.001 – 0.014)	0.085		
Gender (male)	-0.266 (-0.489 - -0.042)	0.021*	-0.163 (-0.385 – 0.059)	0.148
Hypertension	0.404 (0.141 – 0.666)	0.003*	0.324 (0.068 – 0.580)	0.014*
Smoking	-0.335 (0.553 – -0.011)	0.003*	-0.205 (-0.435 – 0.024)	0.079
FBS	-0.014 (-0.174 – 0.145)	0.856		
Aortic SUVmax (late)				
Age	0.003 (-0.011 – 0.016)	0.703		
Gender (male)	-0.405 (-0.795 - -0.014)	0.042*	-0.251 (-0.648 – 0.147)	0.211
Hypertension	0.639 (0.179 – 1.098)	0.007*	0.521 (0.062 – 0.980)	0.027*

Smoking	-0.504 (-0.889 – -0.120)	0.011*	-0.299 (-0.711 – 0.112)	0.150
FBS	0.076 (-0.199 – 0.350)	0.582		

b: Coefficient of Linear regression); *: *p* value < 0.05

SVC SUV_{mean} (early): R²: 0.338; SVC SUV_{mean} (late): R²: 0.249; aortic SUV_{max} (early): R²: 0.266; aortic SUV_{max} (late): R²: 0.212

DISCUSSION

We applied optimum patients' preparation and PET imaging parameters to quantifying arterial ¹⁸F-FDG uptake and found an improvement in the measured quantitative parameters. Arterial SUV_{max}, a marker of the intensity of ¹⁸F-FDG uptake in the arterial wall, increased by a mean of 70%. This improvement in aortic SUV_{max} indicates an improvement in tracer uptake with improved imaging parameters and prolonged uptake time. SVC SUV_{mean}, a marker of the blood-pool background activity, declined by 52% between the early un-optimized imaging and delayed imaging optimized for vascular inflammation imaging. TBR, a ratio of arterial SUV_{max} and venous SUV_{mean}, showed a tremendous improvement of 122% between the unoptimized early imaging and the delayed imaging. Our data confirm that the application of the specific set of parameters recommended by the cardiovascular committee of the EANM is necessary for adequate quantification of ¹⁸F-FDG uptake in the arterial wall.¹³ Our results suggest that data from routinely acquired PET imaging for other indications may significantly underestimate the quantitation of vascular tracer uptake.

Many authors have identified difficulties with quantitation of vascular uptake of ¹⁸F-FDG with a call to standardize patient preparation and imaging parameters.^{8,9,14} Many studies have since been published evaluating the feasibility and the optimum imaging conditions of vascular atheromatous inflammation in different arterial beds.^{6,10,11,15} In a large study by Bucarius et al, there was an increase in the aortic TBR with increasing uptake time.¹⁰ Unlike in our study, aortic SUV_{max} decreased with increased uptake time. A significant difference between this study and ours is that patients in our study were imaged at two-time-points using two different PET imaging parameters. The longer acquisition time of 8 minutes per bed position compared with the early imaging (acquired at 3 minutes per bed position), as well as reconstruction protocols on the delayed imaging optimized for vascular inflammation imaging (higher iterations, no post-filtering) contributed to reducing the impact of partial volume effect on the aortic SUV_{max}.¹³ The CT parameters were similar for the early and delayed imaging. The increase in aortic

SUVmax, decline in SVC SUVmean, and consequently increase in TBR, therefore, result from multiple factors including prolonged uptake time and optimized PET imaging parameters. Other factors such as activity of ^{18}F -FDG and blood sugar levels at the time of tracer injection which are known to influence the SUV parameters were similar for both imaging time-points.

Patients included in our study had their delayed imaging acquired at a variable time from 120 to 245 minutes. We determined the impact of further delay in acquiring PET imaging and found a significant decline in SVC SUVmean and an improvement in TBR across different delayed imaging time-points up till beyond 180 minutes. The increase in aortic SUVmax with delayed imaging was significant up till the 180-minute imaging time-point, but not beyond. Our findings suggest that the increase seen in TBR when imaging is delayed beyond 180 minutes is due to an improvement in blood-pool background activity clearance without any significant improvement in arterial uptake of ^{18}F -FDG. The recommendation of the EANM cardiovascular imaging committee regarding the time of imaging is a compromise agreed on to achieve an acceptable image quality without making patients observe a long uptake time with a potential to disrupt the schedule of other patients being imaged with the same PET/CT scanner for other indications. While our results support the compromised recommendation of the EANM that imaging for vascular inflammation is done after a 2-hour uptake time which is a better imaging time than an earlier imaging, a longer uptake time up till 180 minutes will be more ideal. In an early work by Tawakol et al, good TBR of atheromatous lesions was obtained on PET imaging done after a 3- hour uptake time.¹⁵ In a study with a contrary finding, Menezes et al could not demonstrate a significant difference in arterial ^{18}F -FDG uptake between imaging done at one and three hours post tracer injection. This study done in a limited number of patients with aortic aneurysm has some methodological differences with most studies published on this topic especially regarding the authors' choice of vessel for background correction.¹⁶ Menezes and colleagues obtained their blood-pool background activity from the lumen of the diseased artery rather than from an adjacent vein.¹⁶

Among the factors we tested for their ability to predict the level of arterial ^{18}F -FDG uptake and blood-pool background activity clearance, systemic hypertension was the most consistent predictor in both simple and multiple linear regressions. Individuals with systemic hypertension generally have hypertrophied smooth muscle in their vessel wall. As an adaptive response to sustained elevated blood pressure, the vessels of hypertensive patients develop

concentric thickening with luminal narrowing.¹⁷ Increase in the thickness of arterial wall improves quantification of tracer uptake with it. Thinner vessels in younger individuals without cardiovascular disease are associated with a significant underestimation of arterial ¹⁸F-FDG quantification.⁹ We performed image analysis using the ascending aorta as the arterial bed of interest. The ascending aorta is a large artery with a thick wall that reduces the extent of the underestimation of the measured parameters that may be caused by partial volume effect. Others have shown that TBR measured are similar across different arterial territories.¹⁸ Age was a significant predictor of early and late SVC SUVmean in a simple linear regression. This may be due to better renal function in younger individuals with prompt background activity clearance compared with older population. The impact of age lost its significance of multiple linear regression. Serum blood sugar at the time of ¹⁸F-FDG administration had no impact on any of the parameters tested. This may be due to the strict fasting blood sugar level we used as an entry criterion for this study implying that patients we included were most likely non-diabetic or well-controlled diabetic patients. Male gender significantly predicts background clearance on the early image, but not on the delayed image. We speculate that this finding may mean that males have an early rapid background activity clearance, which equates with the clearance rate in females beyond 60 minutes.

Inflammation plays an important role in the formation and progression of vascular atheroma.³ Agents with anti-inflammatory effects are now being evaluated for their potential for primary and secondary prevention of atherosclerotic cardiovascular diseases.¹⁹ ¹⁸F-FDG PET/CT holds a great potential for non-invasive evaluation of the effectiveness of these therapeutic agents.²⁰ There are, however, several drawbacks to the widespread clinical application of ¹⁸F-FDG PET/CT for arterial inflammation imaging. The most significant of these drawbacks is the lack of specificity of ¹⁸F-FDG. Within the atheromatous lesion, ¹⁸F-FDG is taken up by the inflammatory cells and the hypertrophied vascular smooth muscle cells as well. Similarly, there is high physiologic ¹⁸F-FDG uptake in the myocardium and soft tissues of the neck which may compromise quantification of arterial ¹⁸F-FDG uptake in the coronary and carotid arteries, respectively. There are now concerted efforts to develop more specific tracers which do not suffer from these drawbacks experienced with ¹⁸F-FDG use.^{3,21,22}

Our study is unique in the fact that we compared two sets of imaging conditions, one optimized for vascular inflammation imaging and the other not, in the same set of patients in a

test-retest setting. Our study design allows for each patient to serve as their own control which removes inter-individual variability as a confounding factor. Despite this, our study suffers from some limitations including the group of patients we studied. Our patients have apparently healthy aortas without atheromatous lesions. Also, we did not fully characterize the cardiovascular risk of our patients, and hence we could not perform a sub-group analysis of our study population based on their cardiovascular risk grouping. These limitations of our study must be borne in mind while applying our findings to imaging of atheromatous lesions in patients with established cardiovascular diseases. We recruited a modest study population due to the radiation burden patients were exposed to in this test-retest study design. Despite this modest study population, we performed sub-group analyses on the patients categorized according to the time of delayed imaging and found statistically significant differences in the quantified parameters between groups in most cases. Only one reader performed image analysis in this study. This was based on the widely acknowledged excellent inter-observer agreement in vascular ^{18}F -FDG uptake quantification informing a single-reader image analysis in some recent studies.^{7,10,18} Image analysis by two readers has also been reported in recent studies and its application could have provided a more robust quantification of vascular ^{18}F -FDG uptake in this study.²³

CONCLUSION

Vascular inflammation imaging with ^{18}F -FDG PET requires optimized imaging conditions. These imaging conditions enable improved vascular quantification through increased vascular tracer uptake and improved blood-pool background activity clear.

NEW KNOWLEDGE GAINED

Application of the ^{18}F -FDG PET imaging conditions recommended by the cardiovascular committee of the EANM leads to an improvement in quantified arterial tracer uptake and better background clearance. There is an increase in arterial ^{18}F -FDG uptake and venous blood-pool clearance up till 180 minutes post tracer injection. Delaying imaging beyond 180 minutes post tracer injection leads to further improvement of blood-pool background activity clearance, but not an increase in vascular ^{18}F -FDG uptake.

Acknowledgments

IOL is a PhD student at the time this study was performed. He receives a monthly stipend from the Nuclear Medicine Research Infrastructure (NuMeRI) hosted at the Department of Nuclear Medicine, University of Pretoria. All authors wish to thank members of staff at the Department of Nuclear Medicine, Steve Biko Academic Hospital and University of Pretoria, Pretoria, South Africa.

Disclosures

Ismaheel O. Lawal, Kgomotso G. Mokoala, Gbenga O. Popoola, Thabo Lengana, Alfred O. Ankrah, Anton C. Stoltz, and Mike M. Sathekge declare that they have no conflict of interest.

References

1. Roth GA, Abate D, Abate KH, Abay SM, Abbafati C, Abbasi N, et al. Global, regional, and national age- sex-specific mortality for 282 causes of death in 195 countries and territories, 1980-2017: a systematic analysis for the Global Burden of Disease Study 2017. *Lancet*. 2018;392:1736-1788.
2. Libby P. Inflammation and cardiovascular disease mechanisms. *Am J Clin Nutr*. 2016;83(suppl):456S-460S.
3. Lawal IO, Ankrah AO, Stoltz AC, Sathekge MM. Radionuclide imaging of inflammation in atherosclerotic vascular disease among people living with HIV infection: current practice and future perspective. *Eur J Hybrid Imaging*. 2019;3:5.
4. Lawal I, Sathekge M. F-18 FDG PET/CT imaging of cardiac and vascular inflammation and infection. *Br Med Bull*. 2016;120:55-74.
5. Lawal IO, Ankrah AO, Popoola GO, Lengana T, Sathekge MM. Arterial inflammation in young patients with human immunodeficiency virus infection: a cross-sectional study using F-18 FDG PET/CT. *J Nucl Cardiol*. Epub ahead of print on 07 February 2018.
6. Rudd JHF, Warburton EA, Fryer TD, Jones HA, Clark JC, Antoun N, et al. Imaging atherosclerotic plaque inflammation with [¹⁸F]-Fluorodeoxyglucose positron emission tomography. *Circulation*. 2002;105:2708-2711.
7. Figueroa AL, Abdelbaky A, Truong QA, Corsini E, MacNabb MH, Lavender ZR, et al. Measurement of arterial activity on routine FDG PET/CT images improves prediction of risk of future CV event. *JACC Cardiovasc Imaging*. 2013;6:1250-1259.
8. Huet P, Burg S, Le Guludec D, Hyafil F, Buvat I. Variability and uncertainty of ¹⁸F-FDG PET imaging protocols for assessing inflammation in atherosclerosis: suggestions for improvement. *J Nucl Med*. 2015;56:552-559.
9. Burg S, Dupas A, Stute S, Dieudonné A, Huet P, Le Guludec D, et al. Partial volume effect estimation and correction in the aortic vascular wall in PET imaging. *Phys Med Biol*. 2013;58:7527-7542.
10. Bucierius J, Mani V, Moncrieff C, Machac J, Fuster V, Farkouh ME, et al. Optimizing ¹⁸F-FDG circulation time, injected dose, uptake parameters, and fasting blood sugar levels. *Eur J Nucl Med Mol Imaging*. 2014;41:369-383.

11. Blomberg BA, Thomassen A, Takx RA, Hildebrandt MG, Simonsen JA, Buch-Olsen KM, et al. Delayed ¹⁸F-fluorodeoxyglucose PET/CT imaging improves quantification of atherosclerotic plaque inflammation: results from the CAMONA study. *J Nucl Cardiol.* 2014;21:588-597.
12. Subramanian S, Tawakol A, Burdo TH, Abbara S, Wei J, Vijayakumar J, et al. Arterial inflammation in patients with HIV. *JAMA.* 2012;308:379-386.
13. Bucnerius J, Hyafil F, Verberne HJ, Slart RHJA, Linder O, Sciagra R, et al. Position paper of the Cardiovascular Committee of the European Association of Nuclear Medicine (EANM) on PET imaging of atherosclerosis. *Eur J Nucl Med Mol Imaging.* 2016;43:780-792.
14. Sadeghi MM. ¹⁸F-FDG PET and vascular inflammation; time to reflect the paradigm? *J Nucl Cardiol.* 2015;22:319-324.
15. Tawakol A, Migrino RQ, Bashian GG, Bedri S, Vermylen D, Cury RC, et al. In vivo ¹⁸F-fluorodeoxyglucose positron emission tomography imaging provides a noninvasive measure of carotid plaque inflammation in patients. *J Am Coll Cardiol.* 2006;48:1818-1824.
16. Menezes LJ, Kotze CW, Hutton BF, Endozo R, Dickson JC, Cullum I, et al. Vascular inflammation imaging with ¹⁸F-FDG PET/CT: when to image? *J Nucl Med.* 2009;50:854-857.
17. Mitchell RN. Blood vessels. In: Kumar V, Abbas AK, Aster JC, (eds). *Robins and Cotran pathologic basis of disease.* 9th ed. Saunders Elsevier: Philadelphia;2015. p. 483-522.
18. Knudsen A, Hag AMF, Loft A, von Benzon E, Keller SH, Møller HJ, et al. HIV infection and arterial inflammation assessed by ¹⁸F-fluorodeoxyglucose (FDG) positron emission tomography (PET): A prospective cross-sectional study. *J Nucl Cardiol.* 2015;22:372-380.
19. Ridker PM, Everett BM, Thuren T, MacFadyen JG, Chang WH, Ballantyne C, et al. Antiinflammatory Therapy with Canakinumab for Atherosclerotic Disease. *N Engl J Med.* 2017;377:1119-1131.
20. Hsue PY, Li D, Ma Y, Ishai A, Manion M, Nahrendorf M, et al. IL-1 β inhibition reduces atherosclerotic inflammation in HIV infection. *JACC.* 2018;72:2809-2810.

21. Vigne J, Thackeray J, Essers J, Makowski M, Varasteh Z, Curaj A, et al. Current and emerging preclinical approaches for imaging-based characterization of atherosclerosis. *Mol Imaging Biol.* 2018;20:869-887.
22. Bucorius J, Dijkgraaf I, Mottaghy FM, Schurgers LJ. Target identification for the diagnosis and intervention of vulnerable atherosclerotic plaques beyond ¹⁸F-fluorodeoxyglucose positron emission tomography imaging: promising tracers on the horizon. *Eur J Nucl Med Mol Imaging.* 2019;46:251-265.
23. Toczek J, Hillmer AT, Han J, Liu C, Peters D, Emami H, et al. FDG PET imaging of vascular inflammation in post-traumatic stress disorder: A pilot case-control study. *J Nucl Cardiol.* Epub ahead of print on 09 May 2019.

Chapter 6

[⁶⁸Ga]Ga-Pentixafor for PET imaging of vascular expression of CXCR-4 as a marker of arterial inflammation in HIV-infected patients: A comparison with ¹⁸F-FDG PET imaging

Ismaheel O. Lawal^{1,2}, Gbenga O. Popoola³, Johncy Mahapane⁴, Jens Kaufmann⁵, Cindy Davis⁴, Honest Ndlovu^{1,4}, Letjie C. Maserumule^{1,4}, Kgomotso M.G. Mokoala^{1,2,4}, Hakim Bouterfa⁵, Hans-Jürgen Wester⁶, Jan Rijn Zeevaart^{2,7}, Mike M. Sathekge^{1,2,4}

1. Department of Nuclear Medicine, University of Pretoria, Pretoria, South Africa
2. Nuclear Medicine Research Infrastructure (NuMeRI), Steve Biko Academic Hospital, Pretoria, South Africa
3. Department of Epidemiology and Community Health, University of Ilorin, Ilorin, Nigeria
4. Department of Nuclear Medicine, Steve Biko Academic Hospital, Pretoria, South Africa
5. PentixaPharm GmbH, Wuerzburg, Germany
6. Pharmazeutische Radiochemie, Technische Universität München, 85748 Garching, Germany
7. Nuclear Energy Corporation of South Africa (NECSA), Pelindaba, South Africa

Biomolecules. 2020;10(12):1629.

Abstract

People living with human immunodeficiency virus (PLHIV) have excess risk of atherosclerotic cardiovascular disease (ASCVD). Arterial inflammation is the hallmark of atherogenesis and its complications. In this study we aimed to perform a head-to-head comparison of ^{18}F -FDG PET/CT and [^{68}Ga]Ga-pentixafor PET/CT for quantification of arterial inflammation in PLHIV. We prospectively recruited HIV-infected patients to undergo ^{18}F -FDG PET/CT and [^{68}Ga]Ga-pentixafor PET/CT within two weeks of each other. We quantified the levels of arterial tracer uptake on both scans using maximum standardized uptake value (SUVmax) and target-background-ratio. We used Bland and Altman plots to measure the level of agreement between tracer quantification parameters obtained on both scans. A total of 12 patients were included with a mean age of 44.67 ± 7.62 years. The mean duration of HIV infection and mean CD⁺ T-cell count of the study population were 71.08 ± 37 months and 522.17 ± 260.33 cells/ μL , respectively. We found a high level of agreement in the quantification variables obtained ^{18}F -FDG PET and [^{68}Ga]Ga-pentixafor PET. There is a good level of agreement in the arterial tracer quantification variables obtained on ^{18}F -FDG PET/CT and [^{68}Ga]Ga-pentixafor PET/CT in PLHIV. This suggests that [^{68}Ga]Ga-pentixafor may be applied in the place of ^{18}F -FDG PET/CT for the quantification of arterial inflammation.

Keywords

HIV infection, [^{68}Ga]Ga-pentixafor PET/CT, ^{18}F -FDG PET/CT, Arterial Inflammation, Atherosclerotic Cardiovascular Diseases

INTRODUCTION

The risk of atherosclerotic cardiovascular disease (ASCVD) is twice as high in people living with human immunodeficiency virus (PLHIV) compared with people without human immunodeficiency virus (HIV) infection [1]. Factors responsible for the excess risk of ASCVD among PLHIV include the impact of the virus itself, the atherogenic effect of antiretroviral therapy (ART) used in HIV treatment, and preponderance of traditional cardiovascular risk factors among PLHIV [2]. Inflammation is a hallmark feature of atherogenesis and its progression [3]. Atherogenesis evolves over decades and endothelial dysfunction characterized by invasion of vascular endothelium by inflammatory cells is present long before atheroma develops. The critical role inflammation plays in atheroma formation and its progression informs the new interest in developing therapeutic agents that inhibit inflammation in attempt to stem the tide of the increasing incidence of ASCVD [4]. Radionuclide imaging techniques are a viable option for non-invasive quantification of arterial inflammation to assess patient risk for ASCVD and to directly monitor the impact of anti-inflammatory therapy.

^{18}F -FDG PET imaging is the most commonly used radionuclide technique for arterial inflammation quantification. In an early study, Subramanian et al., using arterial FDG uptake as a surrogate marker of inflammation, reported higher arterial inflammation in patients with HIV compared with their age-, gender-, and Framingham risk score-matched controls [5]. In the study, arterial inflammation in HIV-infected patients was comparable to that observed in older HIV-uninfected patients with established ASCVD. Our group has also recently reported a higher level of arterial inflammation among young PLHIV without risk for ASCVD, except for HIV infection, compared with age- and gender-matched HIV-uninfected controls [6]. Despite the huge experience with the use of ^{18}F -FDG PET for arterial inflammation imaging, there are several limitations associated with its use in this clinical setting, including the need for extensive patient preparation. More importantly, physiologic ^{18}F -FDG uptake in the myocardium and structures in the neck makes accurate quantification of its arterial uptake difficult. There is, therefore, a need to evaluate other radionuclide tracers without these shortcomings for their use in arterial inflammation imaging.

^{68}Ga [Ga]-Pentixafor is a novel tracer that targets chemokine receptor-4 (CXCR-4) expressed on inflammatory and cancer cells. In a proof-of-concept study, Hyafil et al. demonstrated specific localization of ^{68}Ga [Ga]-Pentixafor to macrophage-rich atheromatous

lesions [7], while Weiberg et al. have shown correlations between the level of [⁶⁸Ga]Ga-Pentixafor in arterial lesions and ASCVD risk factors [8]. No study, however, has evaluated the utility of [⁶⁸Ga]Ga-Pentixafor for quantification of arterial inflammation in PLHIV or has performed a prospective head-to-head comparison between it and ¹⁸F-FDG PET imaging. The aim of our study was to report our preliminary experience of a head-to-head comparison of [⁶⁸Ga]Ga-Pentixafor and ¹⁸F-FDG for PET imaging of arterial inflammation among PLHIV. To achieve an objective comparison, we applied the optimized imaging criteria for arterial inflammation recommended by the Cardiovascular committee of the European Association of Nuclear Medicine (EANM) for ¹⁸F-FDG PET imaging [9].

MATERIALS AND METHODS

Between September 2019 and October 2020, we prospectively recruited HIV-infected patients who had been on ART for 24 months or more, had achieved undetectable plasma HIV viremia, and were without a history of change in their ARV regimens in the preceding six months. We collected detailed histories regarding ASCVD risks in the patients. We also measured serum levels of lipids, haemoglobin, and C-reactive protein (CRP). We documented the most recent CD4+ T-cell count in all qualifying patients. Patients were subsequently scheduled to undergo alternating [⁶⁸Ga]Ga-pentixafor and ¹⁸F-FDG PET/CT imaging within two weeks. All participants gave a written informed consent prior to enrolment into this study. The study was conducted in accordance with the Declaration of Helsinki, and the study protocol was approved by the Research Ethics Committee of the Faculty of Health Sciences, University of Pretoria (approval number:242/2018).

¹⁸F-FDG PET: Image acquisition and analysis

Standard patient preparation was observed that included a minimum of six-hour period of fasting. Blood glucose was less than 7.1 mmol/L at the time of ¹⁸F-FDG administration. Sixty minutes after intravenous administration of 3-5MBq/Kg of ¹⁸F-FDG, vertex to mid-thigh CT followed PET imaging was acquired using standard oncologic PET imaging parameters on a Biograph 40 hybrid PET/CT scanner (Siemens Healthineers, Erlangen, Germany). This early PET/CT imaging was followed by a delayed imaging commenced at 120 minutes post ¹⁸F-FDG injection. The delayed imaging was optimized for vascular inflammation imaging as

recommended by the Cardiovascular Committee of the EANM and has we have previously reported [9,10]. Briefly, PET/CT imaging was acquired from the base of skull to the level of the diaphragm at 8 minutes/bed position in 3D mode.

Image analysis was performed on a dedicated workstation equipped with a Syngo.via software (Siemens Healthineers, Erlangen, Germany) as previously reported [10]. Briefly, we obtained SUVmax of arterial ^{18}F -FDG uptake in the ascending aorta and the common carotid artery by averaging values obtained from multiple regions of interest (ROIs) drawn encircling the arterial wall and lumen. For background activity correction, we averaged SUVmean obtained from multiple ROIs placed within the lumen of the superior vena cava (SVC) and internal jugular vein (IJV). We obtained target-to-background ratio (TBR) for the ascending aorta and the carotid artery by dividing the aortic SUVmax by SVC SUVmean and carotid SUVmax by IJV SUVmean, respectively. These parameters were obtained on the early (early-aortic-SUVmax, early-SVC-SUVmean, early-aortic-TBR, early-carotid-SUVmax, early-IJV-SUVmean, and early-carotid-TBR) and delayed (late-aortic-SUVmax, late-SVC-SUVmean, late-aortic-TBR, late-carotid-SUVmax, late-IJV-SUVmean, and late-carotid-TBR) ^{18}F -FDG PET imaging.

[^{68}Ga]Ga-pentixafor: Tracer synthesis, PET imaging, and image analysis

An 1850 MBq loaded $^{68}\text{Ge}/^{68}\text{Ga}$ generator (iThemba LABS, Somerset West, South Africa) was used in-house to provide ^{68}Ga radioactivity to label with precursor pentixafor (ABX advanced biochemical compounds, Biomedizinsche Forschungsreagenzien GmbH, Radeberg, Germany). A buffered ^{68}Ga radioactivity (1 ml) was labelled with pentixafor (50 μg). The reaction mixture at pH 3.5 - 4 was heated in a heating block (95 $^{\circ}\text{C}$) for 10 minutes. Post incubation, radiolabeled [^{68}Ga]Ga-pentixafor was purified using solid phase extraction (Sep Pack C-18-light cartridge (Waters Corporation, Massachusetts, USA)). An instant thin layer chromatography (ITLC) was performed to ascertain the radiochemical purity of the labeled product before administration into patients. A sample (5 μl) of [^{68}Ga]Ga-pentixafor was spotted on ITLC strip (ITLC-silica gel paper (Agilent, Forrest Lake, USA) and developed in a mobile phase solution (Sodium Citrate (pH-5)). The developed ITLC strip (radioactivity) was counted and recorded on radio-chromatogram (($R_f = 0.0 - 0.2$ ([^{68}Ga]Ga-pentixafor (> 95%)), $R_f = 0.8 - 1.0$ (free $^{68}\text{Ga}/^{68}\text{Ga}$ -colloids (<5%))).

Sixty minutes after intravenous administration of [⁶⁸Ga]Ga-pentixafor, vertex to mid-thigh PET/CT imaging was acquired. No special patient preparation was observed before PET imaging. PET imaging was done in 3D mode at 3 minutes/bed position.

Image analysis was similar as described for ¹⁸F-FDG PET imaging. Only a 60-minute [⁶⁸Ga]Ga-pentixafor PET/CT imaging was obtained. Aortic-SUVmax, SVC-SUVmean, aortic-TBR, carotid-SUVmax, IJV-SUVmean, and carotid-TBR were obtained on [⁶⁸Ga]Ga-pentixafor PET/CT images.

Statistical analysis

We performed descriptive statistics of baseline clinical and demographic information of patients. Categorical data are presented as frequencies while continuous variables are presented as mean ± standard deviation (SD) or as median (interquartile range, IQR). We compared the early and late ¹⁸F-FDG PET variables using Paired Sample T test. We used Bland and Altman plots to show the level of agreement in arterial tracer quantification variables derived from ¹⁸F-FDG PET versus those derived from [⁶⁸Ga]Ga-pentixafor PET imaging. We also used Spearman correlation check for correlation between the arterial tracer quantification variables derived from ¹⁸F-FDG PET versus those derived from [⁶⁸Ga]Ga-pentixafor PET imaging. Statistical significance was set at p<0.05. We performed statistical analysis using IBM SPSS Statistics 21.0 (IBM Corp, Armonk, New York USA).

RESULTS

A total of 12 HIV-infected adults with suppressed HIV viremia were included, mean age was 44.67 ± 7.62 years. There were eight women (66.7%). The mean duration of HIV infection and mean CD⁺ T-cell count of the study population were 71.08 ± 37 months and 522.17 ± 260.33 cells/ μ L, respectively. The mean activity of administered ¹⁸F-FDG was significantly higher than that of [⁶⁸Ga]Ga-pentixafor (7.84 ± 1.17 mCi and 4.70 ± 2.12 mCi, p<0.001). The median interval between the two scans was 2 days (range=1-11 days). Table 1 shows the details of the baseline clinical and demographic characteristics of the study population.

Table 1 Demographic and clinical variables of the study population

Variable	Frequency	Percent (%)
Age (years)		
Mean \pm SD	44.67 \pm 7.62	
Range	38 – 65	
Gender		
Male	4	33.3
Female	8	66.7
BMI		
Underweight	1	8.3
Normal	7	58.3
Overweight	3	25.0
Obese	1	8.3
Mean \pm SD	24.18 \pm 3.45	
Range	17.84 – 32.07	
Smoking		
Yes	1	8.3
No	11	91.7
HTN		
Yes	2	16.7
No	10	83.3
DM		
Yes	1	8.3
No	11	91.7
ART		
2NRTI+1INSTI	1	8.3
2NRTI+1NNRTI	9	75.0
2NRTI+1PI	2	16.7
Family history of CVD		
Yes	2	16.7
No	10	83.3
FRS risk		
Low	8	66.7
Moderate	3	25.0
High	1	8.3
Mean \pm SD		
CD4+ T-cell count (cells/ μ L)	522.17 \pm 260.33	

D:A:D risk score	2.59 ± 2.35
C-reactive protein	11.08 ± 4.72
Hemoglobin (g/dL)	11.59 ± 1.96
FBS (mmol/L)	5.88 ± 1.51
Lipid profile	
Triglyceride (mmol/L)	0.91 ± 0.21
LDL cholesterol (mmol/L)	2.71 ± 0.56
HDL cholesterol (mmol/L)	1.23 ± 0.19
Total cholesterol (mmol/L)	4.33 ± 0.83

BMI: Body Mass Index; **HTN:** Hypertension; **DM:** Diabetes Mellitus; **ART:** Antiretroviral Therapy; **NRTI:** Nucleoside Reverse Transcriptase Inhibitor; **NNRTI:** Non-Nucleoside Reverse Transcriptase Inhibitor; **PI:** Protease Inhibitor; **INTSTI:** Integrase Strand Transfer Inhibitor; **CVD:** Cardiovascular Disease; **FRS:** Framingham Risk Score; **LDL:** Low-Density Lipoprotein; **HDL:** High-Density Lipoprotein; **FBS:** Fasting Blood Sugar

Comparison between early and late ¹⁸F-FDG PET quantification variables

Table 2 shows the details regarding comparison between the variables derived from the early and late scan. For the two arterial beds of interest, there was a significant increase in SUVmax in the late scan compared with the early scan. Venous blood pool activity showed a significant decrease between the early and the late scan measured by venous SUVmean. The decline in SUVmean between the early and the late scans did not reach a statistical significance in the IJV. Consequent to an improvement in arterial SUVmax and a decline in venous SUVmean, there was a significant increase in the arterial TBR for both the aortic and carotid arterial beds.

Table 2 Comparison between early and late ¹⁸F-FDG PET/CT-derived parameters

Variable	Early	Late	t	p value
	Mean ± SD	Mean ± SD		
Aortic SUVmax	2.21 ± 0.39	2.85 ± 0.45	-5.160	<0.001*
Superior vena cava SUVmean	1.28 ± 0.26	1.06 ± 0.22	2.701	0.021*
Aortic TBR	1.76 ± 0.30	2.76 ± 0.52	-5.783	<0.001*
Carotid SUVmax	1.66 ± 0.43	2.21 ± 0.64	-4.074	0.002*
Internal jugular vein SUVmean	1.13 ± 0.31	1.05 ± 0.58	0.765	0.460
Carotid TBR	1.51 ± 0.38	2.38 ± 0.66	-4.741	0.001*

t: Paired Samples T test; *: p value <0.05 (i.e. statistically significant); **SUVmax:** maximum Standardized Uptake Value; **SUVmean:** mean Standardized Uptake Value; **TBR:** Target-to-Background Ratio

Level of agreement between ^{18}F -FDG PET and $[^{68}\text{Ga}]\text{Ga}$ -pentixafor PET-derived variables

There is a high level of agreement between the ^{18}F -FDG PET-derived quantification variables and the $[^{68}\text{Ga}]\text{Ga}$ -pentixafor PET-derived variables in the aortic and carotid arterial beds (Figs 1-3). The level of agreement was higher for early ^{18}F -FDG PET-derived quantification variables and $[^{68}\text{Ga}]\text{Ga}$ -pentixafor PET-derived variables than for the comparison between late ^{18}F -FDG PET-derived quantification variables and $[^{68}\text{Ga}]\text{Ga}$ -pentixafor PET-derived variables.

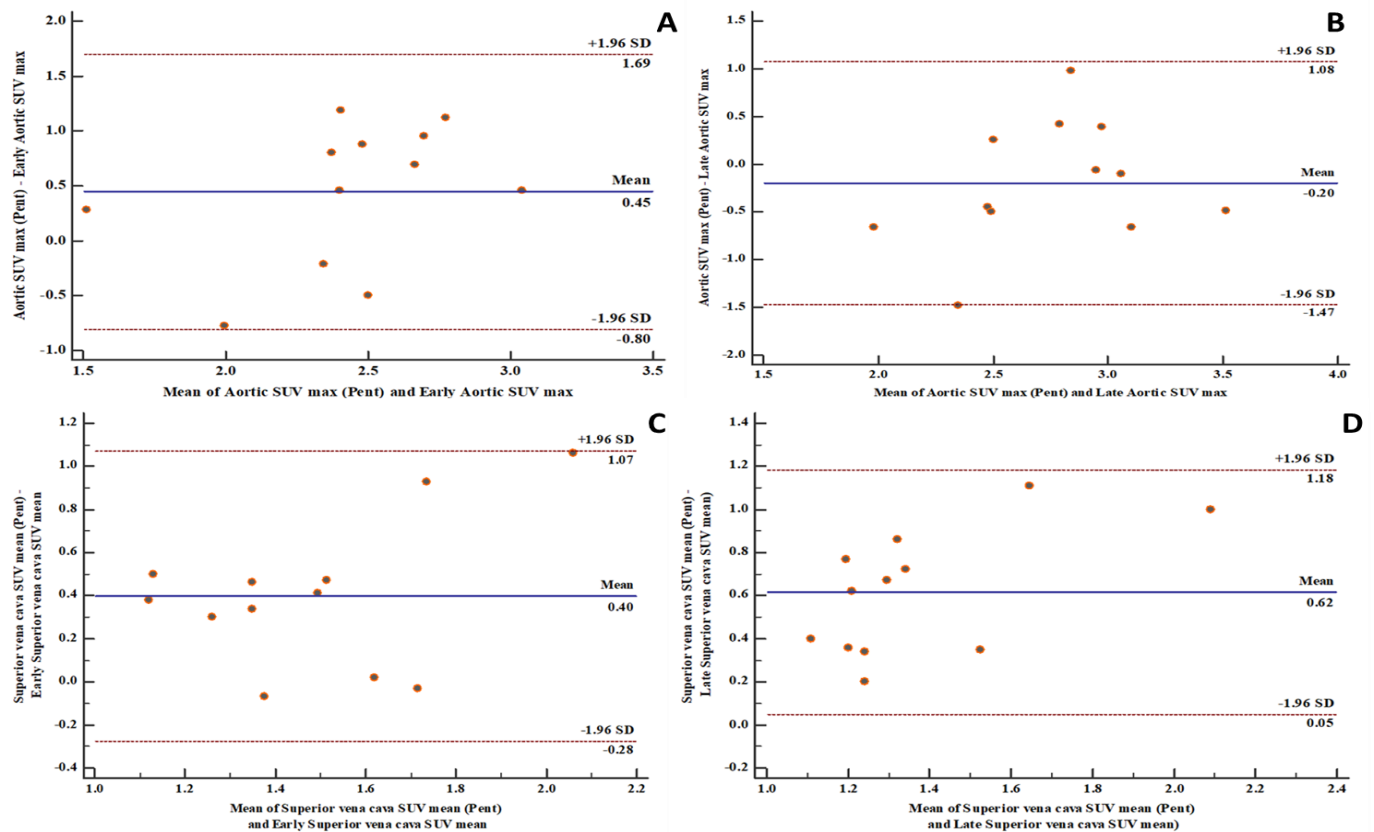


Fig 1 Bland and Altman plots showing good levels of agreement between ^{18}F -FDG PET/CT and $[^{68}\text{Ga}]\text{Ga}$ pentixafor PET/CT-derived variables: (A) a good level of agreement between $[^{68}\text{Ga}]\text{Ga}$ -pentixafor PET-derived aortic SUVmax and ^{18}F -FDG PET-derived early aortic SUVmax with 100% of measurements within the limits of agreement; (B) a good level of agreement between $[^{68}\text{Ga}]\text{Ga}$ -pentixafor PET-derived aortic SUVmax and ^{18}F -FDG PET-derived late aortic SUVmax with 91.7% of measurements within the limits of agreement; (C) a good level of agreement between $[^{68}\text{Ga}]\text{Ga}$ -pentixafor PET-derived superior vena cava SUVmean and ^{18}F -FDG PET-derived early superior vena cava SUVmean with 100% of measurements within the limits of agreement; (D) a good level of agreement between $[^{68}\text{Ga}]\text{Ga}$ -pentixafor PET-derived superior vena cava SUVmean and ^{18}F -FDG PET-derived late superior vena cava SUVmean with 100% of measurements within the limits of agreement

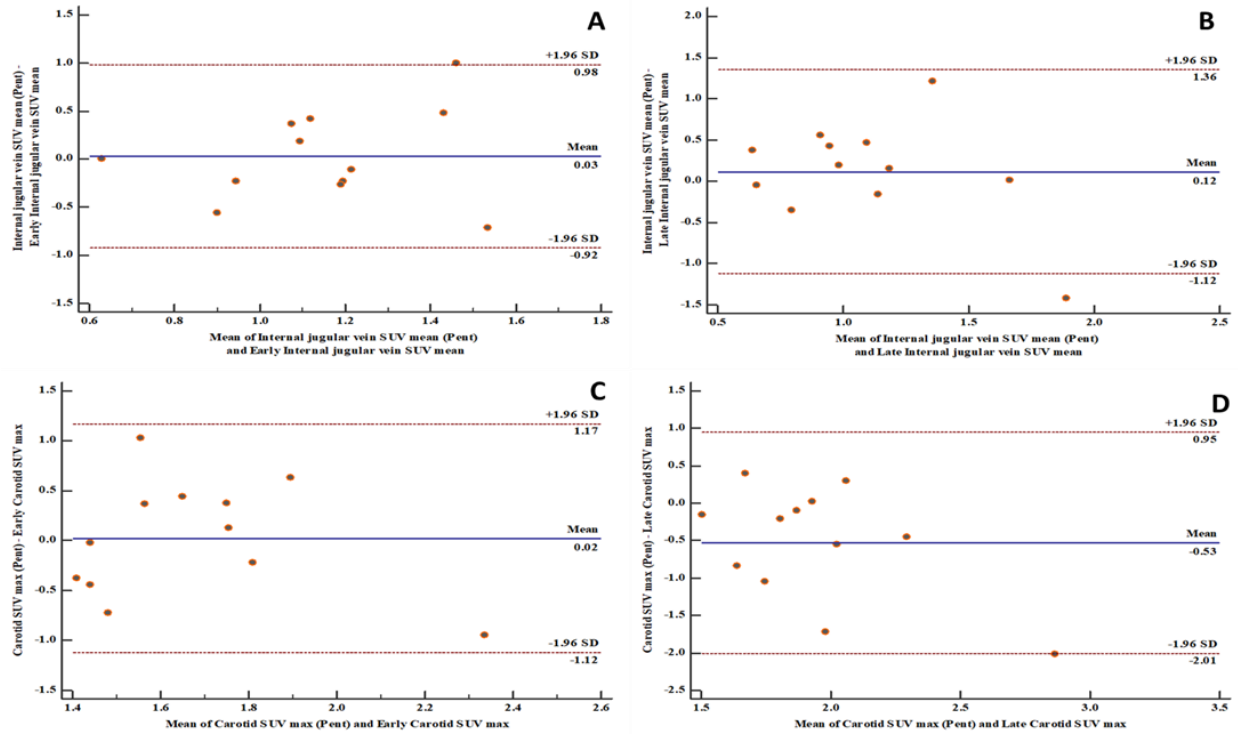


Fig 2 Bland and Altman plots showing good levels of agreement between ^{18}F -FDG PET/CT and ^{68}Ga]Ga-pentixafor PET/CT-derived variables: (A) a good level of agreement between ^{68}Ga]Ga-pentixafor PET-derived internal jugular vein SUVmean and ^{18}F -FDG PET-derived early internal jugular vein SUVmean with 91.7% of measurements within the limits of agreement; (B) a good level of agreement between ^{68}Ga]Ga-pentixafor PET-derived internal jugular vein SUVmean and ^{18}F -FDG PET-derived late internal jugular vein SUVmean with 91.7% of measurements within the limits of agreement; (C) a good level of agreement between ^{68}Ga]Ga-pentixafor PET-derived carotid SUVmax and ^{18}F -FDG PET-derived early carotid SUVmax with 100% of measurements within the limits of agreement; (D) a good level of agreement between ^{68}Ga]Ga-pentixafor PET-derived carotid SUVmax and ^{18}F -FDG PET-derived late carotid SUVmax with 91.7% of measurements within the limits of agreement

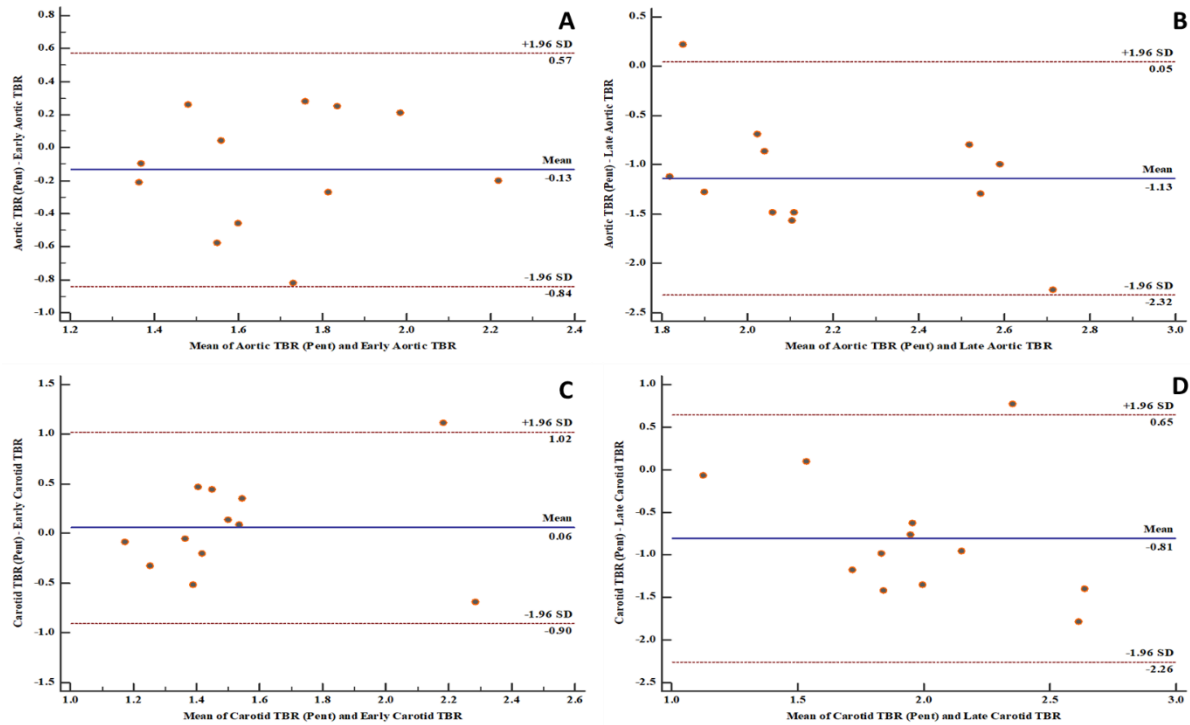


Fig 3 Bland and Altman plots showing good levels of agreement between ^{18}F -FDG PET/CT and ^{68}Ga]Ga-pentixafor PET/CT-derived variables: (A) a good level of agreement between ^{68}Ga]Ga-pentixafor PET-derived aortic target-to-background ratio (TBR) and ^{18}F -FDG PET-derived early aortic target-to-background ratio (TBR) with 91.7% of measurements within the limits of agreement; (B) a good level of agreement between ^{68}Ga]Ga-pentixafor PET-derived aortic target-to-background ratio (TBR) and ^{18}F -FDG PET-derived late aortic target-to-background ratio (TBR) with 91.7% of measurements within the limits of agreement; (C) a good level of agreement between ^{68}Ga]Ga-pentixafor PET-derived carotid target-to-background ratio (TBR) and ^{18}F -FDG PET-derived early carotid target-to-background ratio (TBR) with 91.7% of measurements within the limits of agreement; (D) a good level of agreement between ^{68}Ga]Ga-pentixafor PET-derived carotid target-to-background ratio (TBR) and ^{18}F -FDG PET-derived late carotid target-to-background ratio (TBR) with 91.7% of measurements within the limits of agreement

Correlation between ^{18}F -FDG PET and ^{68}Ga]Ga-pentixafor PET-derived variables

In the aortic arterial bed, we found a positive correlation between early and late aortic SUVmax, SVC SUVmean, aortic TBR derived from ^{18}F -FDG PET versus aortic SUVmax, SVC SUVmean and aortic TBR derived from ^{68}Ga]Ga-pentixafor (table 3). None of these positive correlations reached a statistical significance. In the carotid arterial bed, we found a negative correlation between early and late carotid SUVmax and early IJV SUVmean derived from ^{18}F -FDG PET versus carotid SUVmax and IJV SUVmean derived from ^{68}Ga]Ga-pentixafor PET/CT. In contrast, we found positive correlations between late IJV SUVmean and early and late carotid TBR derived from ^{18}F -FDG PET/CT and IJV SUVmean and carotid TBR derived

from [⁶⁸Ga]-Ga-pentixafor PET/CT (table 3). Like findings in the aortic arterial bed, these correlations did not reach statistical significance.

Table 3 Correlation between ¹⁸F-FDG PET and [⁶⁸Ga]Ga-pentixafor PET-derived variables

¹⁸ F-FDG PET/CT	[⁶⁸ Ga]Ga-pentixafor PET/CT	
	r	p value
	Aortic SUVmax	
Early Aortic SUVmax	0.077	0.812
Late Aortic SUVmax	0.189	0.557
	Superior vena cava SUVmean	
Early Superior vena cava SUVmean	0.560	0.058
Late Superior vena cava SUVmean	0.235	0.463
	Aortic TBR	
Early Aortic TBR	0.344	0.274
Late Aortic TBR	0.225	0.483
	Carotid SUV max	
Early Carotid SUVmax	-0.403	0.194
Late Carotid SUVmax	-0.200	0.532
	Internal jugular vein SUVmean	
Early Internal jugular vein SUVmean	-0.168	0.602
Late Internal jugular vein SUVmean	0.217	0.499
	Carotid TBR	
Early Carotid TBR	0.123	0.704
Late Carotid TBR	0.295	0.352

r: Spearman Correlation Coefficient; **SUVmax**: maximum Standardized Uptake Value; **SUVmean**: mean Standardized Uptake Value; **TBR**: Target-to-Background Ratio

DISCUSSION

¹⁸F-FDG PET/CT is the most used radionuclide imaging technique for arterial inflammation imaging. In this prospective study, we evaluated the level of agreement in arterial tracer uptake quantification between ¹⁸F-FDG PET/CT and [⁶⁸Ga]Ga-pentixafor PET/CT. We found a high level of agreement between the quantitative parameters obtained on both imaging techniques. Our findings suggest that [⁶⁸Ga]Ga-pentixafor may be as effective in quantifying arterial inflammation as ¹⁸F-FDG PET/CT without experiencing the challenges associated with clinical ¹⁸F-FDG PET/CT imaging. We chose to make the comparison in PLHIV because of the elevated

risk of ASCVD in them [1]. PLHIV represents a group where arterial inflammation is present from a young age even in the absence of traditional ASCVD risk factors and despite effective ART [6].

Some important studies have shown the utility of ^{18}F -FDG PET/CT in quantifying arterial inflammation in PLHIV [11,12]. ^{18}F -FDG PET/CT studies have shown elevated arterial inflammation in PLHIV compared with age- and gender-matched control [5,6]. In another study, ^{18}F -FDG PET/CT was used to demonstrate residual arterial inflammation in patients who were treated with effective ART [13]. More recently, Hsue and colleagues demonstrated the utility of ^{18}F -FDG PET/CT for treatment response assessment in HIV-infected people treated with canakinumab, an interleukin- 1β inhibitor targeting arterial inflammation [14]. Some other studies have failed to show a significantly higher burden of arterial inflammation in PLHIV compared with non-HIV infected controls [15-17]. These contradictory findings may be related to the limitations associated with ^{18}F -FDG PET/CT for arterial inflammation imaging [18]. Apart from the need for patients to fast and stop certain medications that can interfere with ^{18}F -FDG biodistribution, there are important hurdles encountered when using ^{18}F -FDG PET/CT for arterial inflammation quantification. The intense ^{18}F -FDG accumulation in the myocardium and soft tissues of the neck precludes accurate arterial ^{18}F -FDG uptake quantification in the coronary and carotid arteries, two of the most important arterial beds involved in ASCVD. During arterial ^{18}F -FDG quantification for vascular inflammation imaging, the goal is to quantify ^{18}F -FDG uptake by inflammatory cells. In ASCVD, ^{18}F -FDG uptake in the vascular smooth muscle contributes significantly to the PET signal recorded during quantification [19].

In view of the limitations associated with the use of ^{18}F -FDG PET/CT for arterial inflammation quantification, it is therefore important to evaluate other tracers for this indication. We chose [^{68}Ga]Ga-pentixafor due to its specific binding to macrophages and not to other components of arterial wall [7]. Also, [^{68}Ga]Ga-pentixafor does not show high physiologic uptake in multiple organs like ^{18}F -FDG. In the study by Hyafil and colleagues, only few organs, including spleen, adrenals and bone marrow, show significant physiologic [^{68}Ga]Ga-pentixafor uptake. This allows for accurate quantification of tracer uptake in any arterial bed of interest. High expression of CXCR-4 in high-risk atheromatous lesions and precursor pre-atheromatous lesions makes [^{68}Ga]Ga-pentixafor a viable tool for non-invasive imaging of arterial inflammation [20]. Good reproducibility of TBR quantification in atheromatous plaques makes

[⁶⁸Ga]Ga-pentixafor PET/CT a technical feasible modality for arterial inflammation imaging [21].

PET imaging of arterial inflammation presents a peculiar limitation due to the limited spatial resolution of the PET system causing significant underestimation of quantified arterial tracer uptake. To reduce the degree of this under-estimation, the Cardiovascular Committee of the EANM proposed certain imaging conditions to be observed while applying ¹⁸F-FDG PET/CT for atherosclerotic vascular inflammation imaging. In this study, we performed a dual-time-point imaging, using the routine oncologic imaging parameters and subsequently applied the EANM recommendations, to achieve a robust comparison of arterial quantification with both tracers evaluated in this study. While there was a significant increase in arterial ¹⁸F-FDG uptake and reduction in background blood-pool activity between the early and late imaging, the quantified [⁶⁸Ga]Ga-pentixafor showed a good level of agreements with the ¹⁸F-FDG PET quantification parameters obtained on the early and late imaging. A study has previously evaluated the correlation between ¹⁸F-FDG PET/CT and [⁶⁸Ga]Ga-pentixafor PET/CT in the quantification of tracer uptake in arterial lesion [22]. This study was a retrospective analysis of data obtained in oncologic patients imaged with both tracers. Like in our study, the authors also reported a weak correlation, albeit with a statistical significance. Our study differs from this previous study regarding the study population (we studied HIV-infected patients while the previous study included HIV-uninfected oncologic patients) and the optimization of ¹⁸F-FDG PET imaging criteria applied in a prospective setting in our study. The weak and statistical insignificant correlations seen in our study despite a good agreement in quantification parameters between the two imaging modalities may be related to the differences in target between the two tracers. There is significant ¹⁸F-FDG uptake in all components of the arterial wall [19], while [⁶⁸Ga]Ga-pentixafor is more specific for macrophages within the vascular endothelium [7]. Another possible contributor to a lack of statistical significance in the level of correlation in quantification parameters between the two imaging modalities may be related to the significant difference in the activity of tracer injected for the two imaging studies.

As done for ¹⁸F-FDG PET/CT imaging of atherosclerotic vascular inflammation, it may be necessary to perform similar standardization for [⁶⁸Ga]Ga-pentixafor PET/CT imaging of arterial inflammation imaging. This standardization may reduce the under-estimation of arterial tracer quantification. Respiratory and cardiac motion causes image blurring and results in under-

estimation in PET signal quantification due to partial volume averaging. Gating of PET acquisition may be a viable way to standardized vascular inflammation imaging. This was confirmed in the study by Derlin et al. where the highest number of coronary lesions were seen in dual-gated imaging (corrected for respiratory and cardiac motion) compared with single or ungated [^{68}Ga]Ga-pentixafor PET acquisition [23].

The strength of our study lies in its novelty. We performed a head-to-head comparison of ^{18}F -FDG PET/CT and [^{68}Ga]Ga-pentixafor PET/CT for arterial inflammation using standardized imaging criteria for the ^{18}F -FDG PET/CT imaging. Our study included PLHIV, a group of patients in which ASCVD is a rising cause of morbidity and mortality but with limited data showing the role of radionuclide imaging for disease characterization in them [24]. Our study has got some limitations, the most important being the small study population. Despite this limited study population, we were able to demonstrate a high level of agreement between the two imaging modalities. Our study population has a low prevalence of ASCVD risks. PLHIV are at risk of ASCVD even in the absence of a high traditional cardiovascular risks.

CONCLUSION

There is a high level of agreement in the vascular tracer quantification as a marker of arterial inflammation between ^{18}F -FDG PET/CT and [^{68}Ga]Ga-pentixafor PET/CT in people living with HIV. We found no significant correlation in the quantification variables between the two imaging modalities. Optimization of imaging conditions for ^{18}F -FDG PET/CT improves the level of arterial tracer uptake and background blood-pool clearance.

Acknowledgements

We are grateful to PENTIXAPHARM, Wuerzburg, Germany for providing us with pentixafor used in this study. We also express our gratitude to all staff members of the department of Nuclear Medicine at Steve Biko Academic Hospital and NuMeRI, South Africa. We thank our patients who volunteered to participate in this South study.

Author contributions:

Conceptualization: I.O.L.; M.M.S.

Methodology: I.O.L.; J.P.; C.D.; J.K.; H.B.; H.J.W.; M.M.S.

Formal analysis: I.O.L.; G.O.P.

Investigation: I.O.L.; J.P.; C.D.; H.D.; L.C.M.; K.M.G.M.; J.R.Z.

Resources: J.R.Z.; J.K.; H.B.; H.J.W.; M.M.S.

Data Curation: I.O.L.; G.O.P.; K.M.G.M.

Writing – original draft preparation: I.O.L.

Writing – review and editing: I.O.L.; G.O.P.; J.P.; J.K.; C.D.; H.D.; L.C.M.; K.M.G.M.; H.B.; H.J.W.; J.R.Z.; M.M.S.

Supervision: J.R.Z.; M.M.S.

Funding acquisition: J.R.Z.; M.M.S

Conflicts of Interest:

Jens Kaufmann and Hakim Bouterfa are employees of PentixaPharm. Hans-Jürgen Wester is a founder, shareholder, and advisory board member of Scintomics GmbH, Fuerstenfeldbruck, Germany. The other authors declare no conflict of interest.

References

1. Shah ASV, Stelzle D, Lee KK, Beck EJ, Alam S, Clifford S, et al. Global burden of atherosclerotic cardiovascular disease in people living with HIV: Systematic review and meta-analysis. *Circulation*. 2018;138:1100-1112.
2. Triant VA, Grinspoon SK. Epidemiology of ischaemic heart disease in HIV. *Curr Opin HIV AIDS*. 2017;12:540-547.
3. Libby P, Ridker PM, Hansson GK; Leducq Transatlantic Network on Atherothrombosis. Inflammation in atherosclerosis: from pathophysiology to practice. *J Am Coll Cardiol*. 2009;54:2129-2138.
4. Ridker PM, Everett BM, Thuren T, MacFadyen JG, Chang WH, Ballantyne C, et al. Antiinflammatory Therapy with Canakinumab for Atherosclerotic Disease. *N Engl J Med*. 2017;377:1119-1131.
5. Subramanian S, Tawakol A, Burdo TH, Abbara S, Wei J, Vijayakumar J, et al. Arterial inflammation in patients with HIV. *JAMA*. 2012;308:379-386.
6. Lawal IO, Ankrah AO, Popoola GO, Lengana T, Sathekge MM. Arterial inflammation in young patients with human immunodeficiency virus infection: A cross-sectional study using F-18 FDG PET/CT. *J Nucl Cardiol*. 2019;26:1258-1265.
7. Hyafil F, Pelisek J, Laitinen I, Schottelius M, Mohring M, Döring Y, et al. Imaging the cytokine receptor CXCR4 in atherosclerotic plaques with the radiotracer ⁶⁸Ga-pentixafor for PET. *J Nucl Med*. 2017;58:499-506.
8. Weiberg D, Thackeray JT, Daum G, Sohns JM, Kropf S, Wester HJ, et al. Clinical Molecular Imaging of Chemokine Receptor CXCR4 Expression in Atherosclerotic Plaque Using ⁶⁸Ga-Pentixafor PET: Correlation with Cardiovascular Risk Factors and Calcified Plaque Burden. *J Nucl Med*. 2018;59:266-272.
9. Bucerius J, Hyafil F, Verberne HJ, Slart RH, Lindner O, Sciagra R, et al. Position paper of the Cardiovascular Committee of the European Association of Nuclear Medicine (EANM) on PET imaging of atherosclerosis. *Eur J Nucl Med Mol Imaging*. 2016 Apr;43(4):780-92. doi: 10.1007/s00259-015-3259-3. Epub 2015 Dec 17. PMID: 26678270; PMCID: PMC4764627.
10. Lawal IO, Mokoala KG, Popoola GO, Lengana T, Ankrah AO, Stoltz AC, et al. Impact of optimized PET imaging conditions on ¹⁸F-FDG uptake quantification in patients with

- apparently normal aortas. *J Nucl Cardiol*. Epub ahead of print on 06 August 2019. doi: 10.1007/s12350-019-01833-6.
11. Schoepf IC, Buechel RR, Kovari H, Hommoud DA, Tarr PE. Subclinical atherosclerosis imaging in people living with HIV. *J Clin Med*. 2019;8:1125.
 12. Lawal IO, Ankrah AO, Stoltz AC, Sathekge MM. Radionuclide imaging of inflammation in atherosclerotic vascular disease among people living with HIV infection: current practice and future perspective. *Eur J Hybrid Imaging*. 2019;3:5.
 13. Zanni MV, Toribio M, Robbins GK, Burdo TH, Lu MT, Ishai AE, et al. Effects of antiretroviral therapy on immune function and arterial inflammation in treatment-naïve patients with human immunodeficiency virus infection. *JAMA Cardiol*. 2016;1:474-480.
 14. Hsue PY, Li D, Ishai A, Manion M, Nahrendorf M, Ganz P, et al. IL-1 β inhibition reduces atherosclerotic inflammation in HIV infection. *J Am Coll Cardiol*. 2018;72:2809-2811.
 15. Knudsen A, Fisker AM, Loft A, von Benzon E, Keller SH, Møller HJ, et al. HIV infection and arterial inflammation assessed by ^{18}F -fluorodeoxyglucose (FDG) positron emission tomography (PET): A prospective cross-sectional study. *J Nucl Cardiol*. 2015;22:372-380.
 16. Yarasheski KE, Laciny E, Overton ET, Reeds DN, Harrod M, Baldwin S, et al. ^{18}F FDG PET-CT imaging detects arterial inflammation and early atherosclerosis in HIV-infected adults with cardiovascular disease risk factors. *J Inflamm*. 2012;9:26.
 17. Lo J, Lu MT, Ihenachor EJ, Wei J, Looby SE, Fitch KV, et al. Effects of statin therapy on coronary artery plaque volume and high risk plaque morphology in HIV-infected patients with subclinical atherosclerosis: a randomized double-blind placebo-controlled trial. *Lancet HIV*. 2015;2:e52-e63.
 18. Rogers IS, Tawakol A. Imaging of coronary inflammation with FDG-PET: Feasibility and clinical hurdles. *Curr Cradiol Rep*. 2011;13:138-144.
 19. Al-Mashhadi RH, Tolbod LP, Bloch LØ, Bjørklund MM, Nasr ZP, Al-Mashhadi Z, et al. ^{18}F Fluorodeoxyglucose accumulation in arterial tissues determined by PET signal analysis. *J Am Coll Cardiol*. 2019;74:1220-1232.

20. Li X, Yu W, Wollenweber T, Lu X, Wei Y, Beitzke D, et al. [⁶⁸Ga]Pentixafor PET/MR imaging of chemokine receptor 4 expression in human carotid artery. *Eur J Nucl Med Mol Imaging*. 2019;46:1616-1625.
21. Li X, Heber D, Leike T, Beitzke D, Lu X, Zhang X, et al. [⁶⁸Ga]Pentixafor-PET/MRI for the detection of chemokine receptor 4 expression in atherosclerotic plaques. *Eur J Nucl Med Mol Imaging*. 2018;45:558-566.
22. Kircher M, Tran-Gia J, Kemmer L, Zhang X, Schirbel A, Wernal RA, et al. Imaging inflammation in atherosclerosis with CXCR4-directed ⁶⁸Ga-pentixafor PET/CT: Correlation with ¹⁸F-FDG PET/CT. *J Nucl Med*. 2020;61:751-756.
23. Derlin T, Sedding DG, Dutzmann J, Haghikia A, König T, Napp LC, et al. Imaging of chemokine receptor CXCR4 expression in culprit and nonculprit coronary atherosclerotic plaque using motion-corrected [⁶⁸Ga]pentixafor PET/CT. *Eur J Nucl Med Mol Imaging*. 2018;45:1934-1944.
24. Lawal IO, Stoltz AC, Sathekge MM. Molecular imaging of cardiovascular inflammation and infection in people living with HIV infection. *Clin Transl Imaging*. 2020;8:141-155.

CHAPTER 7

FDG PET/CT for evaluating systemic arterial inflammation induced by anthracycline-based chemotherapy of Hodgkin lymphoma: A retrospective cohort study

Ismaheel O. Lawal^{1,2} MD; Akintunde T. Orunmuyi³ MD; Gbenga O. Popoola⁴ MD; Thabo Lengana^{1,5} MD; Kgomotso M.G. Mokoala¹ MD; Alfred O. Ankrah^{1,6} MD; Mike M. Sathekge^{1,2} MD, PhD

1. Department of Nuclear Medicine, University of Pretoria, Pretoria, South Africa.
2. Nuclear Medicine Research Infrastructure (NuMeRI), Steve Biko Academic Hospital, Pretoria, South Africa.
3. Department of Nuclear Medicine, University of Ibadan, Ibadan, Nigeria.
4. Department of Epidemiology and Community Health, University of Ilorin, Ilorin, Nigeria.
5. KVNR Nuclear and Molecular Imaging, South Africa.
6. Department of Nuclear Medicine and Molecular Imaging, University of Groningen, Groningen, The Netherlands.

Medicine (Baltimore). 2020;99(48):e23259.

Abbreviations

ABVD	Adriamycin, Bleomycin, Vinblastine, Dacarbazine
ASCVD	Atherosclerotic Cardiovascular Disease
BMI	Body mass Index
FDG PET/CT	Fluorine-18 fluorodeoxyglucose Positron Emission Tomography/ Computed Tomography
HIV	Human Immunodeficiency Virus
HL	Hodgkin Lymphoma
SUVmax	maximum Standardized Uptake Value
TBR	Target-to-Background ratio

Abstract

Objectives. To evaluate arterial fluorine-18 fluorodeoxyglucose (^{18}F -FDG) uptake as a marker of arterial inflammation in multiple vascular beds in patients treated with anthracycline-based chemotherapy for Hodgkin lymphoma (HL).

Methods. We used standardized maximum uptake value (SUVmax) and target-to-background ratio (TBR) to quantify arterial ^{18}F -FDG uptake in the carotid artery, ascending aorta, abdominal aorta and femoral artery obtained on positron emission tomography/computed tomography (PET/CT) imaging performed at baseline before chemotherapy and after completion of chemotherapy in patients with HL treated with an anthracycline-containing regimen. We compared the SUVmax and TBR obtained at baseline with that obtained post-chemotherapy for each arterial bed to evaluate the effect of anthracycline-based chemotherapy. We evaluated the effect of cardiovascular risk factors such as human immunodeficiency virus (HIV) infection, smoking, hypertension, and diabetes on the changes in SUVmax and TBR seen in the different arterial beds after anthracycline-based chemotherapy.

Results. Fifty-two patients were included with a mean age of 34.56 ± 10.19 years. There were 33 males, and 18 patients were HIV-infected. The mean interval between completion of chemotherapy and follow-up ^{18}F -FDG PET/CT scan was 65 weeks. We found no significant difference in arterial FDG uptake measured by SUVmax and TBR in all arterial beds between the pre- and post-chemotherapy ^{18}F -FDG PET/CT. There was no significant impact of HIV infection, smoking, and hypertension on the changes in arterial ^{18}F -FDG uptake following treatment with anthracycline-based chemotherapy.

Conclusion. In patients with HL who were treated with anthracycline-based chemotherapy, we found no significant increase in arterial inflammation measured by ^{18}F -FDG PET/CT after an average follow-up period of about 65 weeks since completion of chemotherapy.

Keywords

Arterial inflammation, ^{18}F -FDG PET/CT, Anthracyclines, Hodgkin lymphoma

INTRODUCTION

Hodgkin lymphoma (HL) is a malignant disease with an excellent response to therapy. Ten-year overall survival is reported in over 80% of patients treated for HL [1,2]. Over 90% of patients treated for HL in their childhood or adolescence survive into adulthood [3]. Anthracyclines are a group of anti-cancer chemotherapeutic agents that form the backbone of HL treatment. Avoiding them in HL treatment leads to less favorable treatment outcome [4]. Despite their efficacy, anthracyclines increase cardiovascular mortality and morbidity of patients in the long run. One of the pathogenic mechanisms by which anthracyclines predispose to atherosclerotic cardiovascular disease (ASCVD) is by causing impairment in the repair of endothelial injury. Anthracycline agents cause an increase in the circulating level of functionally incapacitated endothelial progenitor cells [5], which are responsible for the repair of endothelial injury through the process of re-endothelization after injury [6]. Unrepaired endothelial injury is the bedrock lesion for the formation of vascular atheroma formation.

Long-term survival of patients treated for HL and the negative impact of anthracycline on vascular endothelial function, therefore, expose these patients to significant cardiovascular morbidity and mortality. A recent study with an extended follow-up of 40 years post HL treatment reported a 4- to 7-fold increased risk of coronary artery disease among HL survivors compared with the general population, which translates to 857 excess cardiovascular events per 10 000 person-years [7].

Inflammation is the hallmark process that drives vascular atheroma formation, progression, and its catastrophic completion [8]. The prominent role played by inflammation in ASCVD has formed the basis for the keen interest in the use of anti-inflammatory agents as a primary and secondary preventive therapeutic intervention in many recent randomized trials [9,10]. Fluorine-18 fluorodeoxyglucose (^{18}F -FDG) is a radioactive analog of glucose which is trapped by cancer cells and activated inflammatory cells. Photons emitted when ^{18}F -FDG undergoes radioactive decay can be imaged using hybrid Positron emission tomography and computed tomography (PET/CT) scanner. ^{18}F -FDG PET/CT has, therefore, emerged in the last two decades as a sensitive tool for non-invasive imaging of biological processes, including inflammation, infection, and neoplasm. The intensity of ^{18}F -FDG uptake in the vessel has been shown to correlate with the level of vascular macrophage invasion [11,12]. Abdelbaky et al.

showed, in a longitudinal ^{18}F -FDG PET/CT study, that arterial inflammation precedes subsequent calcification in the same location as a marker of plaque progression [13]. The level of inflammation in the vessel in general or in an atherosclerotic lesion in specific correlates with the risk of cardiovascular events in a patient [14-16]. ^{18}F -FDG PET/CT is the most accurate imaging modality for the staging and re-staging of HL and is the most commonly used imaging modality for these indications in routine clinical practice [17,18]. ^{18}F -FDG PET/CT can, therefore, serve the dual role for evaluating HL and vascular inflammation as a risk for ASCVD in patients treated with anthracycline-based chemotherapy. To our knowledge, no published study has evaluated the clinical utility of ^{18}F -FDG PET/CT in characterizing arterial inflammation in the patients treated with anthracycline-based chemotherapy for HL. In this study, we aimed to evaluate arterial ^{18}F -FDG uptake as a marker of arterial inflammation in multiple vascular beds of patients treated with anthracycline-based chemotherapy for HL. We hypothesized that arterial ^{18}F -FDG uptake would be higher on post-chemotherapy ^{18}F -FDG PET/CT compared with pre-therapy ^{18}F -FDG PET/CT.

MATERIAL AND METHODS

Patients

We performed a retrospective review of ^{18}F -FDG PET/CT scans of patients referred to the Department of Nuclear Medicine at Steve Biko Academic Hospital, Pretoria, between August 2015 and September 2019 for baseline staging and Post-chemotherapy assessment of HL. We included patients who were aged 18 years and older and were treated with a standard course of adriamycin, bleomycin, vinblastine, and dacarbazine (ABVD). We excluded patients in whom arterial FDG uptake could not be quantified without interference from adjacent lymphoma. Other exclusion criteria were renal failure (estimated glomerular filtration rate of <60 ml/min/m²), treatment with a chemotherapy regimen other than ABVD, additional radiotherapy, technically inadequate scans, ongoing use of steroid or other anti-inflammatory medications, and suspected or confirmed vasculitis. We reviewed the patients' hospital records to obtain their demographic information, the associated co-morbidities, and social history. Patients were defined as smokers if they smoked at least a stick of cigarette per day. Patients were classified as hypertensive or diabetic if they self-identified as such based on previous hospital diagnosis, or were on treatment

for these chronic medical conditions. Our institutional review board approved the study and waived the need for patients' consent due to the retrospective design of this study.

¹⁸F-FDG PET/CT scan imaging

¹⁸F-FDG PET/CT scan imaging was performed as previously described and according to published guidelines [19,20]. Briefly, all patients had a minimum of four hours of fasting. The blood sugar level was less than 11.1 mmol/L in all patients at the time of ¹⁸F-FDG injection. The activity of ¹⁸F-FDG administered was adjusted for patient weight. Imaging commenced 60 minutes after the intravenous administration of ¹⁸F-FDG. Imaging was acquired on a Biograph 40 Truepoint hybrid PET/CT scanner (Siemens Medical Solution, Illinois, USA). Imaging was acquired from vertex to mid-thigh. PET imaging was acquired in 3D mode at 3 minutes per bed position with a 50% overlap. We performed image reconstruction using the ordered subset expectation maximization algorithm (4 iterations and 8 subsets) with a Gaussian filter applied at full-width half-maximum of 5.0mm.

Image analysis

We performed image analysis on a dedicated workstation equipped with a Syngo.via software. We used the maximum standardized uptake value (SUVmax) and the target-to-background ratio (TBR) as the parameters for arterial ¹⁸F-FDG uptake quantification following the recommendation of the Cardiovascular Committee of the European Association of Nuclear Medicine (EANM) [21]. To evaluate systemic arterial inflammation using vascular ¹⁸F-FDG uptake, we selected the distal common carotid artery, the ascending aorta, the infra-renal abdominal aorta, and the proximal femoral artery as the representative arterial beds on both the baseline and post-chemotherapy ¹⁸F-FDG PET/CT scans. We determined SUVmax and TBR at these arterial beds. For SUVmax, we drew multiple regions of interest (ROI) around the arterial bed of interest and obtained the mean of the SUVmax measurements obtained from each ROI. For TBR (target-to-background ratio), the target represents the mean SUVmax obtained in the arterial bed of interest, while background represents the mean of SUVmean obtained from multiple ROI drawn in the lumen of the vein adjacent to the arterial bed of interest. For the common carotid artery, venous SUVmean was obtained from the adjacent internal jugular vein, superior vena cava for the ascending aorta, the inferior vena cava for the abdominal aorta, and

the femoral vein for the femoral artery. TBR was obtained by dividing the mean arterial SUVmax by the mean venous SUVmean. In patients who had multiple ^{18}F -FDG PET/CT scans after completion of chemotherapy, the analysis was done on the latest scan to obtain the maximum interval between completion of chemotherapy and follow-up ^{18}F -FDG PET/CT.

Statistical analysis

We expressed continuous variables as mean \pm standard deviation (SD). We expressed categorical data as proportions (percentages). We used the Paired Samples T-test to compare SUVmax and TBR obtained at the four arterial beds of interest between the pre-chemotherapy and post-chemotherapy ^{18}F -FDG PET/CT scans. We also compared the patients' parameters such as fasting blood sugar, the activity of ^{18}F -FDG administered for PET/CT scan, patients' weight, and patients' body mass index between the pre- and post-chemotherapy ^{18}F -FDG PET/CT scans. We performed subgroup analysis in patients with human immunodeficiency virus (HIV) infection by comparing pre- and post-chemotherapy variables using Independent Samples T-test. We evaluated the impact of specific cardiovascular risk factors, including smoking, hypertension, and diabetes mellitus, on the changes in arterial ^{18}F -FDG uptake in response to chemotherapy. All statistical analyses were two-tailed, and p-value <0.05 was considered statistically significant. We performed statistical analyses using the IBM SPSS Statistics 21.0 (IBM Corp, Armonk, New York, USA).

RESULTS

A total of 52 patients were included with a mean age of 34.56 ± 10.19 years. There were 33 males, and 18 patients were HIV-infected. The mean duration between the pre- and post-chemotherapy ^{18}F -FDG PET/CT scan was 24.06 months, while the average interval between completion of chemotherapy and follow-up ^{18}F -FDG PET/CT was 65 weeks. Table 1 shows the baseline clinical and demographic characteristics of the patients included.

Table 1 Baseline clinical and demographic characteristics of the patients

Variable	Frequency	Percent (%)
Age (years)		
Mean \pm SD	34.56 \pm 10.19	
Range	18 – 60	
Gender		
Male	33	63.5
Female	19	36.5
HIV		
Yes	18	34.6
No	34	65.4
Smoking		
Yes	15	28.8
No	37	71.2
HTN		
Yes	3	5.8
No	49	94.2
DM		
Yes	2	3.8
No	50	96.2
Weight (Kg)		
Mean \pm SD	70.62 \pm 17.90	
BMI (Kg/m²)		
Mean \pm SD	25.23 \pm 5.98	
CD4 (cells/μL)		
Mean \pm SD	282.44 \pm 131.94	
Interval between the two PET scans (months)		
Mean \pm SD	24.06 \pm 21.53	
Interval between completion of chemotherapy and post-chemo-PET scan (weeks)		
Mean \pm SD	64.67 \pm 88.41	

HIV: Human Immunodeficiency Virus; HTN: Systemic Hypertension; DM: Diabetes Mellitus; BMI: Body Mass Index; CD4: Cluster of Differentiation 4; PET: Positron Emission Tomography

Patients' weight and, consequently, their BMI were significantly higher at the time of post-chemotherapy ¹⁸F-FDG PET/CT compared with pre-chemotherapy ¹⁸F-FDG PET/CT. Fasting blood sugar at the time of ¹⁸F-FDG administration was similar between pre- and post-

chemotherapy ^{18}F -FDG PET/CT scans. Similarly, the activity of ^{18}F -FDG administered for both pre- and post-chemotherapy scans were comparable. We found no significant difference in the SUVmax and TBR measured in the carotid artery, ascending aorta, abdominal aorta, and femoral artery between the pre- and post-chemotherapy ^{18}F -FDG PET/CT scans. Table 2 shows a detailed comparison between pre- and post-chemotherapy ^{18}F -FDG PET/CT scans.

Table 2 Comparison of parameters obtained at pre-chemotherapy and post-chemotherapy ^{18}F -FDG PET/CT scans

Variable	Pre-chemo Mean \pm SD	Post-chemo Mean \pm SD	t	p-value
Weight (Kg)	70.62 \pm 17.90	74.51 \pm 14.38	-3.092	0.003*
BMI (Kg/m ²)	25.23 \pm 5.98	26.73 \pm 5.25	-3.230	0.002*
FBS (mmol/L)	5.94 \pm 1.66	5.54 \pm 1.20	1.461	0.150
Administered ^{18}F -FDG (mCi)	8.78 \pm 2.32	9.05 \pm 2.15	-1.281	0.206
Ascending aorta				
SUV max	2.67 \pm 0.75	2.66 \pm 0.65	0.144	0.886
TBR	1.77 \pm 0.38	1.83 \pm 0.48	-0.765	0.448
Carotid artery				
SUV max	2.02 \pm 0.59	2.01 \pm 0.53	0.039	0.969
TBR	1.44 \pm 0.35	1.45 \pm 0.41	-0.076	0.940
Abdominal aorta				
SUV max	2.63 \pm 0.81	2.47 \pm 0.61	1.363	0.179
TBR	1.81 \pm 0.46	1.69 \pm 0.35	1.410	0.164
Femoral artery				
SUV max	1.48 \pm 0.49	1.50 \pm 0.47	-0.314	0.755
TBR	1.28 \pm 0.31	1.38 \pm 0.36	-1.390	0.171

t: Paired Samples T test; *****: $p < 0.05$; **BMI:** Body Mass Index; **FBS:** fasting Blood Sugar; **FDG:** Fluorodeoxyglucose; **SUVmax:** maximum Standardized Uptake Value; **TBR:** Target-to-Background Ratio; **t:** Paired Samples T test; *****: $p < 0.05$; **BMI:** Body Mass Index; **FBS:** fasting Blood Sugar; **^{18}F -FDG:** Fluorodeoxyglucose; **SUVmax:** maximum Standardized Uptake Value; **TBR:** Target-to-Background Ratio

We compared HIV-infected patients, and those without regarding changes in baseline characteristics and PET derived variables. There was no significant difference in the weight and BMI of HIV-infected patients and those who were not. Similarly, there was no significant difference in the activity of ^{18}F -FDG administered for PET/CT scan and the blood sugar levels at the time of ^{18}F -FDG administration between HIV-infected patients versus HIV-uninfected patients. Table 3 shows comparative data between HIV-infected and HIV-uninfected patients

regarding changes in patients' and PET derived variables between pre- and post-chemotherapy variables.

Table 3 Comparison of the change in parameters between the two ¹⁸F-FDG PET/CT scans according to patients' HIV serostatus

Change in parameters	HIV		t	p-value
	Mean ±SD Yes (n=18)	Mean ±SD No (n=34)		
Weight (Kg)	2.77 ± 5.92	4.49 ± 10.41	-0.648	0.520
BMI (Kg/m ²)	1.03 ± 2.10	1.75 ± 3.86	-0.738	0.464
FBS (mmol/L)	0.05 ± 1.2	-0.63 ± 2.21	1.203	0.235
Administered FDG (mCi)	-0.26 ± 1.37	0.55 ± 1.55	-1.875	0.067
Ascending aorta				
SUV max	0.02 ± 0.8`1	-0.04 ± 0.94	0.208	0.836
TBR	0.07 ± 0.42	0.05 ± 0.61	0.085	0.933
Carotid artery				
SUV max	-0.13 ± 0.59	0.06 ± 0.92	-0.803	0.426
TBR	0.01 ± 0.46	0.00 ± 0.57	0.087	0.931
Abdominal aorta				
SUV max	-0.18 ± 1.08	-0.15 ± 0.72	-0.122	0.904
TBR	-0.06 ± 0.66	-0.16 ± 0.62	0.519	0.606
Femoral artery				
SUV max	-0.10 ± 0.36	0.09 ± 0.63	-1.166	0.249
TBR	-0.05 ± 0.45	0.18 ± 0.53	-1.548	0.128

t: Independent Samples T test; HIV: Human Immunodeficiency Virus; BMI: Body Mass Index; FBS: fasting Blood Sugar; ¹⁸F-FDG: Fluorodeoxyglucose; SUVmax: maximum Standardized Uptake Value; TBR: Target-to-Background Ratio

We evaluated the effects of the presence of certain ASCVD risk factors on the differences in ¹⁸F-FDG PET-derived variables between the two scans. We found no significant difference between patients who were smokers versus those who were not (table 4). Regarding systemic hypertension, we did not find any significant difference between hypertensive and normotensive patients (table 5). Among patients who were diabetic, there was a mean decline in patients' weight of 10.10 kg between pre- and post-chemotherapy ¹⁸F-FDG PET/CT scan while weight increased by a mean of 4.46 kg among non-diabetic patients (p=0.025). Consequently, there was a significant difference in weight and BMI between patients grouped based on a history of diabetes mellitus between the two ¹⁸F-FDG PET/CT scans. We found no significant difference in

the activity of We found no significant difference in the activity of ^{18}F -FDG administered and the blood sugar level between patients who were diabetic and those who were not (table 6). Among the changes in PET-derived variables between the pre- and post-therapy ^{18}F -FDG PET/CT, patients who were diabetic, had a decline in SUVmax measured at the ascending aorta while non-diabetic patients had an increase in the same parameter ($p=0.035$). In the femoral artery, diabetic patients had a significant rise in TBR compared with non-diabetic patients, $p=0.002$ (table 6). The rest of the quantitative parameters were not significantly different between diabetics and non-diabetics.

Table 4 Comparison between patients grouped according to smoking history

Change in parameters	Smoking		t	p-value
	Yes Mean \pm SD	No Mean \pm SD		
Weight (Kg)	2.97 \pm 12.93	4.27 \pm 7.17	-0.462	0.646
BMI (Kg/m ²)	1.21 \pm 4.65	1.62 \pm 2.73	-0.398	0.692
FBS (mmol/L)	-0.51 \pm 2.28	-0.35 \pm 1.83	-0.263	0.794
Administered ^{18}F -FDG (mCi)	0.33 \pm 1.93	0.25 \pm 1.36	0.185	0.854
Ascending aorta				
SUV max	0.08 \pm 0.79	-0.06 \pm 0.94	0.482	0.632
TBR	0.08 \pm 0.79	-0.06 \pm 0.94	0.180	0.858
Carotid artery				
SUV max	-0.19 \pm 0.81	0.07 \pm 0.82	-1.065	0.292
TBR	-0.21 \pm 0.57	0.09 \pm 0.49	-1.951	0.057
Abdominal aorta				
SUV max	-0.10 \pm 0.88	-0.18 \pm 0.85	0.302	0.764
TBR	-0.22 \pm 0.62	-0.08 \pm 0.63	-0.684	0.497
Femoral artery				
SUV max	0.13 \pm 0.49	-0.02 \pm 0.58	0.850	0.399
TBR	0.16 \pm 0.72	0.07 \pm 0.40	0.534	0.596

t: Independent Samples T test; BMI: Body Mass Index; FBS: fasting Blood Sugar; ^{18}F -FDG: Fluorodeoxyglucose; SUVmax: maximum Standardized Uptake Value; TBR: Target-to-Background Ratio

Table 5 Comparison between patients grouped according to the history of systemic hypertension

Change in parameters	Hypertension		t	p-value
	Yes Mean ±SD	No Mean ±SD		
Weight (Kg)	4.33 ± 9.95	3.87 ± 9.14	0.085	0.932
BMI (Kg/m ²)	1.71 ± 3.74	1.49 ± 3.37	0.108	0.915
FBS (mmol/L)	1.30 ± 2.08	-0.50 ± 1.91	1.576	0.121
Administered ¹⁸ F-FDG (mCi)	1.27 ± 1.27	0.21 ± 1.53	1.168	0.248
Ascending aorta				
SUV max	0.51 ± 1.15	-0.05 ± 0.88	1.049	0.299
TBR	-0.45 ± 0.31	0.09 ± 0.55	-1.680	0.099
Carotid artery				
SUV max	0.55 ± 1.41	-0.04 ± 0.78	1.210	0.232
TBR	0.09 ± 0.23	0.00 ± 0.54	0.281	0.780
Abdominal aorta				
SUV max	0.51 ± 1.13	-0.20 ± 0.83	1.411	0.164
TBR	-0.01 ± 0.15	-0.13 ± 0.64	0.327	0.745
Femoral artery				
SUV max	0.40 ± 0.85	0.00 ± 0.53	1.219	0.288
TBR	0.13 ± 0.07	0/10 ± 0.52	0.112	0.911

t: Independent Samples T-test; BMI: Body Mass Index; FBS: fasting Blood Sugar; FDG: Fluorodeoxyglucose; SUVmax: maximum Standardized Uptake Value; TBR: Target-to-Background Ratio

t: Independent Samples T-test; **BMI**: Body Mass Index; **FBS**: fasting Blood Sugar; **¹⁸F-FDG**: Fluorodeoxyglucose; **SUVmax**: maximum Standardized Uptake Value; **TBR**: Target-to-Background Ratio

Table 6 Comparison between patients grouped according to the history of diabetes mellitus

Change in parameters	Diabetes mellitus		t	p-value
	Yes	No		
	Mean ± SD	Mean ± SD		
Weight (Kg)	-10.10 ± 2.69	4.46 ± 8.79	-2.315	0.025*
BMI (Kg/m ²)	-3.39 ± 0.93	1.69 ± 3.27	-2.183	0.034*
FBS (mmol/L)	-0.10 ± 3.68	-0.41 ± 1.91	0.216	0.830
Administered ¹⁸ F-FDG (mCi)	-0.95 ± 0.21	0.32 ± 1.54	-1.158	0.252
Ascending aorta				
SUV max	-1.32 ± 0.99	0.03 ± 0.86	-2.170	0.035*
TBR	0.68 ± 1.02	0.03 ± 0.53	1.660	0.103
Carotid artery				
SUV max	-0.21 ± 0.04	0.00 ± 0.84	-0.349	0.728
TBR	-0.11 ± 1.72	0.01 ± 0.48	-0.298	0.767
Abdominal aorta				
SUV max	-0.97 ± 0.79	-0.13 ± 0.85	-1.372	0.176
TBR	0.09 ± 0.47	-0.13 ± 0.63	0.474	0.637
Femoral artery				
SUV max	0.48 ± 0.86	0.01 ± 0.54	1.181	0.243
TBR	1.16 ± 1.07	0.06 ± 0.44	3.294	0.002*

t: Independent Samples T test; *: p<0.05; BMI: Body Mass Index; FBS: fasting Blood Sugar; FDG: Fluorodeoxyglucose; SUVmax: maximum Standardized Uptake Value; TBR: Target-to-Background Ratio

t: Independent Samples T test; *: p<0.05; **BMI**: Body Mass Index; **FBS**: fasting Blood Sugar; **¹⁸F-FDG**: Fluorodeoxyglucose; **SUVmax**: maximum Standardized Uptake Value; **TBR**: Target-to-Background Ratio

In order to determine the trends in arterial ¹⁸F-FDG uptake after anthracycline-based chemotherapy, we grouped patients according to the interval between completion of chemotherapy and the time of follow-up ¹⁸F-FDG PET/CT (at increments of four weeks). We plotted SUVmax and TBR obtained on pre- and post-chemotherapy for each arterial bed. At most time points, SUVmax and TBR were lower on the post-chemotherapy ¹⁸F-FDG PET/CT compared with the pre-chemotherapy scan. In patients who had their post-chemotherapy ¹⁸F-FDG PET/CT at 24 weeks or more after completion of chemotherapy, SUVmax and TBR obtained at this follow-up scan were similar or higher than baseline pre-chemotherapy SUVmax and TBR. Figs 1 and 2 show the trends over time of SUVmax and TBR in patients grouped according to the interval between completion of chemotherapy and the follow-up ¹⁸F-FDG PET/CT scan. Fig 3 shows how TBR and SUVmax were computed.

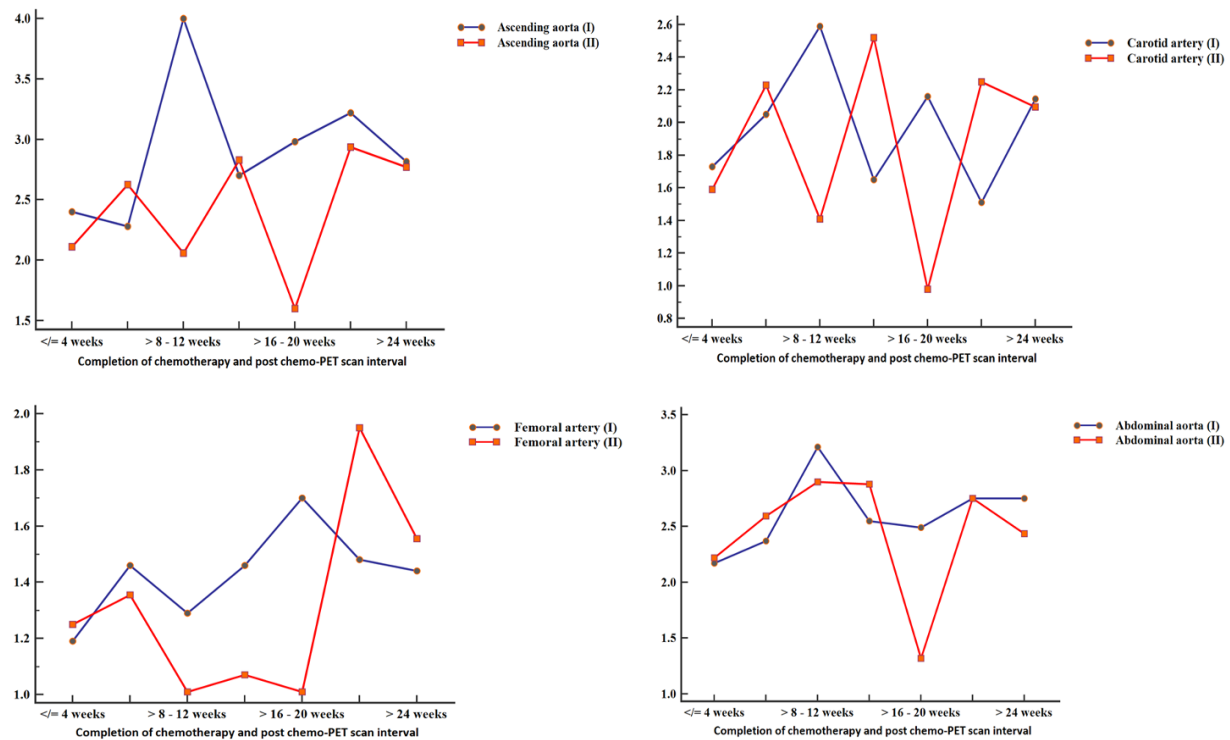


Fig 1 Time trend in SUVmax in patients grouped according to the interval between completion of chemotherapy and the time of follow-up ^{18}F -FDG PET/CT. The blue curve represents the SUVmax obtained on the pre-chemotherapy ^{18}F -FDG PET/CT, while the red curve represents SUVmax obtained in different groups at post-chemotherapy ^{18}F -FDG PET/CT. At more than half of the time-points in the four arterial beds, SUVmax was lower for the post-therapy ^{18}F -FDG PET/CT compared with pre-chemotherapy ^{18}F -FDG PET/CT scan. In the group in whom post-chemotherapy ^{18}F -FDG PET/CT was obtained more than 24 weeks after completion of chemotherapy, SUVmax in the arteries from the post-chemotherapy ^{18}F -FDG PET/CT equaled (ascending aorta and carotid artery) or surpassed (femoral artery) that of the pre-chemotherapy ^{18}F -FDG PET/CT.

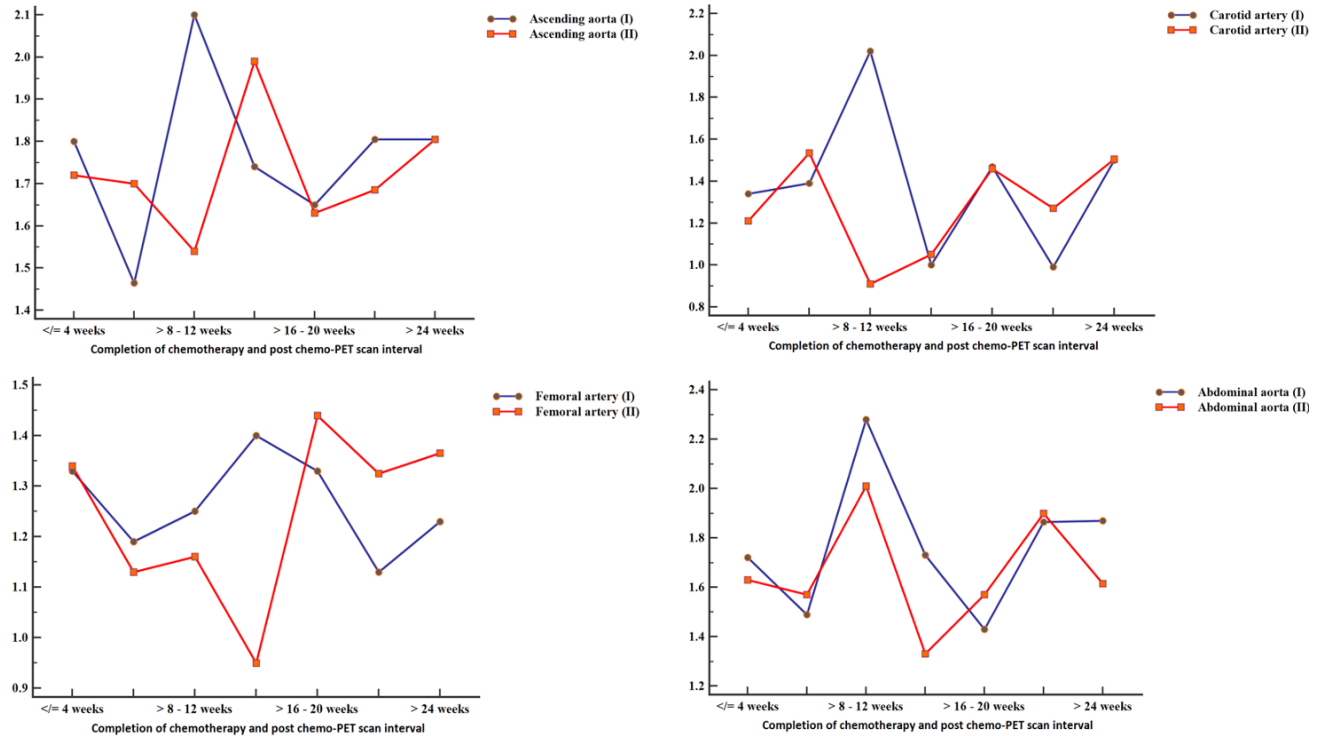


Fig 2 Time trend in TBR in patients grouped according to the interval between completion of chemotherapy and the time of follow-up ^{18}F -FDG PET/CT scan. The blue curve represents the TBR obtained on the pre-chemotherapy ^{18}F -FDG PET/CT, while the red curve represents TBR obtained in different groups at post-chemotherapy ^{18}F -FDG PET/CT. Like for SUVmax shown in fig 1, TBR was lower for the post-therapy ^{18}F -FDG PET/CT compared with pre-chemotherapy ^{18}F -FDG PET/CT in multiple time-points in the trend. In the group in whom post-chemotherapy ^{18}F -FDG PET/CT was obtained more than 24 weeks after completion of chemotherapy, TBR in the arteries from the post-chemotherapy ^{18}F -FDG PET/CT equaled (ascending aorta, carotid artery) or surpassed (femoral artery) that of the pre-chemotherapy ^{18}F -FDG PET/CT. TBR of post-chemotherapy ^{18}F -FDG PET/CT remained below that of the pre-chemotherapy ^{18}F -FDG PET/CT scan in the abdominal aorta.

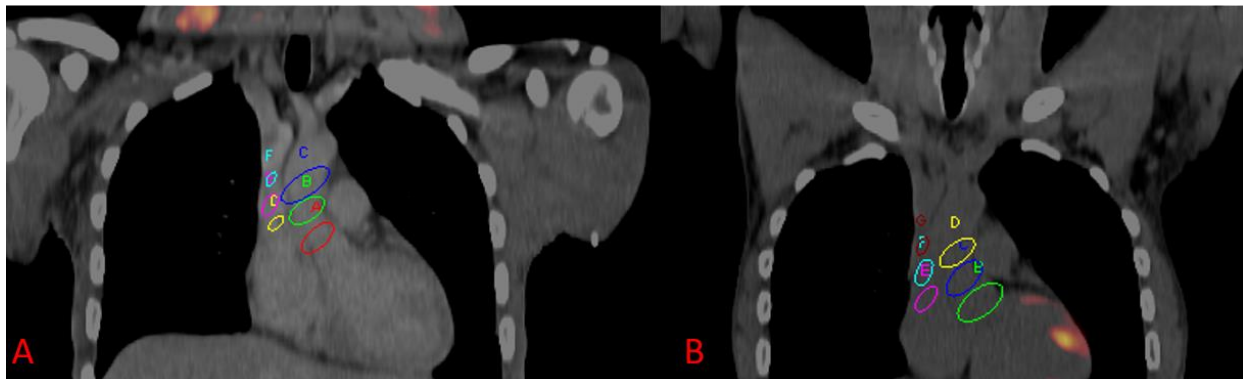


Fig 3 Fused ^{18}F -FDG PET/CT images through the chest of a 40-year-old male who had baseline (A) and follow-up imaging post-chemotherapy (B) for Hodgkin lymphoma. This figure depicts how SUVmax and TBR were calculated for each arterial bed using the ascending aorta and the superior vena cava for demonstration. Multiple regions of interests (ROI) are shown encircling the ascending aorta. The mean SUVmax obtained from these ROIs represents the aortic SUVmax. Multiple ROIs are shown within the lumen of the superior vena cava (SVC). The mean of the SUVmean from these ROIs represent the SVC SUVmean. TBR for the ascending aorta was computed by dividing

the aortic SUVmax by the SVC SUVmean. Aortic SUVmax and aortic TBR were computed for the baseline and post-chemotherapy ^{18}F -FDG PET/CT scans. These parameters were also obtained for the coronary vessels, the abdominal aorta (using the inferior vena cava for background correction), and the femoral vessels.

DISCUSSION

We evaluated systemic arterial inflammation in patients treated with anthracycline-based chemotherapy for HL and found no significant difference in the pre- and post-chemotherapy arterial ^{18}F -FDG uptake. We selected four arterial beds; carotid artery in the neck, ascending aorta in the chest, infra-renal abdominal aorta in the abdomen, and the proximal femoral artery in the proximal lower limbs; for a holistic evaluation of the effect of anthracycline-based chemotherapy on the systemic arterial vascular wall. Several observational studies have reported a higher incidence of cardiac morbidity and mortality contributed by ASCVD in patients treated with anthracycline-based chemotherapy for HL [7,22,23]. Invasion of the arterial wall by inflammatory cells is one of the earliest events in the formation of vascular atheroma, which makes arterial inflammation an early process in ASCVD. Arterial ^{18}F -FDG accumulation is a commonly used technique to measure arterial inflammation in cardiovascular risk assessment [15,24]. An increase in arterial ^{18}F -FDG accumulation over time is associated with the progression of ASCVD [25].

In our study, we could not demonstrate an increase in arterial ^{18}F -FDG uptake as a marker of arterial inflammation. Many factors could account for this negative result. ASCVD complicating anthracycline treatment occurs after a long latent period. The mean interval between the completion of chemotherapy and follow-up ^{18}F -FDG PET/CT in our study was 65 weeks. It may be possible that a more extended follow-up period is necessary for the development of a significant arterial inflammation that will be detectable by ^{18}F -FDG PET imaging. Another putative reason for our results may be due to the cytokine-induced by HL itself, causing an accentuated arterial ^{18}F -FDG uptake on the baseline pre-chemotherapy ^{18}F -FDG PET/CT scan. This may explain why arterial ^{18}F -FDG uptake was lower post-chemotherapy compared with pre-chemotherapy in some patients who were imaged earlier than 24 weeks after completion of chemotherapy (figs 1 and 2). A recent study found similar levels of circulating dysfunctional endothelial progenitor cells in treatment-naïve HL patients and at two years during remission induced by anthracycline-based chemotherapy [5]. Endothelial progenitor cells are responsible for the repair of endothelial damage induced by factors such as diabetes and

smoking that predispose to vascular atheroma formation. This suggests that both HL and its treatment with an anthracycline-containing chemotherapy regimen increase the risk of ASCVD. The primary pathogenic mechanism by which HL and its treatment predispose to ASCVD has been reported to be through impairment in the re-endothelization of damaged vascular endothelium due to dysfunctional endothelial progenitor cells. This pathogenic mechanism will suggest that a long interval is required after HL and its treatment for sufficient endothelial damage to occur in order to have significant arterial inflammation that may progress to ASCVD.

Other arterial structural changes occurring soon after anthracycline-based chemotherapy have been reported to contribute anthracycline-induced endothelial dysfunction. Aortic stiffness has been reported within four months of treatment with anthracycline-based chemotherapy in a group of oncologic patients [26]. Similar early aortic stiffening (within 6 months of treatment) was confirmed in another study of oncologic patients treated with low dose of anthracycline [27]. Apart from aortic stiffness, flow-mediated dilatation and nitrate-mediated dilatation are two sonographic techniques to measure endothelial dysfunction. In a study by Jenei et al, long term survivors of childhood cancer treated with anthracycline-based chemotherapy experienced marked preclinical vasculopathy characterized by endothelial dysfunction (evaluated by flow-mediated dilatation and nitrate-mediated dilatation) and increased arterial stiffness [28]. Aortic stiffness increases during follow-up of patients receiving anthracycline-based chemotherapy [29]. From the foregoing discussion, it is evident that subclinical ASCVD can be assessed by different noninvasive imaging techniques. Arterial changes such as aortic stiffness and endothelial dysfunction measured by magnetic resonance imaging and ultrasound scan show that the vascular changes due to anthracycline chemotherapy occur early after the initiation of treatment. These findings support the data in the literature showing that the incidence of ASCVD start to rise within five years of anthracycline-based chemotherapy without plateauing throughout the life cancer survivors [23,30]. While arterial inflammation is a very early step in atherogenesis, our failure to demonstrate significant increase in arterial ^{18}F -FDG uptake in our cohort may be due any of several factors including the short-term follow-up and many technical factors that could compromise adequate quantification of arterial ^{18}F -FDG uptake.

Patients infected with HIV are at increased risk of ASCVD. Arterial inflammation measured by the intensity of arterial ^{18}F -FDG uptake is known to be higher in HIV-infected people compared with age- and gender-matched controls [15,31]. We compared the changes in

arterial ^{18}F -FDG uptake between HIV-infected and HIV-uninfected patients and found no significant difference in the two groups. Similarly, in a sub-group analysis where we compared patients who were smokers and those who were hypertensive versus those who were not, we found no significant difference in the groups based on these two variables. An additional factor that may be responsible for the lack of significant differences in these groups relates to the low prevalence of these known cardiovascular risks in our patient population. For example, there were only 15 smokers and three patients with systemic hypertension. Our findings regarding sub-group analysis based on the history of diabetes mellitus was a little different. The patients who were diabetic experience significant weight loss and, consequently, a significant decrease in BMI between the pre- and post-chemotherapy ^{18}F -FDG PET/CT scans. We found a decline in the SUVmax measured in the ascending aorta between the pre- and post-chemotherapy ^{18}F -FDG PET/CT in the diabetic patients while non-diabetic patients experienced a rise in SUVmax of ^{18}F -FDG uptake in the ascending aorta. Similarly, we found a significantly higher rise in TBR of ^{18}F -FDG uptake in the femoral arterial among diabetic patients compared with non-diabetic patients. We doubt if these significant differences found in two of the measured ^{18}F -FDG PET parameters are meaningful, especially considering that there were only two patients in our study patients who were diabetic at the time of the study.

In this study, we showed the utility of ^{18}F -FDG PET/CT obtained for baseline pre-chemotherapy staging and post-chemotherapy re-staging in patients with HL treated with anthracycline-based chemotherapy in the evaluation of arterial inflammation as a risk factor of ASCVD. Evaluation of arterial inflammation in this patient group is essential to evaluate their cardiovascular risk and measure the effectiveness of anti-inflammatory therapy for risk reduction, which has attracted much interest in recent times. Our study has many limitations. Our study population is modest. This is because of the strict selection criteria we applied. Most importantly, we excluded all patients in whom lymphoma involves lymph node groups adjacent to the artery of interest that precluded accurate quantification of arterial ^{18}F -FDG uptake without photon spill-over from the lymph nodes. Lymph nodes are generally located around major vessels; hence a large proportion of patients were excluded for this reason. The retrospective design of our study also precludes the application of imaging conditions, including delayed imaging necessary to optimized arterial ^{18}F -FDG uptake and improve background activity clearance [21,32]. We failed to demonstrate a significant increase in arterial inflammation

following anthracycline-based chemotherapy. We speculate that the short interval between the completion of chemotherapy and the time of follow-up imaging in this study could be a significant contributing factor. Future studies in this area should explore a more extended follow-up interval between the completion of chemotherapy and post-chemotherapy ^{18}F -FDG PET/CT.

CONCLUSION

In patients with Hodgkin lymphoma who were treated with anthracycline-based chemotherapy, we found no significant increase in arterial inflammation measured by ^{18}F -FDG PET/CT after an average follow-up of about 65 weeks since completion of chemotherapy. The presence of systemic hypertension, diabetes mellitus, and smoking history did not seem to impact on arterial inflammation in our study population.

Acknowledgments

We wish to thank all members of staff at the Department of Nuclear Medicine, Steve Biko Academic Hospital, Pretoria, South Africa, for their support during the conduct of this study.

Funding

No external funding was received for the conduct of this study.

References

1. Meyer RM, Gospodarowicz MK, Connors JM, Pearcey RG, Wells WA, Winter JN, et al. ABVD alone versus radiation-based therapy in limited-stage Hodgkin's lymphoma. *N Engl J Med.* 2012;366: 399-408.
2. Moding EJ, Advani R, Rosenberg SA, Hoppe RT. Prognostic factors and patterns of failure in advanced stage Hodgkin lymphoma treated with combined modality therapy. *Radiother Oncol.* 2018;129: 507-512.
3. US Department of Health and Human Services; National Cancer Institute. Cancer incidence and survival among children and adolescents: United States Seer Program 1975-2013. Bethesda, MD, USA: 1-192.
4. Zamorano JL, Lancellotti P, Muñoz DR, Aboyans V, Asteggiano R, Galderisi M, et al. 2016 ESC position paper on cancer treatments and cardiovascular toxicity developed under the auspices of the ESC Committee for Practice Guidelines. *Eur Heart J.* 2016;37: 2768-2801.
5. Wiessman M, Leshem D, Yeshurun M, Yavin H, Iakobishvilli Z, Raanani P, et al. Dysfunctional endothelial progenitor cells in patients with Hodgkin's lymphoma in complete remission. *Cancer Med.* 2019;8: 305-310.
6. Werner N, Kosiol S, Schiegl T, Ahlers P, Walenta K, Link A, et al. Circulating endothelial progenitor cells and cardiovascular outcomes. *N Engl J Med.* 2005;353: 999-1007.
7. van Nimwegan FA, Schaapveld M, Janus CPM, Krol ADG, Petersen EJ, Raemaekers JMM, et al. Cardiovascular disease after Hodgkin lymphoma treatment: 40-year disease risk. *JAMA Intern Med.* 2015;175: 1007-1017.
8. Wong BW, Meredith A, Lin D, McManus BM. The biological role of inflammation in atherosclerosis. *Can J Cardiol.* 2012;28: 631-641.
9. Ridker PM, Everett BM, Thuren T, MacFadyen JG, Chang WH, Ballantyne C, et al. Antiinflammatory Therapy with Canakinumab for Atherosclerotic Disease. *N Engl J Med.* 2017;377: 1119-1131.
10. Tardif JC, Kouz S, Waters DD, Bertrand OF, Diaz R, Maggioni AP, et al. Efficacy and safety of low-dose colchicine after myocardial infarction. *N Engl J Med.* 2019;381: 2497-2505.

11. Tawakol A, Migrino RQ, Bashian GG, Bedri S, Vermylen D, Cury RC, et al. In Vivo ¹⁸F-Fluorodeoxyglucose Positron Emission Tomography Imaging Provides a Noninvasive Measure of Carotid Plaque Inflammation in Patients. *J Am Coll Cardiol*. 2006;48:1818-1824.
12. Graebe M, Pedersen SF, Borgwardt L, Højgaard L, Sillesen H, Kjaer A. Molecular pathology in vulnerable carotid plaques: correlation with [18]-fluorodeoxyglucose positron emission tomography (FDG-PET). *Eur J Vasc Endovasc Surg*. 2009;37:714-721.
13. Abdelbaky A, Corsini E, Figueroa AL, Fontanez S, Subramanian S, Ferencik M, et al. Focal arterial inflammation precedes subsequent calcification in the same location: a longitudinal FDG-PET/CT study. *Circ Cardiovasc Imaging*. 2013;6: 747-754.
14. Rominger A, Saam T, Wolpers S, Cyran CC, Schmidt M, Foerster S, et al. 18F-FDG PET/CT identifies patients at risk for future vascular events in an otherwise asymptomatic cohort with neoplastic disease. *J Nucl Med*. 2009;50:1611-1620.
15. Lawal IO, Ankrah AO, Popoola GO, Lengana T, Sathekge MM. Arterial inflammation in young patients with human immunodeficiency virus infection: A cross-sectional study using F-18 FDG PET/CT. *J Nucl Cardiol*. 2019;26: 1258-1265.
16. Figueroa AL, Abdelbaky A, Truong QA, Corsini E, MacNabb MH, Lavender ZR, et al. Measurement of arterial activity on routine FDG PET/CT images improves prediction of risk of future CV event. *JACC Cardiovasc Imaging*. 2013;6:1250-1259.
17. Lawal IO, Nyakale NE, Harry LM, Modiselle MR, Ankrah AO, Msomi AP, et al. The role of F-18 FDG PET/CT in evaluating the impact of HIV infection on tumor burden and therapy outcome in patients with Hodgkin lymphoma. *Eur J Nucl Med Mol Imaging*. 2017;44: 2025-2033.
18. Kostakoglu L, Cheson BD. Current role of FDG PET/CT in lymphoma. *Eur J Nucl Med Mol Imaging*. 2014;41: 1004-1027.
19. Lawal I, Lengana T, Ololade K, Boshomane T, Reyneke F, Modiselle M, et al. ¹⁸F-FDG PET/CT in the detection of asymptomatic malignant melanoma recurrence. *Nuklearmedizin*. 2017;56: 83-89.
20. Boellaard R, Delgado-Bolton R, Oyen WJG, Giammarile F, Tatsch K, Eschner W, et al. et al. FDG PET/CT: EANM procedure guidelines for tumour imaging: version 2.0. *Eur J Nucl Med Mol Imaging*. 2015;45: 328-354.

21. Bucerius J, Hyafil F, Verberne HJ, Slart RHJA, Lindner O, Sciagra R, et al. Position paper of the Cardiovascular Committee of the European Association of Nuclear Medicine (EANM) on PET imaging of atherosclerosis. *Eur J Nucl Med Mol Imaging*. 2016;43: 780-792.
22. Bhakta N, Liu Q, Yeo F, Baassiri M, Ehrhardt M, Srivastava DK, et al. Cumulative burden of cardiovascular morbidity in paediatric, adolescent, and young survivors of Hodgkin's lymphoma: an analysis from the St Jude Lifetime Cohort Study. *Lancet Oncol*. 2016;17: 1325-1334.
23. Maraldo MV, Giusti F, Vogelius IR, Lundemann M, van der Kaaij MAE, Ramadan S, et al. Cardiovascular disease after treatment for Hodgkin's lymphoma: an analysis of nine collaborative EORTC-LYSA trials. *Lancet Haematology* 2015;2: e492-502.
24. Takx RAP, MacNabb MH, Emami H, Abdelbaky A, Singh P, Lavender ZR, et al. Increased arterial inflammation in individuals with stage 3 chronic kidney disease. *Eur J Nucl Med Mol Imaging*. 2016;43: 333-339.
25. Joseph P, Ishai A, Mani V, Kallend D, Ruff JH, Fayad ZA, et al. Short-term changes in arterial inflammation predict long-term changes in atherosclerosis progression. *Eur J Nucl Med Mol Imaging*. 2017;44: 141-150.
26. Chaosuwannakit N, D'Agostino Jr R, Hamilton CA, Lane KS, Ntim WO, Lawrence J, et al. Aortic stiffness increases upon receipt of anthracycline chemotherapy. *J Clin Oncol*. 2010;28: 166-172.
27. Drafts BC, Twomley KM, D'Agostino Jr R, Lawrence J, Avis N, Ellis LR, et al. Low to moderate dose anthracycline-based chemotherapy is associated with early noninvasive imaging evidence of subclinical cardiovascular disease. *JACC Cardiovasc Imaging*. 2013;6:877-885.
28. Jenei Z, Bárdi E, Magyar MT, Horváth A, Paragh G, Kiss C. Anthracycline causes impaired vascular endothelial function and aortic stiffness in long term survivors of childhood cancer. *Pathol Oncol Res*. 2013;19: 375-383.
29. Daskalaki M, Makris T, Vassilakopoulos T, Moyssakis I, Siakantaris M, Angelopolou M, et al. Effects of anthracyclines on aortic distensibility in patients with lymphomas: A prospective study. *Hellenic J Cardiol*. 2014;55: 191-196.

30. Rugbjerg K, Mellekjær L, Boice JD, Køber L, Ewertz M, Olsen JH. Cardiovascular disease in survivors of adolescent and young adult cancer: A Danish cohort study, 1943-2009. *J Natl Cancer Inst.* 2014;106: dju110.
31. Lawal IO, Ankrah AO, Stoltz AC, Sathekge MM. Radionuclide imaging of inflammation in atherosclerotic vascular disease among people living with HIV infection: current practice and future perspective. *Eur J Hybrid Imaging.* 2019;3:5.
32. Lawal IO, Mokoala KG, Popoola GO, Lengana T, Ankrah AO, Stoltz AC, et al. Impact of optimized PET imaging conditions on ^{18}F -FDG uptake quantification in patients with apparently normal aortas. *J Nucl Cardiol.* Epub ahead of print on August 06, 2019.

Chapter 8

Summary

The critical role inflammation plays in the evolution and catastrophic complication of atherosclerotic cardiovascular disease (ASCVD) is now well-known. This makes targeting inflammation for risk assessment and as target for therapy promising. Combination antiretroviral therapy (cART) is now remarkably effective in reversing the severe immunosuppression associated with human immunodeficiency (HIV) infection. Its wide availability has translated into a significant reduction in the incidence and severity of opportunistic infections among people living with HIV (PLHIV) infection. ASCVD is an HIV-associated morbidity whose incidence is still on the increase even in the cART era. The efficacy of cART has translated into the aging of the HIV-infected population, indicating that the burden of ASCVD will continue to increase further among PLHIV. Since cART alone is not sufficient to protect against ASCVD among PLHIV, additional therapy including therapeutics targeting inflammation may be necessary for risk reduction. Novel biomarkers are necessary to identify patients at risk to select them for therapy and for therapy response assessment.

¹⁸F-FDG PET/CT is a useful modality to image arterial inflammation as a risk for ASCVD and to assess for response to anti-inflammatory therapy. Data on the application of ¹⁸F-FDG PET/CT for arterial inflammation imaging in PLHIV are presented in chapters 2 and 3. ASCVD is a chronic condition with a prolonged preclinical phase characterized by arterial inflammation and endothelial dysfunction. In chapter 4, data on the use of ¹⁸F-FDG PET/CT as a non-invasive biomarker for arterial inflammation in young HIV-infected patients with otherwise no risk factors for ASCVD are presented. In this original study, higher arterial inflammation was demonstrated in HIV-infected patients compared with age- and gender-matched control, indicating that HIV and its treatment are significant risk factors to kickstart atherogenesis from a young age even when other ASCVD risk factors are absent. The implications for this study include the need for the institution of anti-inflammatory therapy for ASCVD risk reduction earlier in PLHIV compared with HIV-uninfected people.

The PET system has a limited resolution which may impair accurate quantification of arterial inflammation. In chapter 5, data are presented showing that applying a set of imaging criteria recommended by the Cardiovascular Committee of the European Association of Nuclear Medicine leads to an improvement in the quantified arterial tracer uptake and reduction in background blood-pool activity. Standardization of imaging may improve the accuracy of PET for arterial inflammation quantification.

^{18}F -FDG is an analogue of glucose and is trapped by many tissues in the body. This is a limitation due to photon contamination from tissues with physiologic ^{18}F -FDG uptake during arterial tracer quantification. Tracers without these limitations with potential for use in PET imaging of arterial inflammation are presented in chapter 2. Chapter 6 reports the head-to-head comparison of ^{18}F -FDG PET/CT and [^{68}Ga]Ga-pentixafor PET/CT for arterial inflammation imaging in PLHIV. The data show a good agreement between the two imaging modalities suggesting that the latter may be used in the place of ^{18}F -FDG PET/CT.

PLHIV are also at increased risk of malignancies including lymphomas. Hodgkin lymphoma (HL) is treated with anthracycline-based chemotherapy, a treatment regimen associated with ASCVD in the long-term. Chapter 7 contains an original report on the performance of ^{18}F -FDG PET/CT to measure arterial inflammation in a mixed population of patients treated with anthracycline-containing chemotherapy for HL. No significant increase in arterial inflammation measured by arterial ^{18}F -FDG uptake was found between post-chemotherapy and baseline scans. This negative finding may be related to the short interval between the two scans since anthracycline-induced ASCVD is known to only occur after many decades.

Chapter 9

General Conclusion and Future Perspectives

General conclusion

The risk of atherosclerotic cardiovascular disease (ASCVD) is higher in people living with the human immunodeficiency virus (PLHIV) infection. As a precursor lesion of ASCVD, arterial inflammation is present at a young age even in HIV-infected patients without other cardiovascular risk factors. ^{18}F -FDG PET/CT can be used as a non-invasive biomarker to assess arterial inflammation in this young HIV-infected population. The accuracy of arterial ^{18}F -FDG uptake quantification, a surrogate marker of arterial inflammation, can be improved by applying a set of criteria including prolonged uptake time as recommended by the Cardiovascular Committee of the European Association of Nuclear Medicine. Based on the data presented in this work, it is clear that the routine oncologic PET imaging parameters severely underestimate signal intensity during ^{18}F -FDG PET/CT imaging of arterial inflammation.

Non-specific ^{18}F -FDG uptake in normal tissues surrounding the arterial bed of interest is an important challenge in photon quantification. This challenge can be addressed by substituting ^{18}F -FDG for other radiotracers targeting inflammatory cells for specific inflammation imaging. [^{68}Ga]Ga-pentixafor, a radiotracer that targets chemokine receptor-4 (CXCR4) expressed on activated inflammatory cells, may be a good substitute for ^{18}F -FDG for arterial inflammation imaging in PLHIV. In a study included in this work, PET quantification parameters of arterial [^{68}Ga]Ga-pentixafor uptake shows a good level of agreement with similar parameters obtained from both early and delayed ^{18}F -FDG PET/CT imaging.

Anthracycline-based chemotherapy, like HIV and its treatment, increases the risk of ASCVD. The higher risk of Hodgkin lymphoma in PLHIV and its treatment with anthracycline-containing chemotherapy regimen further increases the risk of ASCVD in this population. In a study included in this work, a higher level of arterial ^{18}F -FDG uptake was not demonstrated after anthracycline-based chemotherapy in a mixed population of HIV-infected and HIV-uninfected patients.

Future perspectives

The clinical experience with the use of ^{18}F -FDG PET for non-invasive imaging of arterial inflammation in HIV-infected patients remained extremely limited. More work is needed in the future to better define the role of this radionuclide technique for arterial inflammation imaging.

For example, in chapter 4, evidence was presented showing higher arterial wall ^{18}F -FDG uptake among young HIV-infected patients compared with age- and gender-matched controls, suggesting the presence of arterial inflammation as a biomarker of subclinical ASCVD in the HIV-infected patients. A need exists for a longitudinal study to follow-up these two populations (HIV-infected patients and their age- and gender-matched controls) to determine if this arterial inflammation seen in the HIV-infected patients translates into higher incidence of clinical ASCVD in the long-term. Apart from identifying the population at risk to select them for preventive therapy, there is a need for studies interrogating the performance of PET technique for response assessment of anti-inflammatory therapy as a means to stemming the tide of ASCVD in the HIV-infected population.

Owing to the challenges associated with the use of ^{18}F -FDG for PET imaging of arterial inflammation, a need exists to explore other PET tracers that target inflammation in assessing arterial inflammation in PLHIV.

Gallium-68 is an attractive positron emitter for PET imaging due to its availability from a $^{68}\text{Ge}/^{68}\text{Ga}$ generator. Prolonging uptake time has been shown to increase arterial tracer uptake and lead to an improvement in background blood-pool activity clearance. The short physical half-life of ^{68}Ga (68 minutes), while advantageous from a radiation protection perspective, is impracticable for delayed imaging. Complexing of small peptides targeting inflammation to longer-lived radionuclide with positron energy comparable to ^{18}F is needed in the future to allow for delayed imaging without compromising imaging resolution that may be degraded by using radionuclides with longer positron range and lower abundance. Copper-64 with a physical half-life of 12.7 hours appears promising for delayed imaging based on the limited experience with the use of ^{64}Cu -DOTA-peptide for inflammation imaging in ASCVD among HIV-uninfected patients.

Beyond the limited spatial resolution of the PET system, motion caused by the cardiac and respiratory cycles contribute to image degradation due to photon smearing. Image acquisition with dual respiratory and cardiac gating will go a long way in reducing the underestimation in photon quantification during arterial inflammation imaging. As newer generations of PET systems with the capability for this dual gating become more readily available, it is hoped that more robust data may emerge on the clinical application of PET techniques for vascular inflammation imaging. Coupling of PET camera to MR (magnetic

resonance) as hybrid PET/MR is another technological advancement in camera design with the potential for improving the sensitivity of characterizing inflammatory lesions, especially in small tissues such as the vessel wall. As PET/MR systems gain more prominent clinical utility and its availability increases, arterial inflammation in PLHIV may better be characterized using this more sensitive hybrid imaging modality than the traditional PET/CT system.

Total body PET/CT is the latest advancement in radionuclide imaging allowing for a more sensitive imaging of the entire body at a single bed position. In arterial inflammation imaging, the potential utility of the total body PET/CT camera will include whole body dynamic imaging which will allow for the computation of arterial tracer kinetics in real-time. This may go a long way in mitigating many of the limitations encountered in the use of the currently available clinical PET systems. The better sensitivity and resolution of the newer system may result in less underestimation of arterial wall signal allowing for a more accurate quantification of the arterial tracer uptake as a surrogate marker of arterial inflammation.

Annexures

The Research Ethics Committee, Faculty Health Sciences, University of Pretoria complies with ICH-GCP guidelines and has US Federal wide Assurance.

- FWA 00002567, Approved dd 22 May 2002 and Expires 03/20/2022.
- IRB 0000 2235 IORG0001762 Approved dd 22/04/2014 and Expires 03/14/2020.



UNIVERSITEIT VAN PRETORIA
UNIVERSITY OF PRETORIA
YUNIBESITHI YA PRETORIA

Faculty of Health Sciences Research Ethics Committee

28/06/2018

Approval Certificate
New Application

Ethics Reference No: 242/2018

Title: Ga-68 pentixafor PET/CT imaging of vascular expression of chemokine receptor 4 (CXCR4) as a marker of arterial inflammation in patients with human immunodeficiency virus infection and its comparison with F-18 FDG PET/CT Imaging.

Dear Dr Ismaheel Lawal

The **New Application** as supported by documents specified in your cover letter dated 7/06/2018 for your research received on the 7/06/2018, was approved by the Faculty of Health Sciences Research Ethics Committee on its quorate meeting of 27/06/2018.

Please note the following about your ethics approval:

- Ethics Approval is valid for 2 years
- Please remember to use your protocol number (**242/2018**) on any documents or correspondence with the Research Ethics Committee regarding your research.
- Please note that the Research Ethics Committee may ask further questions, seek additional information, require further modification, or monitor the conduct of your research.

Ethics approval is subject to the following:

- The ethics approval is conditional on the receipt of **6 monthly written Progress Reports**, and
- The ethics approval is conditional on the research being conducted as stipulated by the details of all documents submitted to the Committee. In the event that a further need arises to change who the investigators are, the methods or any other aspect, such changes must be submitted as an Amendment for approval by the Committee.

We wish you the best with your research.

Yours sincerely

Dr R Sommers; MBChB; MMed (Int); MPharMed, PhD

Deputy Chairperson of the Faculty of Health Sciences Research Ethics Committee, University of Pretoria

The Faculty of Health Sciences Research Ethics Committee complies with the SA National Act 61 of 2003 as it pertains to health research and the United States Code of Federal Regulations Title 45 and 46. This committee abides by the ethical norms and principles for research, established by the Declaration of Helsinki, the South African Medical Research Council Guidelines as well as the Guidelines for Ethical Research: Principles Structures and Processes, Second Edition 2015 (Department of Health).

☎ 012 356 3084

✉ deepeka.behari@up.ac.za / fhsethics@up.ac.za

🌐 <http://www.up.ac.za/healthethics>

✉ Private Bag X323, Arcadia, 0007 - Tswelopele Building, Level 4, Room 60 / 61, 31 Bophelo Road, Gezina, Pretoria

The Research Ethics Committee, Faculty Health Sciences, University of Pretoria complies with ICH-GCP guidelines and has US Federal wide Assurance.

- FWA 00002567, Approved dd 22 May 2002 and Expires 03/20/2022.
- IRB 0000 2235 IORG0001762 Approved dd 22/04/2014 and Expires 03/14/2020.

17 July 2019

**Approval Certificate
Annual Renewal**

Ethics Reference No.: 242/2018

Title: Ga-68 pentixafor PET/CT imaging of vascular expression of chemokine receptor 4 (CXCR4) as a marker of arterial inflammation in patients with human immunodeficiency virus infection and its comparison with F-18 FDG PET/CT Imaging

Dear Dr IO Lawal

The **Annual Renewal** as supported by documents received between 2019-06-18 and 2019-07-17 for your research, was approved by the Faculty of Health Sciences Research Ethics Committee on its quorate meeting of 2019-07-17.

Please note the following about your ethics approval:

- Renewal of ethics approval is valid for 1 year, subsequent annual renewal will become due on 2020-07-17.
- Please remember to use your protocol number (242/2018) on any documents or correspondence with the Research Ethics Committee regarding your research.
- Please note that the Research Ethics Committee may ask further questions, seek additional information, require further modification, monitor the conduct of your research, or suspend or withdraw ethics approval.

Ethics approval is subject to the following:

- The ethics approval is conditional on the research being conducted as stipulated by the details of all documents submitted to the Committee. In the event that a further need arises to change who the investigators are, the methods or any other aspect, such changes must be submitted as an Amendment for approval by the Committee.

We wish you the best with your research.

Yours sincerely



Dr R Sommers

MBChB MMed (Int) MPharmMed PhD

Deputy Chairperson of the Faculty of Health Sciences Research Ethics Committee, University of Pretoria

The Faculty of Health Sciences Research Ethics Committee complies with the SA National Act 61 of 2003 as it pertains to health research and the United States Code of Federal Regulations Title 45 and 46. This committee abides by the ethical norms and principles for research, established by the Declaration of Helsinki, the South African Medical Research Council Guidelines as well as the Guidelines for Ethical Research: Principles Structures and Processes, Second Edition 2015 (Department of Health)

Institution: The Research Ethics Committee, Faculty Health Sciences, University of Pretoria complies with ICH-GCP guidelines and has US Federal wide Assurance.

- FWA 00002567, Approved dd 22 May 2002 and Expires 03/20/2022.
- IORG #: IORG0001762 OMB No. 0990-0279 Approved for use through February 28, 2022 and Expires: 03/04/2023.

17 July 2020

**Approval Certificate
Annual Renewal**

Ethics Reference No.: 242/2018

Title: Ga-68 pentixafor PET/CT imaging of vascular expression of chemokine receptor 4 (CXCR4) as a marker of arterial inflammation in patients with human immunodeficiency virus infection and its comparison with F-18 FDG PET/CT Imaging

Dear Dr IO Lawal

The **Annual Renewal** as supported by documents received between 2020-06-30 and 2020-07-15 for your research, was approved by the Faculty of Health Sciences Research Ethics Committee on its quorate meeting of 2020-07-15.

Please note the following about your ethics approval:

- Renewal of ethics approval is valid for 1 year, subsequent annual renewal will become due on 2021-07-17.
- Please remember to use your protocol number (242/2018) on any documents or correspondence with the Research Ethics Committee regarding your research.
- Please note that the Research Ethics Committee may ask further questions, seek additional information, require further modification, monitor the conduct of your research, or suspend or withdraw ethics approval.

Ethics approval is subject to the following:

- The ethics approval is conditional on the research being conducted as stipulated by the details of all documents submitted to the Committee. In the event that a further need arises to change who the investigators are, the methods or any other aspect, such changes must be submitted as an Amendment for approval by the Committee.

We wish you the best with your research.

Yours sincerely



Dr R Sommers

MBChB MMed (Int) MPharmMed PhD

Deputy Chairperson of the Faculty of Health Sciences Research Ethics Committee, University of Pretoria

* The Faculty of Health Sciences Research Ethics Committee complies with the SA National Act 61 of 2003 as it pertains to health research and the United States Code of Federal Regulations Title 45 and 46. This committee abides by the ethical norms and principles for research, established by the Declaration of Helsinki, the South African Medical Research Council Guidelines as well as the Guidelines for Ethical Research: Principles Structures and Processes, Second Edition 2015 (Department of Health)



UNIVERSITEIT VAN PRETORIA
UNIVERSITY OF PRETORIA
YUNIBESITHI YA PRETORIA

Faculty of Health Sciences

12 July 2018

Prof MM Sathekge
HoD: Nuclear Medicine
University of Pretoria

Dear Prof Sathekge

STUDENT : O LAWAL (PhD MEDICAL NUCLEAR SCIENCE)

Ga-68 pentixafor PET/CT imaging of vascular expression of chemokine receptor 4 (CXCR4) as a marker of arterial inflammation in patients with human immunodeficiency virus infection and its comparison with F-18 FDG PET/CT imaging

The above-mentioned student's protocol has been approved by the PhD committee.

We wish the student all the best with his studies.

Kind regards

A handwritten signature in black ink, appearing to read 'V Steenkamp'.

PROF V STEENKAMP
CHAIR: PhD COMMITTEE

Pharmacology Dept., BMS Building
University of Pretoria, Private Bag X323
Arcadia 0007, South Africa
Tel +27 (0)12 319 2254
Email: vanessa.steenkamp@up.ac.za

Fakulteit Gesondheidswetenskappe
Lefapha la Disaense tša Maphelo